EFFECTS OF INTRINSIC NEURONAL PROPERTIES IN NEURAL DYNAMICS

Grupo de Neurocomputación Biológica
Departamento de Ingeniería Informática
Escuela Politécnica Superior
Universidad Autónoma de Madrid

Fabiano Baroni
fabiano.baroni@uam.es
June 2010

Work supervised by Pablo Varona Martínez

Acknowledgements

I am grateful to the GNB members, in particular Francisco Rodríguez, Luis Lago, Manuel Sánchez-Montañes, Eduardo Serrano, Carlos Aguirre, Juan Alberto Sigüenza, David Domínguez and especially my advisor Pablo Varona for his availability, patience and supportive attitude. To my lab colleagues, in particular Srikanth Ramaswamy, Bóris Marin, Carlos Muñíz, Fernando Herrero and Pablo Chamorro. During my doctoral studies I could benefit from several research stays which have been very useful in my training. I am especially grateful to Ron Calabrese, Angela Wenning, Andrey Olypher, Mikhail Rabinovich, Ramón Huerta, Marcelo Bussotti Reyes, Mark van Rossum, Irina Erchova and Thomas Nowotny. To other scientists who played an important role in my training, in particular Joaquín Torres Agudo, Gonzalo de Polavieja, Rafael Levi, Reynaldo Pinto and Tim Pearce. To my friends and family. This thesis was supported by grants from CAM.

Summary

This thesis belongs to the area of computational neuroscience, a discipline devoted to an understanding of the functions of nervous systems from the perspective of information processing through experimental recordings in living neurons, along with computer simulations and mathematical analysis. In particular, this work focuses on the effects of intrinsic, single-cell dynamics upon neural activity. This aspect has been investigated at different levels of description of the nervous system with the aid of mathematical models.

In the first part of the thesis, the interplay between membrane voltage and intracellular calcium concentration has been characterized in heart interneurons and motoneurons of the leech *Hirudo Medicinalis*, a very well known model system in the study of rhythmic motor generation. This analysis reveals a complex bidirectional interaction between these coupled dynamics, which is only revealed if the correspondent time series are analyzed at multiple time scales.

In the second part of this thesis, I describe how the interplay between intrinsic subthreshold oscillations and after-spike refractoriness shape the input-output transformation between trains of input pulses and evoked postsynaptic action potentials. The third part of the thesis extends these results by defining a measure of the propensity to firing of a cell in a given time. This measure evolves in time in a history-dependent fashion, allowing the quantitative assessment of the mnemonic features resulting from intrinsic neuronal dynamics.

Finally, the fourth part of the thesis investigates the effects of the intrinsic properties of a single neuron upon the weight dynamics of the connections impinging on it, subjected to activity-dependent plasticity rules. These effects are particularly evident when an oscillatory component is present in the input to the cell. In this case, its intrinsic properties will bias its average phase and hence the weight dynamics arising from a temporally sensitive plasticity rule.

Resumen

Esta tesis pertenece al campo de la neurociencia computacional, una disciplina dedicada a la comprensión de las funciones del sistema nervioso desde la perspectiva del procesamiento de información a través de registros experimentales, así como de simulaciones por ordenador y análisis matemático. En particular, este trabajo se centra en los efectos de la dinámica intrínseca de las neuronas individuales sobre la actividad neuronal. Este aspecto se ha investigado en diferentes niveles del sistema nervioso con la ayuda de modelos matemáticos.

En la primera parte de la tesis, se caracteriza la interacción entre el potencial de membrana y la concentración intracelular de calcio en interneuronas y motoneuronas de la sanguijuela *Hirudo Medicinalis*, un modelo experimental muy conocido en el estudio de la generación de patrones motores rítmicos. Este análisis revela una interacción bidireccional entre estas dinámicas acopladas, que se hizo patente sólo con un análisis de las correspondientes series temporales en múltiples escalas de tiempo.

En la segunda parte de la tesis, describo como la interacción entre oscilaciones subumbrales intrínsecas y las propiedades refractarias que siguen la generación de potenciales de acción modulan la transformación entre los trenes de entrada y los potenciales de acción evocados. La tercera parte de la tesis extiende estos resultados con la definición de una medida de la propensidad al disparo en un cierto instante de tiempo. Esta medida evoluciona en el tiempo de una forma dependiente de la historia, permitiendo un análisis cuantitativo de las características mnemónicas derivantes de las propiedades dinámicas intrínsecas de las neuronas individuales.

Finalmente, la cuarta parte de la tesis investiga los efectos de las propiedades intrínsecas de las neuronas individuales sobre la dinámica de los pesos sinápticos de las conexiones que convergen a la neurona, bajo una reglas de plasticidad dependientes de la actividad. Estos efectos son particularmente evidentes cuando la entrada a la neurona incluye una componente osciladora. En este caso, las propiedades intrínsecas de la neurona determinan su fase promedio, y por consecuencia la dinámica de los pesos sinápticos subyacentes a una regla de plasticidad sensible a la estructura temporal relativa de la actividad pre y post sináptica.

Contents

List of Figures

4.6 **Intrinsic discriminability as a function of input statistics for different model neurons.** A: Mean discriminability between input triplets with exponentially distributed ISIs, as a function of the input mean ISI, for the GIF and the IF neuron. Shades from brown to orange indicate GIF neurons with increasing values of the intrinsic frequency ω (see legend), while the black line indicates the IF neuron. The membrane rate constant μ was fixed at its canonical value of 1. B: The same as in A, but μ has been varied while ω was fixed at its canonical value of 2. Shades from brown to orange indicate increasing values of μ (see legend). GIF neurons, solid lines; IF neurons, dashed lines. C, D: Probability densities of the discriminability between input triplets with exponentially distributed ISIs, as a function of the input mean ISI, for the GIF (C) and the IF (D) neuron. E: The same as in A and B, but μ and ω have been scaled proportionally in order to maintain a fixed $\frac{\mu}{\omega}$ ratio of 0.5. Lighter colors indicate greater values of μ and ω. F: The same as in A, for gaussianly distributed input ISIs. Summarizing, increasing ω increases the discriminability at high input rates, while decreasing μ increases the discriminability especially for middle and low frequency inputs. 68

Chapter 1

Introduction

1.1 Behavioral demands span several time scales, and so do neuronal dynamics

1.1.1 Evolutionary origin of neurobiology

Most animals are endowed with an effector system which allows them to move in their environment to escape predators, and find food and mates, in a quest for survival. Through evolution, they have been pushed towards developing increasingly more sophisticated sensors and effectors, and later, more sophisticated decision processes and survival strategies. In contrast, plants and other non-moving organisms do not have this possibility, and have not been evolutionarily pushed in that direction. Indeed, they do not possess a nervous system, even if some plants and sponges are endowed with excitable cells displaying sensory-evoked and spontaneous electrical activity, and are capable of intelligent behavior in a formal sense (Baluska and Mancuso, 2009a,b). Nervous systems have evolved in order to map sensory stimuli to convenient motor output. For this mapping to be evolutionary advantageous, that is, for giving an individual the possibility of surviving and mating, it needs to be highly flexible, modular, and modifiable in several meaningful ways.

Neurons are specialized cells of the nervous system that have evolved to perform, as a network of connected elements, complex information processing aimed at directing behavior in an effective way. Surviving in a highly competitive environment poses hard cognitive challenges. In certain situations, a hundred millisecond delay in a motor response marks the difference between life and death: hence, certain highly relevant information requires an urgent response and needs to be processed in a direct, straightforward manner. This has

to be implemented through neuronal loops involving fast-conducting, myelinated axons and few synapses, because chemical communication through synaptic transmission is the time bottleneck of information transfer in the nervous system. This neuronal architecture allows high reaction speed, but limited flexibility. The reverberation of neuronal activity in large neuron ensembles with the involvement of many, physically distant layers allows a more flexible and modulable behavior, because information from different sensory modalities and past experiences can be integrated and better informed decisions can be taken. Obviously, information processing through multiple, recurrent loops is not as fast as in the former case. In other situations, relevant information which could be salient for future behavioral responses needs to be retained for a very long time, ideally, for the whole life span of the individual. Different behavioral needs seem to cover the whole time span between these two extremes.

Hence, behavioral needs pushed the nervous system to perform information processing on multiple temporal scales. A solution adopted by the most recently evolved organisms is to devote the tasks of information processing on short, intermediate and long temporal scales to different anatomical structures. For example, involuntary reflexes and the generation of automatic, locomotive movements can be observed in spinal animals (Grillner and Zangger, 1979). On the other extreme of the commonly accepted neuronal hierarchy, the hippocampus is required for the acquirement of new long-term memories (which are thought to be transferred and organized by a bidirectional dialogue with the neocortex), but not for the retainment of information for short periods of time nor for the access to already formed long-term memories (Scoville and Milner, 1957). In spite of this functional specialization, neuronal microcircuits are also capable of bridging over multiple time scales locally, due to the complex and distributed molecular machinary which determine their behavior. In fact, the interaction of fast and slow time scales is also observed at the single cell level, and forms the basis of the generation and recognition of complex temporal patterns, as we will show in the following chapters.

1.1.2 Neuronal dynamics on multiple time-scales

Behavioral demands span time scales from the millisecond range up to the whole life span of the individual. Still, action potentials are commonly assumed to be the main information-carrier events in the brain, and their duration is only a couple of milliseconds. In spite of its extremely fast time course, a single action potential triggers a series of events which

greatly outlast it. Indeed, along evolution, nervous cells developed a sophisticated molecular machinery which bridges several of the time scales required for efficient behavior.

Apart from the opening of voltage-gated ionic channels, whose dynamics can last up to a few hundred milliseconds in certain cases, action potentials result in calcium influx, which can affect ionic channels and interfere with several intracellular processes through molecular cascades (see (Berridge, 1998) for review). Calcium exchange between the intracellular medium and the endoplasmic reticulum (ER) further enhances the computational capabilities of single neurons. Indeed, the distributed morphology of the ER, the presence of specialized receptors with complex dynamics on its surface, and of a positive feedback in the dynamics of calcium flux through its membrane (calcium-induced calcium release) suggest that it could be considered as a neuron-within-a-neuron, integrating the information about the neuron input-output activity over longer time scales than the cytoplasmic membrane. The concentration of calcium in the intracellular medium can be thought of as a mnemonic trace of the recent activity of the cell. In fact, it allows the contextualization of information at the local level by constraining the dynamics of the neuron in a way which depends upon the previous activity and received inputs. Calcium signaling also plays a key role in gene transcription and in the plasticity of ion channels and synaptic machinery (Berridge, 1998), which are phenomena occurring at relatively long time scales.

Bridging over temporal scales is also accomplished through network mechanisms. In particular, the interplay between nested oscillations (typically gamma-theta) and slow neuronal dynamics like short term depression (Leibold et al., 2008) or adaptation (Kropff and Treves, 2008) results in compression of information at behavioral time scales (for instance, regarding a sequence of visited location in space) within each theta cycle, resulting in a compression factor of about 10. Such fast replay of temporal sequences has also been observed in the hippocampus (Nadasdy et al., 1999) and in the prefrontal cortex (Euston et al., 2007) during slow-wave sleep. Nevertheless, the importance of single cell dynamics interacting at multiple time scales, fostering complex information processing at the single cell level, and its relationship to complex, modulable functionality at the network level is only partially understood.

1.2 Lessons from CPGs

The realm of neuroscience where the importance of intrinsic dynamical properties of single neurons for network dynamics was first appreciated in detail is the study of small networks of neurons. In particular, small networks of neurons exhibiting rhythmic, but complex, behavior were studied in great detail by several groups starting from the sixties (reviewed in (Marder and Calabrese, 1996)). These networks, commonly referred to as Central Pattern Generators (CPGs), underlie the generation of rhythmic behaviors like respiration, chewing and locomotion (walking, running, crawling, swimming, flying, and in general any movement intended to propel the body in a certain direction in space). Invertebrate preparations were the most convenient for experimental analysis, because of the small number of cells involved, and their size and resistance to electrode penetration which greatly eased electrophysiological characterization.

For instance, it has been recognized that in some cases the oscillatory behavior of CPGs derives from intrinsic bursting of some of their component neurons. In this case, the intrinsically bursting neurons are called pacemakers, and the other neurons in the network which are not intrinsically bursting, but are entrained to burst rhythmically through network interactions, are called followers. This arrangement is not the only possibility, nor the most common: in many other cases, network oscillatory dynamics emerge from individual elements which are not pacemakers themselves. In this case, network oscillations arise through synaptic interactions.

In the most simple arrangement, a pair of tonically spiking neurons can produce rhythmic out-of-phase oscillations when coupled through mutual inhibition. As inward currents accumulate in one cell during its hyperpolarized phase, they will eventually exceed the total sum of synaptic and intrinsic outward currents thus starting the bursting phase, which in turn results in the termination of their partner's burst (alternation by escape). In this case, some overlap between the bursting phases of the two neurons is observed, and burst duration depends upon the intrinsic properties of the inhibited cell. Alternatively, burst alternation can arise from the withdrawal of firing of the active cell due to the build-up of adapting, outward currents. Its postsynaptic partner will then be released from inhibition and will start its active phase (alternation by release). In this case, no overlap is observed between the bursting phases of the two neurons, and burst duration is controlled by the intrinsic dynamical properties of the active cell. In most practical cases, though, both

dynamical mechanisms are interacting, and network period is controlled in part by both neurons. In fact the time of alternation, when the inactive cell starts its bursting phase, depends upon its intrinsic properties, the intrinsic properties of its partner neuron and the dynamics of the intervening synaptic connection.

As new features of neuronal physiology were discovered, their impact on network dynamics was assessed and the state-of-the-art picture of CPG behavior now comprises a wealth of dynamical mechanisms acting at several spatial and temporal scales, which all intervene in a redundant fashion to guarantee the healthy physiological performance of the network as a whole. For example, the precise phase relationship between the active phases of neurons in the crustacean pyloric CPG, and its maintenance as the network period is manipulated, have been attributed to fine differences in the dynamics of the h current in different cell types, a hyperpolarization-activated inward current which mediates post-inhibitory rebound spiking (Nowotny et al., 2008). Slow potassium currents could also be involved (Hooper et al., 2009; Zhang et al., 2008). Electrical coupling between rhythmically active neurons aids in their coordination with the correct phase relationships (Garcia et al., 2008). As an additional example, short-term synaptic depression can implement a dynamic switch between different functional network configurations (Nadim et al., 1999).

Second-messenger intracellular signaling mediates several dynamical phenomena, like the activity-dependent regulation of gene expression (Dallman et al., 1998; Linsdell and Moody, 1995), the modulation of ion channels on fast time scales in a homeostatic fashion (Meech, 1978; Luthi and Mccormick, 1998), the modulation of synaptic transmission (Ivanov and Calabrese, 2003), and calcium exchange with the endoplasmic reticulum (Berridge, 1998).

In particular, modeling work has shown that calcium exchange through the ER can endow an otherwise regular burster with irregular, chaotic dynamics (Falcke et al., 2000), which can be regularized by mutual interactions with other neurons (Varona et al., 2001). Depending upon the parameters used,the bidirectional coupling between calcium influx and calcium-dependent modulation of ionic conductances alters the phase space structure and can result in regularization of the bursting trajectories (Baroni et al., 2005). Neuromodulation (Warrick and Marder, 1991) can alter network dynamics in an activity-dependent fashion, often mediating homeostatic effects (Thoby-Brisson and Simmers, 1998; Liu et al., 1998), or reshaping functional connectivity in multifunctional networks (Briggman and Kristan, 2008). Even if a defining feature of Central Pattern Generators is their ability

to generate rhythmic dynamics in the absence of sensory information, in normal operating conditions their activity if finely modulated by proprioceptive feedback (Borgmann et al., 2009).

1.3 Large scale network dynamics

More complex networks are expected to operate on similar dynamical principles as CPGs (Yuste et al., 2005). However, most theoretical approaches to network dynamics have adopted very simplified descriptions of single-cell computation, typically relying upon non-dynamical individual units which implement a fixed input-output transformation (Hopfield, 1982). This approach was justified by its simplicity, allowing both analytical treatment and theoretical rigor in extracting results from minimal principles.

Only in the last few decades theoretical work in neuronal network dynamics began considering simple dynamical models for the individual neurons (Amit and Brunel, 1997). In particular, the Integrate and Fire (IF) has been by far the most widely used neuron model in the theoretical investigation of large neuronal network dynamics. It is the most simple dynamical model of neurons. It describes voltage fluctuations of the neuron membrane with a linear differential equation, as in a RC circuit, with the addition of a fixed voltage threshold and a spike reset. This model constituted an important step forward in realism in network modeling, still allowing analytical treatment in many cases of interest. For example, in the thermodynamic limit of an infinite network of identical cells oscillating asynchronously, a neuron output and its input can be related in a self-consistent manner, allowing the analytical calculation of the mean firing frequency and its standard deviation. The inclusion of an oscillatory term $e^{i\omega t}$ in the model equations allows the analytical assessment of the stability properties of the asynchronous state, and in particular the identification of the boundaries of the asynchronous state where oscillatory instabilities develop, and the frequency of the emerging oscillations (Amit and Brunel, 1997; Brunel, 2000).

1.3.1 Which model to use for individual neurons?

The main contribution of the IF neuron is the introduction of spike times in network modeling, while network models based upon non-dynamic individual units could only pro-

vide a spatial description of network activity, with the temporal dimension being blurred by a rate description. Furthermore, IF neurons do not implement a static input-output transformation as non-dynamical models like the perceptron, but one that is affected by previous input-output dynamics. This feature results in history-dependent responses to input stimuli at the single cell level. In addition to this, the after-spike reset of the voltage variable and the possibility of including an absolute refractory period can account for the effects of refractoriness. The inclusion of a non-linear term can account for the rapid activation of sodium channels (this version of the model is known as Exponential Integrate and Fire, or EIF (Fourcaud-Trocmé et al., 2003)), while the addition of another linear dynamical variable can account for subthreshold oscillations (this model is known as Generalized Integrate and Fire (GIF) (Richardson et al., 2003; Schreiber et al., 2004), or Resonate and Fire (Izhikevich, 2001)). In yet another variant, known as the Spike Response Model (SRM), a spike-triggered kernel is added to the voltage equation, representing both action potential shape and after-spike effects such as adaptation (Kistler et al., 1997). Similarly, a spike-triggered kernel can be added to a dynamic threshold for spike generation, yielding a formally equivalent model (Gerstner and Kistler, 2002). In another attempt for generalization, the parameters of the IF neuron has been made voltage-dependent (Abbott and van Vreeswijk, 1993). It should be noted that these extensions of the general IF formalism greatly complicate the analytical treatment of the correspondent network dynamics.

Even when one restricts the analysis to a certain neuron model, network dynamics depends critically upon the specific parameter set chosen. For example, the inclusion of propagation delays along neurites, and synaptic delays in the chemical communication between cells, deeply affect the dynamic repertoire a neuronal network can exhibit (Roxin et al., 2005; Coombes et al., 2003). In addition to this, intrinsic single cell dynamics also has a strong effect upon the resultant network behavior. Not only the adoption of different models for the individual neurons deeply affect the resultant dynamics (Muresan and Savin, 2007), but also does the inclusion of mild heterogeneities in their intrinsic properties (White et al., 1998). These aspects have not been throughly investigated. One of the main reasons is the high dimension of parameter space that one needs to consider when addressing the influence of intrinsic properties in network dynamics.

Depending upon the level of description one wishes to adopt, at least two parameters for each cell (in the case of minimal, phenomenological models like the EIF and the GIF) are needed, and the number of parameters can increase virtually without bound as

conductance-based models, multicompartimental models, and models based on a molecular description are considered. While the constrainment of single neuron parameters from biological experiments is feasible for phenomenological models based on very few parameters, it starts posing important challenges even at the single compartment conductance-based level. Actually, the complete characterization of the ionic channel complement of a given neuron, which can be accomplished through a careful combination of voltage clamp protocols and pharmacological manipulations, as pioneered by Hodgkin and Huxley (Hodgkin and Huxley, 1952), is not expected to result in a close match between the model and the biological behavior when all the acquired knowledge is put together in a single compartment conductance-based model.

This failure is not only due to the known limitations of the conductance based approach, which does not account for ion concentration changes within the cell and in the extracellular medium. The Goldman-Hodgkin-Katz formalism (Hille, 2001), based on ion channel permeabilities rather than conductances, describes ion concentration changes but does not improve much on the prediction side with respect to conductance-based models. In fact, neurons are the cells with the greatest morphological diversity and complexity, which deeply affect the exhibited behavior because of ion diffusion within the cell and in the extracellular medium, and because of the non-uniform and non-random distribution of ion channels along their morphology. Multicompartimental models are a strong computational tool in the description of neuronal behavior, but they require a very high number of parameters whose constrain is hindered by overfitting. Nevertheless, they are the minimal level of description one can adopt when trying to unravel the influence of morphology in neuronal dynamics.

In addition to the bottom-up approach where conductance based neurons are built from the detailed knowledge acquired from each of their ion channel types, the increased computational power available in the last decade has allowed a top-down, brute force search approach in parameter space (Prinz et al., 2004b). In this approach, millions of different neurons are created by randomly sampling a convenient portion of the parameter space, bounded by experimental results. These neurons are then probed with different levels of injected current or other applied stimuli, and only neurons with the desired response are selected. This approach has shown that the same neuronal output can be achieved with widely different parameter sets. However, this approach, albeit increasingly feasible given the great computational power available today, suffers from several problems (Nowotny

et al., 2007). For example, there are no strongly grounded rules for choosing the sampling strategy in parameter space. Neuronal output can be extremely sensitive (up to fractal sensitivity (Komendantov and Kononenko, 1996)) in certain regions and along certain directions in parameter space, and very little sensitive in others. More importantly, the wide diversity of ion channel distribution in "valid" neuron models obtained through the data-base approach doesn't seem to be reflected by an analogous diversity in biological neurons. Indeed, pharmacological manipulations aiming at blocking specific ion channels result in highly reproducible results across preparations, a result which doesn't seem to be consistent with a wide distribution of ion channels (but see (Grashow et al., 2009) for an alternative explanation). Hence, parameter estimation using a database approach can manage to constrain neuronal dynamics for certain input stimuli, but is likely to perform poorly on predictions for other input stimuli which were not included in the fitness function.

Recently, new fitting procedures have been suggested, which aim at finding parameter sets which correspond to valid and sufficiently robust dynamics, while at the same time keeping the computational cost manageable. For example, Nowotny *et. al.* (Nowotny et al., 2008) used a simulated annealing algorithm for parameter estimation, simulating a gap junction between the model output and the target voltage and considering several values of a DC input current in the fitness function. This work highlighted how different parameters are constrained very differently, with some parameters being tightly constrained, and others being almost irrelevant for the enforced dynamics. Others have obtained similar results with genetic algorithms (Tobin and Calabrese, 2006; Vanier and Bower, 1999). In particular, axonal and dendritic recordings are expected to improve the parameter estimation by constraining the model dynamics also in the spatial dimension, with respect to somatic recordings only (Keren et al., 2005). Other authors have performed parameter fitting using Kalman estimation (Ullah and Schiff, 2009). Another possibility for model estimation, which has not been explored in detail so far, is real-time estimation, which consists in actively probing the biological system with stimuli designed to reduce uncertainty in the parameters.

Recently, a spike train prediction contest has been launched (Gerstner and Naud, 2009), which allowed a quantitative comparison of neuron models. As expected, neither the detailed conductance-based neurons, nor the simple IF or related models (EIF, GIF) performed well. The best predictive power was obtained with a nonresetting leaky integrator with a firing threshold adapting on multiple time scales (Kobayashi et al., 2009). The

main advantage of this model neuron is the relatively small number of parameters (2 for the leaky integrator as in the standard LIF model, and 2L+1 for the adapting threshold, where L in the number of time scales considered, usually two or three), and the possibility of accounting for adaptation of slow and fast temporal scales. Indeed, the best predictive power was obtained with L=2.

Still, this model is not expected to faithfully reproduce, as its parameters are varied, a broad range of neuronal dynamical classes. In fact, its adapting threshold makes a good job in determining the output spike times, but the subthreshold dynamics is reduced to a purely passive description and hence cannot reproduce the frequency preference and other dynamical features of neurons with subthreshold resonances. This limitation was not revealed in the spike train prediction context probably because of the limited data set (three data sets in vitro and one in vivo) and the limited classes of inputs considered (random current injection in the in vitro data sets, random optical stimulation of the retina for the in vivo data set).

1.4 Original contribution of the present thesis

This thesis comprises four chapters, each of which resulted in a journal article. All of them deal with the interaction of different dynamical mechanisms in single neurons and its functional consequences for information processing in neural systems.

The first, titled "Time-scales in the interplay between calcium and voltage dynamics" (Ramaswamy et al., 2007), has been a pioneer work in the study of the interactions between membrane voltage and calcium dynamics. As discussed in the previous subsections, the interplay between membrane potential and intracellular calcium concentration has been studied extensively. Nevertheless, most experimental protocols focused upon specific aspects of this interaction, used highly artificial experimental settings and did not consider in detail the physiological, free evolution of the intact system as a whole. According to the dominant view in electrophysiology where neurons respond to input stimuli in a stereotypical manner and do not "produce information" on their own, the wealth of information gathered in these experiments resulted in intracellular calcium being considered as a mere integrator of membrane activity, basically following membrane dynamics with a certain delay as calcium enters the cell through NMDA and voltage-sensitive calcium channels, and is then absorbed into the ER, bound to other molecules or expelled into the

extracellular medium.

In this chapter, we performed long simultaneous recordings of transmembrane potential and intracellular calcium concentration in interneurons and motoneurons of the heart system of the leech, a very well known model system (Calabrese, 1979; Calabrese et al., 1995). We used an *in vitro* preparation comprising the first seven ganglia, thus retaining much of the wiring and complexity of the intact system. We performed correlation analysis between the two signals both at the temporal scale of the whole recording (comprising about ten bursts), and at the scale of individual bursts. Linear correlation performed at different temporal scales revealed that the interaction between voltage and calcium depends upon the temporal scale considered. Importantly, this interaction is not always unidirectional, with calcium responses lagging behind voltage deflections. At the single-burst scale, we often observed voltage deflections lagging behind the corresponding calcium transients.

These experimental results constitute a stringent benchmark for existing models which describe the interaction between calcium and voltage. In principle, they are not incompatible with models where coupling between voltage and calcium results in irregular, chaotic activity at the single cell level (Varona et al., 2001; Falcke et al., 2000). This variability could be constrained but not eliminated by network interactions, resulting in irregular network trajectories which might be more convenient for the exploration of phase space, and ultimately for the proper physiological function of the CPG (Zhurov and Brezina, 2006; Baroni et al., 2005; Baroni, 2005). In particular, this burst-to-burst variability could endow the cardiac CPG with an ability to adapt to developmental or pathological changes in the motor plant (Bucher et al., 2005). The temporal structure of bursting patterns depends upon the interaction between slow and fast dynamics. This interaction is also responsible for the modulation of bursting patterns on a cycle-by-cycle basis, allowing the reverberation of the information about the previous history of activity and stimulation of the cell (Marin et al., 2009). This local form of contextualization of information can form the basis for the emergence of complex discrimination capabilities at the single cell level.

By systematically observing several features of the bursting dynamics in both the voltage and calcium variables, we noticed that some features are strongly correlated, whereas others seem to vary independently. These results have been confirmed in other CPGs, in particular in the pyloric CPG of crustacean (Nowotny et al., 2008; Reyes et al., 2008), and might apply quite generally in the nervous system. One of the possible interpretation of these results is that some forms of variability and irregularity at several levels of the nervous system

(from the genetic underpinnings to the resulting network dynamics) are not only inevitable but also benificial, and that some built-in, distributed molecular machinery could act in a homeostatic fashion to guarantee the production of a "good enough" network output even in the face of variable circuit parameters, by strongly constraining variability in the task-relevant subspaces and letting it accumulate in task-irrelevant subspaces (see also (Scholz and Schöner, 1999; Todorov, 2004) for related ideas applied in motor control).

In the second chapter of this thesis (Baroni and Varona, 2007), we considered a simple, conductance-based model neuron with subthreshold damped oscillations, and studied its response to temporally structured inputs. As reported in the previous subsections, it has been observed both in models and in real cells that intrinsic oscillations act as a band-pass filtering mechanism, enhancing neuronal output when the input frequency matches the intrinsic frequency of the cell (Izhikevich et al., 2003b). In this chapter we showed how the interaction of neuronal dynamics at different time scales, namely the time scale of intrinsic subthreshold oscillations and the time scale of after-spike refractoriness, endows even very simple model neurons with complex input-output relationships which are better defined at the fine temporal scale of individual EPSPs.

To our knowledge, this is the first work that relates intrinsic subthreshold oscillations with the detection and production of precise temporal sequences of spikes. The motivation for studying the discriminability properties offered by subthreshold oscillations in a temporal coding scheme arose from a wealth of experimental studies which reported the non-random and informative nature of temporally precise firing sequences.

Oscillations in the membrane potential, either due to oscillatory inputs or to intrinsic dynamical mechanisms, format the continuos flow of neuronal information, by dividing it in chunks separated by peaks of inhibitory conductances which consistently bring the neuron to a restricted portion of its phase space (Li et al., 2006; Schaefer et al., 2006). Furthermore, oscillations offer a natural substrate for the emergence of informative temporal patterns of firing. During each cycle, the membrane potential is periodically brought closer and further from the firing threshold, resulting in periodical windows of opportunity for the generation of action potentials. In addition to this, the interaction between a neuron's intrinsic properties and its inputs will determine the phase of firing in each given cycle, which will then carry information about both neuron identity and its inputs (Hopfield, 2004; Shamir et al., 2009). This phenomenon results in the self-organization of cell assemblies in temporal coalitions, which would be maximally effective in firing their postsynaptic targets

due to their precise synchrony (Wang et al., 2010).

The third and longer chapter which comprise this thesis stemmed from an attempt of generalization of the results exposed in the previous chapter, with a focus upon subthreshold membrane dynamics (Baroni et al., 2010). Molecular dynamics in single neurons carry information about the previous input-output history, and in turn modulates the output responses to future stimuli. In particular, the state of activation/inactivation of ion channels, and the intracellular concentration of second-messenger molecules such as calcium, reflects the recent activity of the neuron, and their joint dynamics will determine how subsequent inputs will be processed and when, if at all, they will result in the generation of an action potential. This dynamical mnemonic trace allows the interpretation of newly incoming information in the context of the previously received inputs, and hence the discrimination of information at the single-cell level. Hence, this phenomenon can be considered as a single-cell, local form of transient memory, or information contextualization. We suggested a formal definition of neuronal excitability as a measure of the propensity to fire in any moment in time, linking the subthreshold history-dependent dynamics to spike generation. By studying how the excitability trajectories depend upon the statistics and temporal structure of input stimuli, we could assess the extent and characteristics of the intrinsic memory for different single-neuron dynamics and input statistics. The chapter offers a detailed analytical treatment in the case of the IF and GIF neuron with subthreshold oscillations, and also gives precise indications for estimating history-dependent excitability in general model and biological neurons. In particular, the contribution of specific ion channels to single cell memory can be investigated with a combination of modelling and dynamic clamp experiments. The presence of complex forms of local discrimination at the single cell level is likely to be highly relevant for information processing in neural networks, especially in the light of recent experimental accounts which revealed the highly dynamic, transient nature of information processing in the nervous system. The recognition of these cell-specific discrimination properties might further our understanding of neuronal network computations and their relationships to the distribution and functional connectivity of the different neuronal types found in the brain.

The fourth and last chapter is a first attempt to relate the intrinsic neuronal dynamics at the single cell level to functional outcomes at the network level (Baroni and Varona, 2010). In this work we showed that intrinsic neuronal dynamics interact with activity-dependent synaptic plasticity. In particular, when an oscillatory component is present in a neuron

input, typically as the result of emerging network oscillations (Buzsaki, 2006), the intrinsic properties of the neuron will determine its average phase, and hence the direction and extent of plastic changes of the synapses impinging on it. In fact, a form of Hebbian learning which is extremely sensitive to the relative timing of pre and post synaptic firing patterns, known as STDP (Spike Timing-Dependent Plasticity), introduces a differential bias in the weight dynamics which depends upon both the period of the oscillating input modulation and the intrinsic properties of the post synaptic cell. For example, if the post-synaptic cell tends to fire, on average, later than the peak of the oscillating modulation, synaptic weights originating from the oscillating population will be biased towards potentiation. Conversely, a bias towards depression will be observed if the cell tends to fire earlier than the oscillating modulation. Such a phase advance is actually observed in cells displaying inductive dynamics (Richardson et al., 2003; Narayanan and Johnston, 2008). This work suggests that the distribution of intrinsic properties across a neuronal network strongly constrains the possible wiring schemes which would emerge from activity-dependent plasticity rules. Given the wide heterogeneity of intrinsic properties in the nervous system (Soltesz, 2005), and the ubiquitos presence of network oscillations (Buzsaki, 2006), we believe that this mechanism might be highly relevant for structure formation during both development and mature life.

The last three chapters all deal with the computational consequences of intrinsic subthreshold oscillations, both at the level of local (single-cell) information discrimination, and at the level of connectivity development in networks. The four chapters which comprise this thesis offer only a glimpse of the functional complexity arising from intrinsic dynamics at the single cell level.

Chapter 2

Time-scales in the interplay between calcium and voltage dynamics

Abstract

The interaction between dynamics on multiple time scales increases the processing capabilities of neurons. A proper understanding of this interaction has to take into account not only the average behavior, but also the variability which is observed across bursting cycles. We analyze simultaneous voltage and calcium recordings from spiking-bursting neurons, and perform a statistical study of the correlation between both variables. We find a rich repertoire of time scales and correlated and uncorrelated parameters. We interpret these results as an outcome of the interaction between the intracellular slow dynamics and the membrane fast dynamics. This interaction results in complex behavior, where cycle-to-cycle variability is constrained in a highly non-random fashion. We expect our results to be highly relevant for information processing based on multiple codes, where the slow oscillation envelope and fast frequency modulations within bursts may carry complementary information. In particular, the slow calcium signal constitutes an informational inertia which could be a substrate for the contextualization of information at the single cell level.

Keywords: Voltage-calcium correlation, leech heart CPG, calcium dye fluorescence.

2.1 Introduction

The interaction between the fast dynamics of the membrane potential and the slow dynamics of intracellular ion concentration can result in complex neuronal dynamics. Of particular importance is the calcium ion Ca^{2+}, which controls excitability, neurotransmiter release and plasticity (Berridge, 1998). Calcium entering from voltage-dependent channels or released from internal stores controls conductances responsible for slow afterhypolarization or depolarizing afterpotentials following spikes (Meech, 1978; Luthi and Mccormick, 1998). These potentials, in turn, modify the neuronal firing. In effect, the slow dynamics of calcium and its interaction with the neuron's electrical responses is a form of short-term memory (Loewenstein and Sompolinsky, 2003). This memory can be used, for example, as a delay in the computation of motion detection (Barlow, 1996), to adapt to stimulus statistics (Fairhall and Bialek, 2003; Arganda et al., 2007) or to intervene in synaptic integration by affecting the shape of backpropagating action potentials (de Polavieja et al., 2005). Calcium is also a player in the global dynamics of the neuron. It contributes to generate complex patterns of spiking bursting-activity and can also affect the reliability of particular features of the electrical response (Baroni et al., 2005). These two effects, short-term memory and a fundamental role in the single-neuron dynamics, make calcium a mayor player in the network dynamics. We therefore expect calcium to play a role in the regulation of rhythms in the inhibitory loops found in many central pattern generators, in adaptation to statistics or more generally in the processing of recurrent circuits as predicted by realistic conductance-based models (Falcke et al., 2000; Varona et al., 2001). The many computational capabilities arising from the interaction between slow and fast dynamics are best studied in the identified neurons of invertebrates.

The leech is an ideal system to study the roles of calcium in network activity. Calcium imaging experiments in the leech have been used to study the role of calcium dynamics in dendritic processing in the AP neuron (Wessel et al., 1999). The heart interneurons HN, responsible for the CPG of heart beat control (Thompson and Stent, 1976), have been the focus of intensive calcium imaging studies. The modulation of spike-mediated synaptic transmission by presynaptic background Ca^{2+} (Ivanov and Calabrese, 2003) and the relationship between the spatio-temporal patterns of Ca^{2+} changes and the slow wave changes in the voltage dynamics (Ivanov and Calabrese, 2000) are the two main results of these studies. In spite of several modelling efforts, the role of calcium dynamics in shap-

ing membrane potential dynamics is still largely unknown. To further our understanding of the interplay between calcium and voltage dynamics, we have performed a statistical analysis of 50-100 s long recordings of simultaneous calcium and voltage activity in sensory neurons, interneurons and motoneurons. The analysis reveals several time scales in the bidirectional interaction between voltage and calcium, and reveals a complex scenario where some features of this interaction are strongly constrained, while others are almost independent.

2.2 Materials and methods

2.2.1 Experimental recordings

Medicinal Leeches (*Hirudo medicinalis*) were obtained from a German supplier (Zaug GmbH) and maintained in artificial pond water at 15 deg. centigrade in natural light. Standard techniques were used (Muller et al., 1981). In brief, ganglia 1st to 7th ganglion were dissected from the anesthetized animal and pinned ventral side up in standard extracellular solution. Relevant neurons were identified from their position in the ganglia and firing characteristics. The neurons were visualised using 40x water immersion objectives, under a Zeiss Axioskop FS 2 microscope. Intracellular recordings were made using a single quartz microelectrode filled with 4M potassium acetate and potassium chloride, and pulled to resistances of 40-80 Megaohms. Signals were amplified using an Axoclamp 1A amplifier. Calcium Green-1 was delivered into the neuron using a hyperpolarizing current of 0.5nA for about 5 min. Calcium images were acquired using a NeuroCCD system.

2.2.2 Data analysis

Spike detection was performed on the raw voltage traces by thresholding, and verified by visual inspection. The resulting spike trains had a clearly biphasic Inter Spike Interval (ISI) distribution, hence could be chunked into individual bursts without ambiguities. Each burst was temporally defined as the time window between the first and the last spike of the burst. For each burst, the time of maximal instantaneous frequency t_ν was defined as the middle point between the spikes corresponding to the shortest ISI.

Calcium images were temporally and spatially low-pass filtered, and the pixels included in a Region of Interest (ROI), located in the proximal portion of the primary neurite

(Figure 2.1A), were averaged to obtain the scalar signal plotted in Figure 2.1B,C. The maximum of the calcium signal in each burst was extracted. All temporal features were defined with respect to the median spike of each burst, a time reference which corresponds to the least standard deviation when computing cycle period in these cells. If n_s is the number of spikes in a certain burst, the median spike was defined as the spike with index $(n_s - 1)/2 + 1$ if n_s is odd, and as the middle point between the spikes with indexes $n_s/2$ and $n_s/2 + 1$ otherwise. Normalized cross-correlation between the low-pass filtered voltage and calcium signal was computed as

$$\mathcal{C}(n) = \frac{\sum_m v(m)c(m+n)}{\sqrt{\sum_m v(m)v(m+n)}\sqrt{\sum_m c(m)c(m+n)}}$$

where $v(n)$ and $c(n)$ are the time series for voltage and calcium, corresponding to each recording (Figure 2.2A,B) or to each individual burst (Figure 2.2C,D). In each case the maximum of $\mathcal{C}$ (correlation peak) and its position (correlation delay) were extracted. Probability densities have been estimated with a Gaussian kernel. Statistical analysis was performed using custom-built software in Matlab programming language.

2.3 Results

Figure 2.1B shows the somatic voltage in interneuron HN and the simultaneous fluorescence changes obtained with the calcium dye Calcium Green-1 from the region of interest indicated with a closed loop in Figure 2.1A. Eye inspection already indicates that the relationship between calcium and voltage is complex compared to those found in sensory neurons (sensory cells known as N cells, for example, show a clean one-to-one correspondence between single spikes and calcium changes; data not shown).

To better understand the relationship between calcium and voltage dynamics, we calculated the correlation function between the two variables. Figure 2.2 gives the probability density for calcium-voltage correlation peak values and delays for the motoneuron HE (solid line) and for interneuron HN (dashed line). To distinguish between interburst and intraburst characteristics, we have calculated correlation peak values and delays for whole recordings (top row) and single bursts (bottom row). Single burst correlations are computed as the normalized cross-correlation between the calcium signal and the voltage trace in a time window starting 1 s before the first spike and ending 1 s after the last spike for

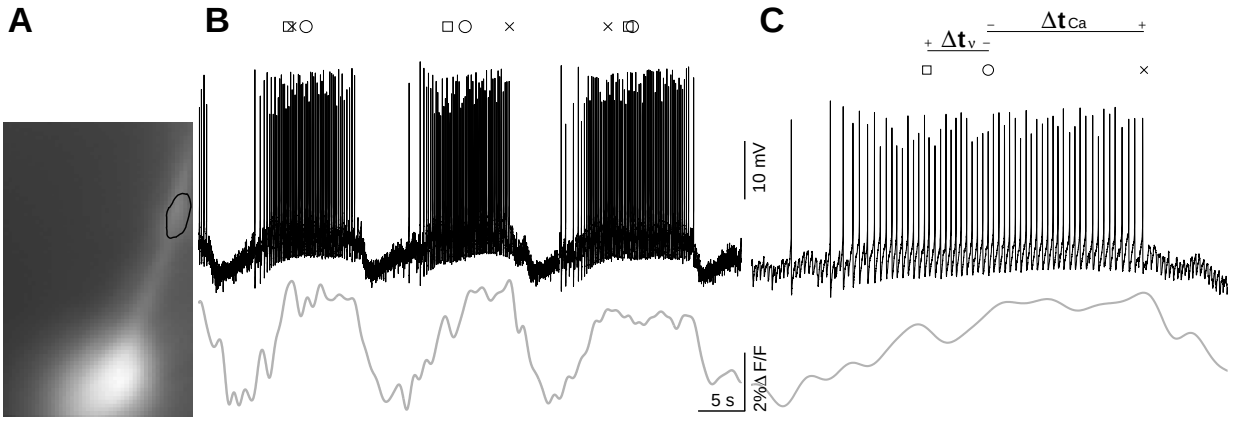

Figure 2.1: Simultaneous recording of calcium dye fluorescence and membrane potential for the HN neuron. (A) single frame showing the calcium dye fluorescence. Black closed loop indicates the region of interest in which we averaged the intensity pixel values for the calculation of a signal proportional to local calcium. (B) Membrane potential (top trace) and calcium (bottom trace). Symbols on top of the bursts indicate: ∘ median spike, □ frequency maxima, × calcium maxima . (C) Enlarged view of the middle burst in (B). Lines on top of the voltage trace denote time intervals used in the analysis. Δt_{Ca} is the time difference between the calcium maximum and the median spike for each burst. Δt_{ν} is the time difference between the maximum frequency and the median spike.

each burst. Whole recording correlations take into account longer time windows comprising 2-10 bursts. Both signals are low-pass filtered before computing correlations. While whole recording correlations contain slow frequencies corresponding to the biphasic rhythm driving the leech hearts, single burst correlations only comprise fast components corresponding to spiking activity.

Ca^{2+} signals were spatially averaged in the proximal portion of the primary neurite, and temporally low-pass filtered before being analyzed. The remaining burst-to-burst observed calcium variability is thought to reflect the variability in the burst structure, i.e. in the profile of the instantaneous firing frequency along the burst. This idea is supported by the single burst correlation analysis, where much higher correlation peaks where observed between corresponding Ca^{2+} and V low-pass filtered signals than when they were randomly shuffled. Furthermore, Ca^{2+} rising slopes lagging the corresponding local increases in firing frequency can be detected by the naked eye in recordings shown in Figure 2.1B. When a softer low pass filter was applied to the Ca^{2+} signal, almost one-to-one correspondence of Ca^{2+} peaks to individual spikes could be observed.

In general, HE cells show a stronger correlation between the voltage and the calcium dynamics, especially when single burst correlations are considered, Figure 2.2A,C. This

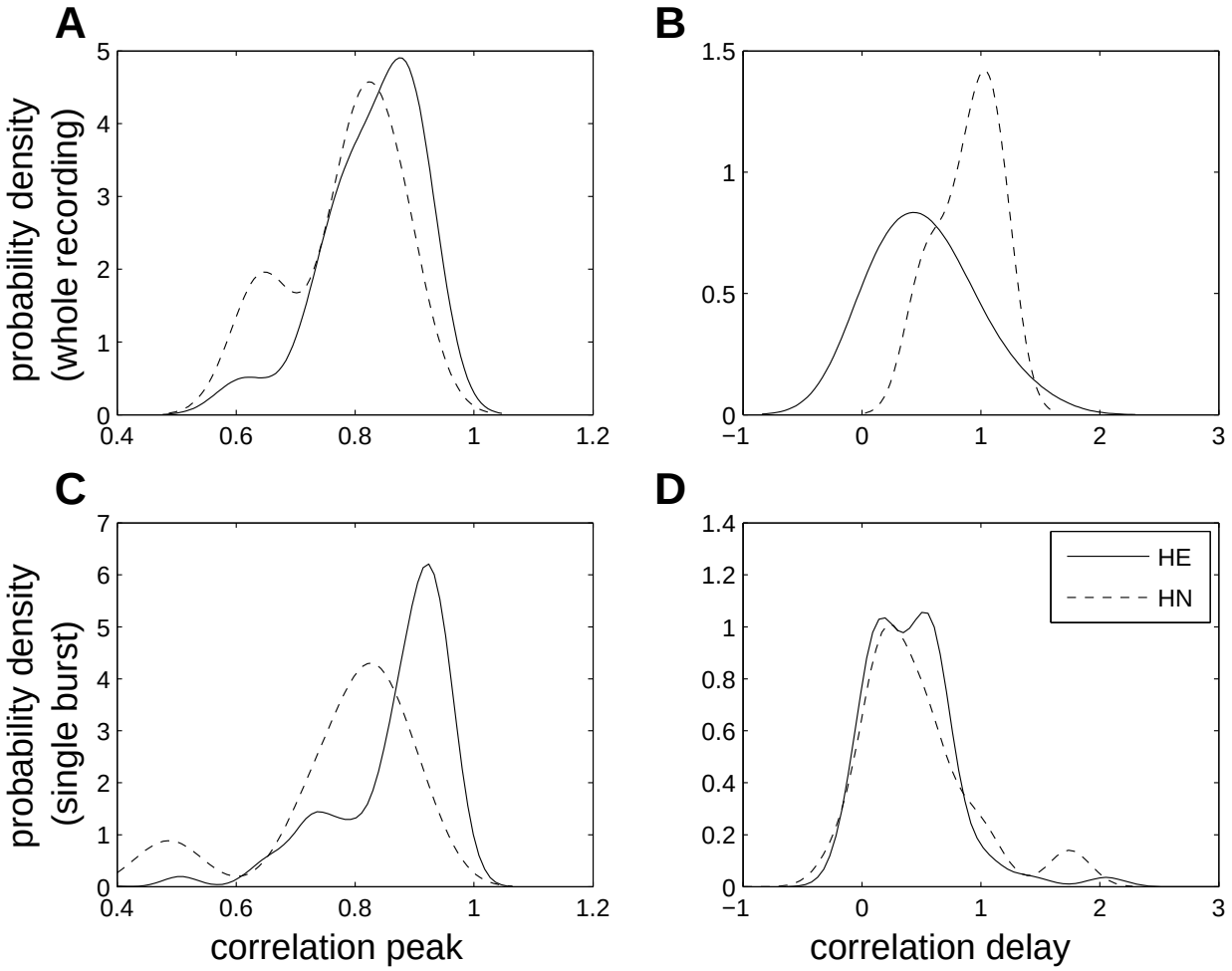

Figure 2.2: Probability density for calcium-voltage correlation peaks (A,C) and corresponding delays (B,D) for HE (solid line) and HN (dashed line). Top row (A,B) corresponds to whole recording correlations, while the bottom row (C,D) to single burst correlations. Correlation delays are measured in seconds.

stronger correlation coexists with a more variable correlation delay (wider curve for HE in Figure 2.2B,D). The correlation between calcium and voltage depends upon the length of the traces: for instance, if single bursts are taken into account, the correlation peak occurs at a shorter delay (compare panels B and D of Figure 2.2) than what observed when longer traces are used. We interpret this phenomenon as evidence for the interplay between calcium and voltage on multiple time scales: in the whole recording correlation analysis the interactions between voltage and calcium due to different cell mechanisms add together and the net result is a delay of calcium centered around 0.5 s for HE and 1 s for HN. On the other hand when we restrict the analysis to the bursting phase the coupling between V and Ca^{2+} is implemented with a different combination of cell mechanisms, resulting in a faster interaction.

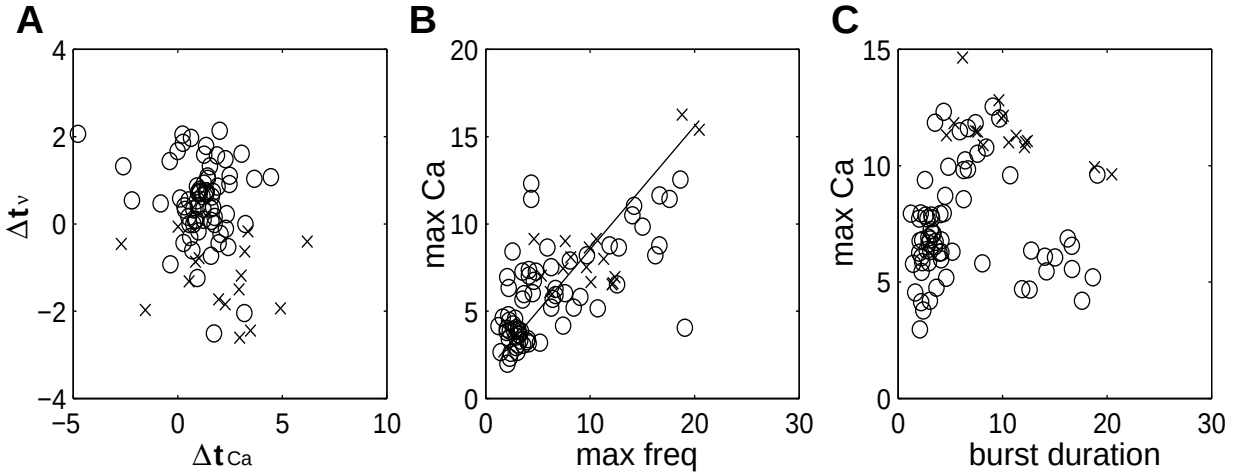

Figure 2.3: Correlated and uncorrelated parameters in the relationship between calcium and voltage for HE and HN neurons. (A) Time for maximum calcium, Δt_{Ca}, is not correlated with time of maximum spike frequency Δt_ν, $p > 0.01$. (B) Maximum calcium value is correlated to maximum spike frequency, $p < 10^{-13}$. (C) Maximum calcium value is not correlated with burst duration, $p > 0.1$. Different symbols indicate different cell types: $\circ$ HE, $\times$ HN. p values and correlation values are computed regardless of the cell type since no significant difference was found between them.

The correlation functions show the more general characteristics of the time-scales in the relation between calcium and voltage. To find which are the key parameters that best describe the correlation between calcium and voltage, we performed a large set of statistical comparisons. Figure 2.3 shows some of the most representative findings. The time corresponding to a maximum of calcium in a burst, Δt_{Ca}, measured from the time corresponding to the median spike (see Figure 2.1C), is not correlated to the time of maximum spike frequency, Δt_ν, also measured from the median spike, Figure 2.3A. This is particularly interesting in view of the fact that the maximum value of the calcium correlates with the maximum spike frequency, Figure 2.3B. Burst duration might be thought to have an impact on the maximum value of calcium but it does not for these spiking-bursting neurons, Figure 2.3C. For these bursting neurons the dynamics of voltage and calcium are surely correlated, but with wide degrees of freedom. Our analysis reveals that the interdependence between the two variables concentrates in some subspace, while in other subspaces they are free to behave almost independently.

2.4 Discussion

In this chapter we showed that the interaction between calcium and voltage is bidirectional, and results in different trajectories in each cycle. Hence, spike bursting in these neurons is not a stereotypical behavior, but one that varies from one burst to the next. Within this variability, some of the parameters describing voltage and calcium trajectories, and their interaction, vary in a strongly correlated fashion, while others vary almost independently. Theoretical work suggests that these features are not incompatible with deterministic models (Falcke et al., 2000; Varona et al., 2001). Nevertheless, stochastic phenomena embedded in a complex phase space, corresponding to chaotic dynamics, are also compatible with our experimental results. We expect our results to constrain future modelling of spike bursting behavior, and help to clarify the relationship between complex, chaotic dynamics and the possible role of stochastic phenomena in the resulting behavior.

Modelling work suggests that calcium modulation of ion channels dynamics can regulate the timing precision of action potentials in specific regions of the burst (Baroni et al., 2005). In accordance with this theoretical predictions, experimental work by our group shows the presence of regions of focalized timing precision in bursting activity (Campos et al., 2007). Future work will test the relevance of calcium for this timing precision. In this work, we did not consider spatial patterns of activity. We expect diffusion to influence the time scales observed. Extension of the present analysis in the time domain to the full spatiotemporal domain will clarify this issue.

Further experiments and analysis are needed to clarify more aspects of the relationship between calcium and voltage. So far, it has been a daunting task to obtain long and stationary calcium imaging recordings. In fact, the toxicity of calcium-sensitive dyes limits the recording time to few hundred seconds. Nowadays, more physiologically compliant dyes have been developed. The long simultaneous recordings of calcium and voltage which will be possible with this technology will allow the application of non-linear analysis tools (such as information and causality analysis), furthering our understanding of the relationship between voltage and calcium (Levi et al., 2010).

Recent modeling results have shown that neural signatures, i.e. cell-specific interspike interval distributions (Szücs et al., 2003), can be part of a multicoding strategy of bursting neurons (Latorre et al., 2006) and convey information about input stimuli received during the hyperpolarized phase (Marin et al., 2009). In this framework, the slow bursting en-

velope and the fast modulations of the instantaneous firing frequency within bursts carry different, complementary information. The analysis presented in this chapter suggests that the interaction between slow and fast dynamics at the single cell level can constitute a dynamical basis for the generation of a variable, informationally rich intraburst structure, while preserving the regularity of the slow wave. As we will discuss in the following chapters, the interaction between intrinsic dynamics at different time scales is also fundamental for the recognition of temporally specific input patterns, hence qualifying as a key ingredient in the complex information processing performed by neuronal cells.

Chapter 3

Subthreshold dynamics and refractoriness shape neuronal input-output relationships

Abstract

The difference between resonator and integrator neurons relies upon a frequency preference for the former, while the latter monotonically increase their spiking probability with the frequency of a periodic input. In model neurons where dynamics on multiple time scales are present (hence ubiquitously in real neurons) the concept of frequency preference can naturally be broadened to take into account preference towards temporally specific n-tuples of presynaptic inputs. As we show in this chapter, single neurons with dynamics on multiple time scales can detect specific temporal patterns. In particular, the interplay between damped subthreshold oscillations and refractory properties results in specific temporal preferences in the input-output transformation performed by an individual neuron.

Keywords: input-output neuronal preference, sparse coding, neural signatures.

3.1 Introduction

Traditionally, model neurons have been classified on the basis of their computational properties as integrators or resonators (Izhikevich, 2006). While integrator neurons are more likely to fire a spike when they receive high frequency inputs, resonator neurons show some preference to spikes with a certain interspike interval (ISI), in the sense that their firing probability is maximum when the presynaptic ISI has a certain non-zero value. This property depends on the kind of bifurcation of the stable equilibrium corresponding to the rest state the neuron is near to. In general, integrator neurons are close to a saddle-node bifurcation (whether off or on a limit cycle) while resonators are close to an Andronov-Hopf bifurcation. In the latter case the stable focus corresponding to the rest state is surrounded by an unstable limit cycle (subcritical Andronov-Hopf bifurcation) or by large amplitude trajectories which will eventually lead the phase point back to the stable focus (supercritical Andronov-Hopf bifurcation). In both cases a displacement of the current phase point from the stable focus might give rise to a small amplitude oscillation, eventually leading the phase point back to the stable focus, or a large amplitude oscillation, corresponding to a spike. In this chapter we focused our analysis in a simple model neuron near a supercritical Andronov-Hopf bifurcation. If we consider the response of the neuron to a pair of inputs (a doublet), the effect of the second input will depend upon its timing with respect to the first, and upon the amplitude of the first input. Indeed the first input will cause a subthreshold oscillation of the phase point, at a frequency that depends upon the amplitude of the oscillation, hence upon the input amplitude. The second pulse might push the phase point to regions of the phase space corresponding to large amplitude trajectories (i.e. spikes), or might as well push the phase point closer to the stable focus, resulting in a dampening of the subthreshold oscillations (e.g. Fig. 7.22 in (Izhikevich, 2006)). When more than one resonant variable is added to the model, the phase space around the stable focus might become very complex, and the frequency of oscillation might depend not only upon the amplitude but also upon the current phase. In addition to this, action potential generation results in activation (inactivation) of outward (inward) currents, globally resulting in a strong or even complete decrease in excitability, known as neuronal refractoriness. This scenario leads to complex input-output relationships, where single neurons might have evolved and developed so as to respond only to certain, precisely timed sequences of inputs. Neuronal preference in terms of temporal structure of incoming inputs has been known for a long time (Segundo et al., 1963), nevertheless few theoretical efforts have been made for

the identification of the minimal ionic mechanisms which can implement it.

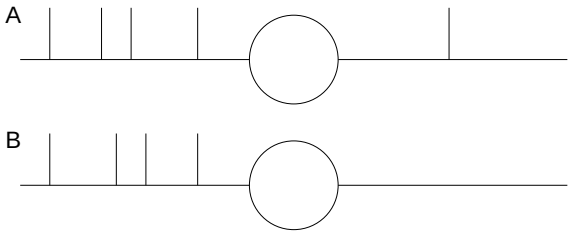

Figure 3.1: Example of input-output preference relationship. The two input patterns are different permutations of the same set of ISIs, but the neuron responds only to input pattern A.

3.2 Model

We argue that the traditional notion of frequency preference can be naturally broadened to take into account n-tuples of presynaptic inputs (Fig. 3.1). The neurocomputational property of frequency preference is based upon a resonance ionic mechanism. For instance, a model neuron with a K^+ activation variable or a Ca^{2+} inactivation variable could, with an adequate choice of the parameters, display a phase portrait close to an Andronov-Hopf bifurcation, and hence show resonant properties. Nevertheless real neurons display several amplifying and resonant variables acting on comparable time scales, hence it is reasonable to hypothesize that such an interaction might give rise to complex input-output relationships. We prove this hypothesis by injecting triplets of presynaptic spikes with different ISIs in a model neuron, and observing whether a triplet elicited a spike or not.

We study this phenomenon in a conductance-based model of a cortical neuron published by Gutfreund *et. al.* (Gutfreund et al., 1995), and in a linear model with after-spike reset exhibiting subthreshold oscillations, known as GIF (Generalized Integrate and Fire).

3.2.1 Conductance-based model

The model by Gutfreund *et. al.* produces subthreshold oscillations through an interplay of a fast and persistent Na^+ current, and a slowly activating K^+ current. EPSPs are modelled as exponentially decaying conductances with a time constant $\tau_{syn} = 0.2$. Postsynaptic spikes are defined as the crossing of a threshold $V_{thr} = -10mV$ with positive slope of the membrane potential variable. The model is described by the following system of differential

equations:

$$\begin{aligned} C_m \frac{dv}{dt} &= -(I_{NaP} + I_{Ks} + I_{Na} + I_K + I_L + I_{syn}) \\ \frac{dh}{dt} &= (h_\infty(v) - h)/\tau_h(v) \\ \frac{dn}{dt} &= (n_\infty(v) - n)/\tau_n(v) \\ \frac{dn_{Ks}}{dt} &= (q_\infty(v) - n_{Ks})/\tau_{Ks} \end{aligned}$$

where the persistent Na^+ current I_{NaP} and the slow K^+ current I_{Ks} are responsible for the subthreshold damped oscillations, and the fast Na^+ and K^+ currents, I_{Na} and I_K, mediate the generation of action potentials. The expressions for the currents are given by

$$\begin{aligned} I_{Na} &= g_{Na} m_\infty^3(v) h (v - E_{Na}) \\ I_K &= g_K n^4 (v - E_K) \\ I_{NaP} &= g_{NaP} p_\infty(v)(v - E_{Na}) \\ I_{Ks} &= g_{Ks} n_{Ks}(v)(v - E_K) \\ I_L &= g_L (v - E_L) \\ I_{syn} &= \sum_{t_s} g_{Syn} \mathrm{e}^{-(t-t_s)/\tau_{syn}} \mathcal{H}(t - t_s) \end{aligned}$$

where $\mathcal{H}(t)$ is the Heaviside function, g_x is a membrane conductance, E_x is a reverse potential, τ_x is a time constant ($x = Na,\ K,\ NaP,\ Ks,\ L,\ syn$), $C_m = 0.37nF$ is the membrane capacitance, $\phi = 26.12$ is a temperature factor. See Tables 3.1 and 3.2 for a complete definition of the remaining functions and parameters.

In general, response to synaptic inputs results in a deformation of the phase space. Even in the case of the widely used synaptic model where each presynaptic spike triggers a synaptic conductance with fixed reversal potential which is an alpha function of time, the time constants of rise and decay of the synaptic conductance are comparable with the time constants governing ion channels kinetics. Hence the dynamical response of the system cannot be qualitatively analyzed unless the system is cast into a higher dimensional state

Table 3.1. Gating variables and parameters for the currents of the Gutfreund neuron.

Current	g_x,μS	E_x, mV	Gating Variables	τ_x, ms
I_{Na}	19.24	55	$m_\infty = \alpha_m/(\alpha_m + \beta_m)$	
			$h_\infty = \alpha_h/(\alpha_h + \beta_h)$	$1/(\phi(\alpha_h + \beta_h))$
I_K	7.4	-90	$n_\infty = \alpha_n/(\alpha_n + \beta_n)$	$1/(\phi(\alpha_n + \beta_n))$
I_{NaP}	0.037	55	$p_\infty(v) = 1/(1 + e^{-(v+51)/5})$	
I_{Ks}	2.59	-90	$q_\infty(v) = 1/(1 + e^{-(v+34)/6.5})$	6
I_L	0.037	-60		

Table 3.2. Values for the functions α and β used in the spike generating currents I_{Na} and I_K.

	α	β
m	$\alpha_m = \frac{-0.1(v+32)}{e^{-0.1(v+32)}-1}$	$\beta_m = 4e^{-(v+57)/18}$
h	$\alpha_h = 0.07e^{-(v+46)/20}$	$\beta_h = \frac{1}{e^{-0.1(v+16)}+1}$
n	$\alpha_n = \frac{-0.01(v+36)}{e^{-0.1(v+36)}-1}$	$\beta_n = 0.125e^{-(v+46)/80}$

space, which additionally complicates the understanding of the dynamics. In this case the values chosen for these parameters correspond to a very fast kinetics if compared to the other variables of the system, hence the synaptic conductances in this model can be considered as instantaneous current pulses which do not affect the vector field in the state space, but only displace the current phase point to the right along the V axis (see Fig. 7.2 in (Izhikevich, 2006)).

3.2.2 Linear model with after-spike reset

The second neuron model we consider is the Generalized Integrate and Fire (GIF) model, described by the following equations:

$$\begin{aligned} \frac{dv}{dt} &= -\alpha v - \beta w + I_{syn} \\ \frac{dw}{dt} &= v - w \end{aligned} \tag{3.1}$$

The model is endowed with an after-spike reset mechanism, so that when v crosses a threshold v_{thr} from below a spike is emitted and the membrane potential is reset to a value

v_{reset}, and kept there for a refractory time t_{refr}. The system (3.1) has proven particularly useful in studying neuronal intrinsic oscillations (Richardson et al., 2003; Izhikevich, 2001; Schreiber et al., 2004): in a certain parameter regime, it is mathematically equivalent to a damped linear oscillator, and thus constitutes an analytically amenable model for the description of neuronal intrinsic oscillations, i.e., oscillations generated by intrinsic ionic mechanisms as the activation of a resonant current or the inactivation of an amplifying current (Hutcheon and Yarom, 2000). The canonical GIF model that we used for most of the thesis has $\alpha = 1$ and $\beta = 4$, resulting in complex conjugate eigenvalues $-1 \pm 2i$ (see the Appendix). Given the wide frequency range of intrinsic oscillations observed in mammalian brains, which spans at least two order of magnitude (from 0.5 Hz until 50 Hz (Hutcheon and Yarom, 2000)), we preferred to keep this model dimensionless.

For the sake of simplicity, and for carrying out analytical calculations, we consider

$$I_{syn} = \sum_{t_s} A\delta(t - t_s)$$

This approximation reduces the synaptic dynamics to an instantaneous and voltage independent shift in the voltage variable. If the considered intrinsic dynamics is slow with respect to the synaptic dynamics, and if the membrane voltage stays in a narrow range with respect to the distance from the synaptic reversal potential, this approximation is reasonable. The model trajectories have been calculated with iterative formulae (see the Appendix).

3.3 Results

3.3.1 Conductance-based model

We show that n-tuples of spikes with the same average frequency can elicit different response patterns depending upon the precise temporal structure of the n-tuples. For visualization purposes triplets of spikes were considered. Fig. 3.2 shows the input-output preference relationship for increasing values of the injected current in the Gutfreund model neuron. The neuron was set at its only stable point, and its response to triplets with different ISIs was considered.

Each triplet of spikes (t_1, t_2, t_3), corresponding to a pair of ISIs $(t_2 - t_1, t_3 - t_2) =$

(ISI_1,ISI_2), is represented with a different colour depending upon the output pattern it produced (see colorbar). In particular, we use shades of blue for input triplets that only elicited one postsynaptic spike, shades of green for input triplets that elicited two postsynaptic spikes, and red for input triplets that elicited three postsynaptic spikes, one in response to each of the incoming EPSPs. Different shades of blue and green indicate different output patterns (see colorbar). For example, light blue indicates triplets that resulted in only one postsynaptic spike, which occurred in response to the first EPSP (between the first and the second EPSPs); light green indicates triplets that resulted in two postsynaptic spike, which occurred in response to the second and third EPSP. Since more than one postsynaptic spike can be produced in this setting, the input-output preference relationship to triplets of spikes that we present here is not only shaped by the subthreshold ionic properties of the model neuron, but also by its refractoriness.

For low synaptic efficacies, only triplets with a sufficiently short ISI_1 or ISI_2 can elicit a spike, thus the neuron acts mainly as an integrator (Fig. 3.2A). Nevertheless specific values for ISI_1 can prevent the neuron from firing in response to the third spike, unless ISI_2 is very short (excitation-induced depression).

As g_{Syn} is raised to $0.27nS$ (Fig. 3.2B), two new regions of preference in the (ISI_1,ISI_2) plane appear: the first corresponds to a resonant ISI_1 which results in a postsynaptic spike after the second input pulse (middle blue vertical stripe); the second corresponds to a resonant ISI_2, which results in a postsynaptic spike after the third input pulse (dark blue horizontal stripe). Note that if ISI_1 is included in a certain region around $18ms$, the resonant region in ISI_2 disappears and a postsynaptic spike is obtained only for very short ISI_2 (excitation-induced depression). The intersection between the horizontal and vertical regions of preference, corresponding to a resonant ISI_2 or ISI_1, respectively, result in light green regions of preference, indicating suprathreshold responses to both the second and the third EPSPs. Note, though, that the contours of the horizontal regions of preference (thus determined by ISI_2) are modulated by ISI_1, reflecting a fine history-dependence of the input-output dynamics. In particular, the ISI_2 coordinate in the light green region depends on whether the first postsynaptic spike was produced by a short ISI_1 or a resonant ISI_1, being slightly shorter in the former case.

Figure 3.2C shows the input-output preference relationships for $g_{Syn} = 0.28nS$, a value of the synaptic conductance which results in a postsynaptic spike in response to a single EPSP. In this case, the neuron entrains 1:1 to the presynaptic input pattern if it is com-

posed of ISIs close to its intrinsic period of oscillation ($\sim 40ms$), or sufficiently long to bypass any refractory effect (ISI$\lesssim$30 ms), or inhibitory effects due to anti-resonant intervals (52ms$\lesssim$ISI$\lesssim$68ms). For input ISIs which interact with neuronal dynamics, a complex description of input-output mapping emerges, where EPSPs might or might not be transmitted depending upon the previous input-output history. In particular, certain EPSPs are blocked (they do not result in a postsynaptic spike) depending upon a complex interplay between refractoriness and subthreshold damped oscillations, which result in excitation-induced inhibition for certain input timing.

For even higher values of g_{Syn}, the region of 1:1 entrainment broadens in the (ISI_1,ISI_2) plane. For high enough values of the synaptic efficacy, inhibitory effects due to anti-resonant input intervals are overcome and 1:1 entrainment is lost only for short ISI_1 or ISI_2, because of refractoriness.

3.3.2 Linear model with after-spike reset

Similar results can be obtained with the GIF model. In this model, the effects of refractoriness can be reproduced by an appropriate choice for V_{reset} and t_{thr}. In Fig. 3.3, we show the same kind of input-output preference relationships as in Fig. 3.2, for different values of the after-spike parameters V_{reset} and t_{thr}. Some of the features observed in the Gutfreund model are recovered in this simple, linear model with after-spike reset. In particular, we can observe the neuron preference for short ISIs only when the synaptic efficacy is weak, and the appearance of horizontal (vertical) stripes of preference corresponding to a resonant ISI_2 (ISI_1) when the synaptic efficacy is increased. We also observe excitation-induced inhibition when $ISI_1 \sim 1.6$, about half of the neuron intrinsic period π. Some history-dependent modulation of the postsynaptic response to ISI_2 is also observed, but it is more simple than in the Gutfreund neuron due to the few time scales involved in the GIF dynamics.

In this model, the values of ISI_2 which will result in a second postsynaptic spike (light green regions) also depends on whether the first postsynaptic spike was produced by a short ISI_1 or a resonant ISI_1. Contrary to the Gutfreund model, they are slightly longer in the former case, at least for the range of parameters we considered. The refractory parameters V_{reset} and t_{thr} affect the regions in the (ISI_1,ISI_2) plane which correspond to two or more postsynaptic spikes, and can be tuned in order to recover the input-output preference relationships of living neurons or more realistic neuron models. In particular, if $V_{reset} =$

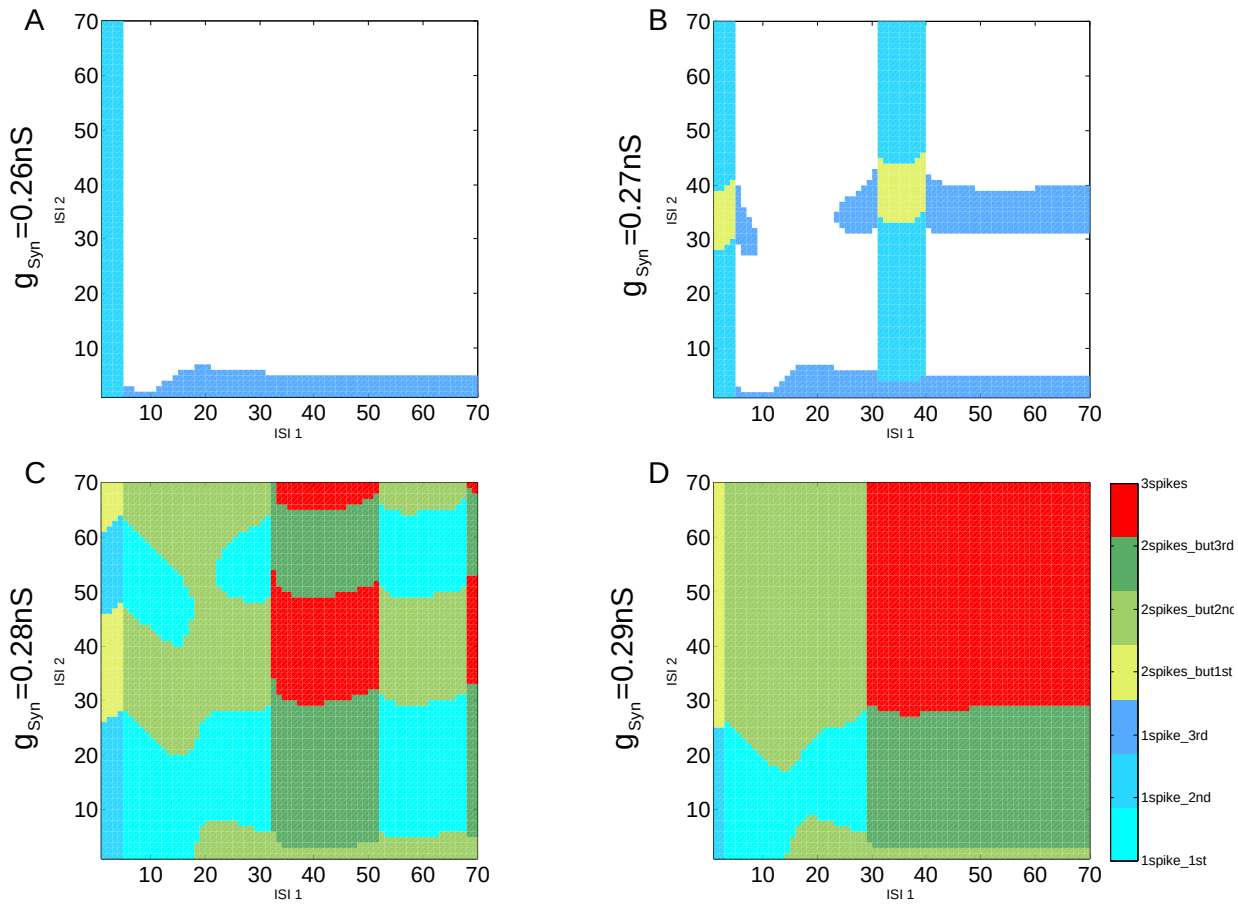

Figure 3.2: Input-output preference relationship for the Gutfreund model neuron. Coloured cells correspond to triplets of spikes that fire the neuron. Different colours correspond to different output responses (see colorbar and main text for details). ISIs are expressed in milliseconds. Panels A, B, C and D depict the preference relation for increasing values of the synaptic efficiency g_{Syn}: $0.26nS$, $0.27nS$, $0.28nS$, $0.29nS$ respectively.

$t_{thr} = 0$, the neuron doesn't show refractory properties in response to suprathreshold inputs and will entrain 1:1 to arbitrarily high input frequencies.

3.4 Discussion

This chapter shows how complex input-output relationships can arise even in a very simple neuronal model: a triplet of inputs with a certain average frequency can elicit a postsynaptic spike, or not, depending upon the precise temporal structure of the triplet, as well as upon the amplitude of each of the inputs. This input-output preference relationship depends upon the parameters of the model neuron. Hence in the context of a network of such neurons with a certain distribution of parameters, a presynaptic spike train can

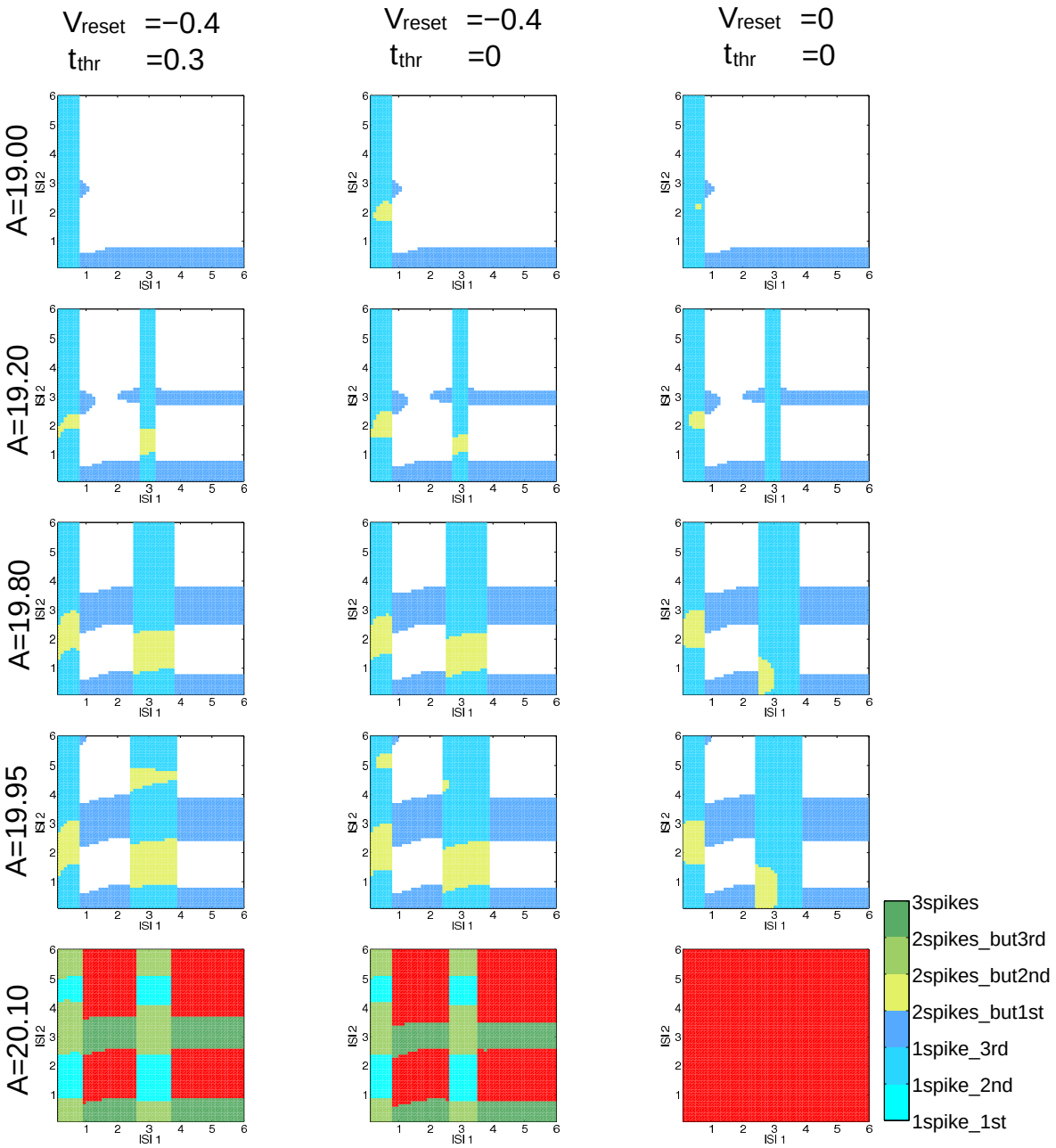
Vreset =−0.4
tthr =0.3
Vreset =−0.4
tthr =0
Vreset =0
tthr =0
A=19.00
A=19.20
A=19.80
A=19.95
A=20.10
ISI 1
ISI 2
3spikes
2spikes_but3rd
2spikes_but2nd
2spikes_but1st
1spike_3rd
1spike_2nd
1spike_1st

elicit spikes in a different postsynaptic cell at different times (Izhikevich et al., 2003a), thus translating a temporal code into a spatiotemporal or purely spatial code. This observation is highly relevant in the context of large networks describing different layers of information processing. In the context of signal propagation, for instance, a large scale network of model neurons with different subthreshold dynamics might display signal propagation to one or another region of the network depending on the temporal structure of the external signal, or could convey different information to different regions. Recent modeling results have shown that neural signatures, i.e. cell-specific interspike interval distributions, can be part of a multicoding strategy of bursting neurons (Latorre et al., 2006). The model presented in this chapter can distinctively react as a reader of these neural signatures.

This study focuses on intrinsic neuronal dynamics and neglects the realistic dynamics of synaptic transmission. Since the frequency of subthreshold oscillations depends upon oscillation amplitude, the input-output temporal preference relationship outlined above is expected to change when short term plasticity is added to the synapses. Synaptic conductances modeled as instantaneous current pulses do not alter the phase portrait of the system but only shift the current phase point to the right along the V axis; obviously the inclusion of more realistic synaptic dynamics, with time constants comparable to ion channels kinetics, would lead to more complicated input-output relationships. Furthermore, in the GIF neuron the dynamics of after-spike refractoriness and subthreshold oscillations do not interact in a realistic fashion. In a real cell, after-spike effects are expected to affect subthreshold dynamics in a complex way, which is shaped by the spatial distribution of fast Na^+ and K^+ channels, underlying the generation of action potentials, and the slower channels mediating I_{NaP} and I_{Ks} which are responsible for slow subthreshold oscillations. These issues will be addressed in spatially extended models and through experimental work. However we proved that a simple, linear neuron with subthreshold damped oscillations and after-spike reset has the computational capabilities for implementing the well known noncommutative summation observed experimentally (Segundo et al., 1963).

Many neural systems encode sensory information using a small number of simulta-

---

Figure 3.3 *(facing page)*: Input-output preference relationship for the GIF model neuron. Color code as in 3.2. ISIs are expressed in arbitrary units. Different columns represent model neurons with different refractory properties. Efficacies of EPSPs increase along rows.

neously active neurons. In fact many areas of the brain are surprisingly very sparsely active (Shoham et al., 2006). One of the proposed explanations to silent neural systems is the presence of sparse stimulus selectivities, i.e. smart neurons that only respond to very specific stimuli (Olshausen and Field, 2004). In this chapter we have explained a simple dynamical mechanism for these preferred input-output relationships.

3.5 Appendix

3.5.1 Integration of the GIF model

The differential equations describing the GIF model can be solved analytically given the initial conditions of the dynamical variables. In the absence of synaptic input ($I_{syn} = 0$), the subthreshold dynamics (3.1) has as a general solution

$$\vec{s}(t) = \mathrm{e}^{-\mu t}(c_1 \mathrm{e}^{i\omega t}\vec{u}_1 + c_2 \mathrm{e}^{-i\omega t}\vec{u}_2) \tag{3.2}$$

where $\mu = \frac{\alpha+1}{2}$ and $\omega = \frac{\sqrt{4\beta-(1-\alpha)^2}}{2}$. The parameter μ determines the membrane time constant, while the parameter ω is the oscillation frequency (in 1/rad), related to the intrinsic period of oscillations $T = \frac{2\pi}{\omega}$. We chose to fix μ at a physiological value ($\mu = 1$). With this choice, $\omega = \sqrt{\beta}$.

The coefficients c_1 and c_2 depends on the initial conditions and can be easily derived analytically. Considering that $\vec{u}_1 = \begin{pmatrix} 1+\lambda_1 \\ 1 \end{pmatrix}$ and $\vec{u}_2 = \begin{pmatrix} 1+\lambda_2 \\ 1 \end{pmatrix}$ are eigenvectors of the system (3.1) associated with the eigenvalues $\lambda_1 = -\mu + i\omega$ and $\lambda_2 = -\mu - i\omega$, respectively, by evaluating (3.2) at $t = 0$ and projecting on the v and w axis one obtains:

$$\begin{aligned} v_0 &= c_1(1+\lambda_1) + c_2(1+\lambda_2) \\ w_0 &= c_1 + c_2 \end{aligned}$$

where v_0 and w_0 are the general initial conditions for the voltage and the slow variable at $t = 0$. By solving for c_1 and c_2 and substituting $\mathrm{e}^{i\omega} = \cos(\omega) + i\sin(\omega)$ one obtains the following expressions for the free evolution of the system (3.1) given the initial condition (v_0, w_0):

$$
\begin{aligned}
v(t) &= \mathrm{e}^{-\mu t}\left(v_0\cos(\omega t) + \frac{v_0(1-\mu) - w_0(1-2\mu+\mu^2+\omega^2)}{\omega}\sin(\omega t)\right) \\
w(t) &= \mathrm{e}^{-\mu t}\left(w_0\cos(\omega t) + \frac{v_0 - w_0(1-\mu)}{\omega}\sin(\omega t)\right)
\end{aligned}
\tag{3.3}
$$

Hence, if we model the EPSPs as instantaneous pulses along the v axis, it is possible to compute analytically the response to a train of presynaptic pulses. The response of the model neuron to a train of synaptic events at times $(t_0^s, t_1^s, \ldots, t_{n-1}^s)$ can be calculated by iterating the following map:

- if $v_{i-1}+A < V_{thr}$ (EPSP is subthreshold), (v_i, w_i) are given by (3.3) with $v_0 = v_{i-1}+A$, $w_0 = w_{i-1}$, $t = \mathrm{ISI_i}$
- else (EPSP is suprathreshold), (v_i, w_i) are given by (3.3) with $v_0 = V_{reset}$, $w_0 = V_{reset} + (w_{i-1} - V_{reset})\mathrm{e}^{-t_{thr}}$, $t = \mathrm{ISI_i} - t_{thr}$

for $i = 1, \ldots, n-1$, where $\mathrm{ISI}_i = t_i^s - t_{i-1}^s$, A is the synaptic strength (assumed to be equal among synaptic events), and (v_i, w_i) are the dynamical variables just before the arrival of the synaptic event at time t_i^s. The voltage variable after the last spike of the train is calculated as

$$v_n = (v_{n-1} + A)$$

In all our simulations we set the initial conditions at the rest state ($v_0 = 0, w_0 = 0$).

Chapter 4

History-dependent excitability as a single-cell substrate of transient memory for information discrimination

Abstract

In the previous chapter we showed how intrinsic neuronal properties, and in particular subthreshold damped oscillations, result in a complex mapping between trains of input pulses and postsynaptic spiking patterns. In particular, we showed how each input pulse affects the neuron state, and will result in temporal windows of opportunity when the neuron will be more excitable, that is, more likely to generate an action potential. The extent and position in time of these windows depend upon the intrinsic dynamical properties of the cell. In this chapter, we intend to explore in a systematic manner how intrinsic neuronal properties in the subthreshold regime shape neuronal responsiveness as a function of the previous input-output history. Neurons react differently to incoming stimuli depending upon their previous history of stimulation. This property can be considered as a single-cell substrate for transient memory, or context-dependent information processing. We propose a formal definition of neuronal excitability as a measure of the propensity to firing in any moment in time, linking the subthreshold history-dependent dynamics with spike generation. This definition allows the quantitative assessment of the intrinsic memory for different single-neuron dynamics and input statistics. We illustrate the concept of history-dependent excitability by considering two general dynamical mechanisms: the passive behavior of an Integrate and Fire (IF) neuron, and the inductive behavior of a Generalized Integrate and Fire (GIF) neuron with subthreshold damped oscillations. This framework allows us to characterize the sensitivity of different model neurons to the detailed temporal structure of incoming stimuli. While a neuron with intrinsic oscillations discriminates equally well between input with the same or different frequency, a passive neuron discriminates better between inputs with different frequencies. This suggests that passive neurons are better suited to rate-based computation, while neurons with subthreshold oscillations are advantageous in a temporal coding scheme. We also address the influence of intrinsic properties in single-cell processing as a function of input statistics, and show that intrinsic oscillations enhance discrimination sensitivity at high input rates. Finally, we discuss the generality of this concept and its application to the study of information discrimination in more complex models and living neurons.

Keywords: intrinsic neuronal dynamics, transient memory, subthreshold oscillations.

4.1 Introduction

Since the beginnings of electrophysiology it has been observed that neuronal firing rate in sensory systems carries information about the presented stimulus (Cooper and Adrian, 1923; De Valois et al., 1962). Still, it has long been recognized that the exact timing of neural firing carries additional information beyond that provided by the mean firing rate. Spike latencies among synchronously active neuronal assemblies have been demonstrated to be highly informative in many sensory and motor systems (see, for example, (Meister et al., 1995; deCharms and Merzenich, 1996; Wehr and Laurent, 1996; Ikegaya et al., 2004)). In addition to electrophysiological studies based on a stimulus-response paradigm, precisely timed spiking patterns have also been observed in the spontaneous activity of a variety of preparations (Luczak et al., 2007; Mao et al., 2001; Cossart et al., 2003). In particular, the observation of precise temporal structures in the activity of cultured slices (Beggs and Plenz, 2003, 2004) suggests their emergence from a self-organized process (Beggs, 2008; Plenz and Thiagarajan, 2007). While these results might not apply universally in the nervous system (Oram et al., 1999; Baker and Lemon, 2000; Johnson and Buonomano, 2007), they are clearly advocating for an important role of precisely timed activity in neural network processing.

The higher information capacity offered by precisely timed firing patterns is likely to be exploited by the nervous system, given that neurons are sensitive to the exact timing of applied stimuli (Ripley and Wiersma, 1953; Segundo et al., 1963), and muscle contraction depends upon the temporal pattern of activity of its innervating motoneurons (Wiersma and Adams, 1950; Zhurov and Brezina, 2006). Nevertheless the dynamical mechanisms underlying the sensitivity to temporally structured inputs are not completely understood.

Many biophysical mechanisms have been proposed as feasible candidates in decoding a temporal code. At the network level, a combination of delay lines (possibly tuned by STDP[1]) and an array of coincidence detectors allow the recognition of certain sequences of ISIs[2] (Hooper, 1998; Abarbanel and Talathi, 2006). At the single-cell level, the interplay between short-term synaptic dynamics and intrinsic neuronal oscillations results in selective transmission of input bursts with a frequency content that matches the synaptic and intrinsic filtering properties (Izhikevich et al., 2003b).

[1]Spike Timing-Dependent Plasticity
[2]Inter Spike Intervals

When dealing with temporally selective neuronal mechanisms, most attention has been drawn on the role of short-term synaptic dynamics (Thomson and Deuchars, 1994; Tsodyks and Markram, 1997; Abbott et al., 1997), based mostly upon mechanisms of vesicle depletion and replenishment which in turn depend upon several pre and post synaptic factors (for reviews see (Zucker and Regehr, 2002; Kavalali and Ege, 2007)). In particular, it has been shown how the random but not independent synaptic transmission between subsequent synaptic event conveys information (in the formal sense of uncertainty reduction) about the timing of previous presynaptic spikes (Fuhrmann et al., 2002; Kleppe and Robinson, 2006).

The present study focuses on the other side of the engram (Zhang and Linden, 2003), that is, on the history-dependent processing capabilities offered by intrinsic neuronal dynamics. These include ion channels activation - inactivation kinetics, intracellular second messenger processes involving calcium up-take and release from intracellular stores, and in general any non-synaptic neuronal process that could possibly alter the cell's excitability or input-output mapping.

The last decades have seen a renewed interest in intrinsic neuronal properties, and in particular in intrinsic oscillations (Llinas, 1988; Hutcheon and Yarom, 2000). Most of this interest has been motivated by the interplay between intrinsic properties and synaptic connectivity in the generation of network oscillations, a widespread phenomenon in the nervous system which has been correlated with several physiological and cognitive processes (Buzsaki, 2006). A more theoretical line of research has focused on intrinsic oscillations as a neuronal band-pass filtering mechanism (Richardson et al., 2003; Schreiber et al., 2004), although most of these studies focused on a rate-coding perspective and missed the potentially important role of intrinsic oscillations in a temporal coding scheme.

Indeed, intrinsic oscillations shape the input-output relationship of single neurons (Baroni and Varona, 2007). For example, a certain neuron will respond to a train of synaptic events in a way that depends upon the precise temporal structure of the input train and upon the neuron's intrinsic properties. This study investigates more deeply into the relationship between intrinsic single-cell properties (in particular, intrinsic oscillations) and the encoding - decoding of a temporal code.

In any moment in time, a neuron carries information about its history of stimulation through its dynamical variables. In particular, the history-dependence of ion channel

dynamics has long been recognized as a single-cell substrate for transient memory (Turrigiano et al., 1996; Marder et al., 1996; Egorov et al., 2002; Nayak and Sikdar, 2007; Winograd et al., 2008). Certain specific ionic currents have been considered as molecular basis for single-cell memory, due to their slow dynamics of activation or inactivation, or the complex temporal profile of their responses (Nayak and Sikdar, 2007; Turrigiano et al., 1996; Winograd et al., 2008). The interplay between calcium influx (through synaptic and voltage-gated channels) and its diffusion and exchange through intracellular stores has also been suggested as a candidate mechanisms for single-cell memory (Loewenstein and Sompolinsky, 2003; Teramae and Fukai, 2005). The positive feedback required for persistent activity can also be provided by a slow excitatory synapse of a neuron onto itself, i.e. an autapse (Seung et al., 2000). Nevertheless, the context-dependent computational capabilities of neurons might be better understood when all the intrinsic neuronal processes that influence its excitability are taken into account, and represented in a dynamical system framework. In the case of a biological neuron, the dynamical processes involved are very diverse in nature and span several time scales, from few milliseconds in the case of fast ion channels' activation-inactivation kinetics, until days or months in the case of neurite growth and protein synthesis. Computational models are extremely useful in taming the enormous complexity arising from such a picture, allowing the theoretical measurement of the discrimination capabilities of simple dynamical mechanisms which are general to several neuron classes.

In this chapter we present a formal measure of the neuron's state directly related to spike generation, namely the intrinsic excitability, which lumps the different history-dependent dynamical variables of an arbitrary model neuron to a single, scalar value that describes its propensity to firing in any moment in time. This dynamical mnemonic trace allows the interpretation of newly incoming information in the context of the previously received inputs, and hence the discrimination of information at the single-cell level. The comparison between the excitability trajectories arising from different input histories quantifies the intrinsic discrimination capabilities of single neurons, and their dependence upon the input statistics and the neuronal dynamics.

Since different physiological processes can yield similar dynamical effects, it is useful to consider general, dynamical neuronal models which abstract from the specific molecular mechanisms involved. In particular, we illustrate the concept of intrinsic excitability with two very general dynamical mechanisms: the RC behavior of a passive membrane, captured

by a simple Integrate and Fire model, and the inductive RLC behavior of a neuron with a resonant current, described in its simplest (linear) form by a Generalized Integrate and Fire model (see Methods). These models are based on analogies with linear electric circuits, a formalism with a long and successful history in the phenomenological characterization of neuronal dynamics (for some early examples, see (Lapicque, 1907; Hill, 1936; Cole, 1932, 1941)).

Before particularizing our analysis to these two simple cases, in the next section we will present a general mathematical framework that allows the quantitative assessment of the history-dependent modulation of intrinsic excitability for arbitrary neuron models.

4.1.1 History-dependent excitability

In the most general mathematical framework a neuron is described as a dynamical system:

$$\frac{d\vec{x}}{dt} = \vec{f}(\vec{x}, I_{syn})$$

where I_{syn} is the sum of all synaptic currents flowing through the neuron's membrane. Every synaptic event will move the current phase point according to the intrinsic and synaptic dynamics, while in between synaptic events, the phase point will evolve according to the intrinsic dynamics only. Since the outcome of a synaptic event depends upon the intrinsic state vector $\vec{x}(t_i^s)$ at the time of the event, and $\vec{x}(t_i^s)$ depends upon the state at the time of the previous synaptic event $\vec{x}(t_{i-1}^s)$ and the time between events $t_i^s - t_{i-1}^s$, the neuron acts as a dynamic encoder of its stimulus history. That is, the neuron state vector will reflect the previous history of stimulation, and will itself determine the following evolution of the neuron as a dynamical system. This property is particularly suited for the encoding of precisely timed stimuli. In this chapter we analyze how the specific form of the system vector field $\vec{f}$ will determine the computational characteristics of the dynamic encoding mechanism, such as its efficiency in the presence of noise and its sensitivity to particular features of the input.

The neuron's state vector $\vec{x}$ encodes stimulus history in an implicit way: the actual values of the dynamical variables are unknown, both to the experimenter and to other neurons in the network. Their values can only be indirectly inferred through their influence on membrane potential or intracellular calcium (the main physiological quantities directly

measurable though standard experimental techniques) and, in particular, on spiking activity.

On the other hand the state vector $\vec{x}$, containing all relevant information about the neuron's dynamic state, directly affects the way the neuron responds to incoming stimuli. From the simplest point of view, input-output history modulates the neuron's excitability, or propensity to firing, as a function of time. More generally, input-output history can affect single-cell processing by varying the output repertoire a neuron can exhibit, for instance by augmenting the probability of short burst emission versus single spike emission in a certain time window. This phenomenon allows for history-dependent information processing: the neuronal input-output transformation is not a static map, but it is changing in time in a history-dependent manner. The influence of the past history on the current input-output transformation can be considered as a cell-based substrate for contextualization of information in the nervous system, or short-term memory (Marder et al., 1996).

Depending on the local context that the neuron 'sees' through the synapses impinging on it in the immediate past, it will differently treat the information it receives. As we will show in this chapter, this context-dependent processing is a very general property of dynamical systems and it can be presented in its simplest form with linear models such as the IF and GIF neuron models.

The state vector contains all relevant information about the dynamic state of the neuron, hence it can be used to predict the neuron's response to an arbitrary stimulus. Nevertheless, it is not easy to deal with directly. In a model neuron the state vector's dimensionality can be high, and obviously it depends upon the specific model considered, making the comparison between different neuron models difficult and somewhat arbitrary. In a real neuron the state vector depends upon the description level one wishes to adopt, and even when just a few channels' activation-inactivation kinetics are taken into account, it is impossible to measure experimentally. Hence, it is useful to introduce a lumped, functional and physiologically motivated measure of the neuron's state, directly related to spike generation. To this end we propose a formal definition of neuronal excitability at any moment in time as the minimal synaptic strength g_{thr} of an excitatory synaptic event that can make the neuron fire. This measure is obviously dependent upon the synaptic kinetics considered. In this work our focus is on intrinsic neuronal dynamics, hence we decided to adopt the simpler synaptic description: EPSPs[3] will be modelled as instantaneous, voltage-independent

[3]Excitatory Post Synaptic Potentials

shifts in the v variable, representing the membrane potential. Numerical simulations with more realistic models, i.e. conductance-based model neurons with exponentially decaying synaptic conductances, yield similar results. As we show in this chapter, the time evolution of neuronal excitability $g_{thr}(t)$ carries information not only about the intrinsic properties of the cell, but also about its input-output history.

4.2 Methods

4.2.1 Neuron models

The first neuron model we consider is the integrate and fire (IF), described by a single linear differential equation:

$$\frac{dv}{dt} = -\mu v + I_{syn} \tag{4.1}$$

The model is endowed with an after-spike reset mechanism, so that when v crosses a threshold v_{thr} from below a spike is emitted and the membrane potential is reset to a value v_{reset}, and kept there for a refractory time t_{refr}. Since this work focuses on subthreshold dynamics, the spike generation mechanisms is disregarded. In its normal form (where time has been properly scaled) this model is described by a single parameter μ, which is the rate of the exponential decay to the rest state in the absence of stimulation ($I_{syn} = 0$). The canonical IF model that we used for most of the chapter has a decay rate $\mu = 1$, but this parameter has been varied in the simulations represented in Figs. 4.3D,F; 4.4; 4.6B,E.

Another simple model that linearly describes the subthreshold dynamics, but with the addition of another dynamical variable w, is the Generalized Integrate and Fire (GIF) model, introduced in the previous chapter. The canonical GIF model that we used for most of the chapter has $\alpha = 1$ and $\beta = 4$, resulting in complex conjugate eigenvalues $-1 \pm 2i$, but these parameters have been varied in the simulations represented in Figs. 4.3D-F; 4.4; 4.6A,B,E,F; 4.7. Given the wide frequency range of intrinsic oscillations observed in mammalian brains, which spans at least two order of magnitude (from 0.5 Hz until 50 Hz (Hutcheon and Yarom, 2000)), we preferred to keep our models dimensionless.

As in the previous chapter, we considered instantaneous synapses

$$I_{syn} = \sum_{t_s} A\delta(t - t_s)$$

This approximation reduces the synaptic dynamics to an instantaneous and voltage independent shift in the voltage variable. If the considered intrinsic dynamics is slow with respect to the synaptic dynamics, and if the membrane voltage stays in a narrow range with respect to the distance from the synaptic reversal potential, this approximation is reasonable. The model trajectories have been calculated with iterative formulae, as in the previous chapter (see the Appendix therein).

4.2.2 Generation of random trains of synaptic events

In the simulations, random trains of synaptic events have been generated by concatenating two or more ISIs generated from an exponential distribution, using the Matlab routine "random". For each value of the ranged parameters, 1000 different trials have been simulated, and the corresponding results have been represented in Figs. 4.6C,D and 4.7. In each block of simulations the random number generator has been initialized with a different seed in order to avoid spurious correlations between the random realizations in different trials.

4.3 Results

4.3.1 Example of single-neuron discriminability in minimal models

Traditionally the detection capabilities of neurons have been assessed by observing how their output changes as a function of their input. For example, two stimuli are considered to be indistinguishable as long as they both result in a single postsynaptic spike, or in the lack of it. We show that this is not necessarily the case: two different input stimuli can still be distinguished if they bring the neuron to a different internal state, and hence change its response properties to future stimuli.

In the case depicted in Fig. 4.1, a GIF neuron with subthreshold damped oscillations (see Methods) receives one of two different input trains, comprising the same constituent ISIs, one long ISI_l and one short ISI_s (Fig. 4.1A). Both input trains evoke subthreshold

responses only, hence no differential information about the input history is delivered to other cells in the network. Importantly though, the information about which of the two input trains has been received is contained in the state variables immediately after the last spike of the train, and can be extracted from the subsequent free evolution of the state vector. The voltage v variable after the last spike of the train is almost identical for both inputs, because the internal variable w counteracts voltage changes, while in the IF neuron the input with increasing frequency evokes a greater depolarization (Fig. 4.1C). Nevertheless, the different histories result in different values of w, which in turn result in a history-dependent free evolution to the rest state (Fig. 4.1D): the v variable decreases smoothly and with a shallow, late sag after the (ISI_s,ISI_l) triplet, while it decreases more abruptly and with a deeper, earlier sag after the (ISI_l,ISI_s) triplet. The black line in Fig. 4.1A shows the correspondent evolution of the instantaneous intrinsic discriminability (a measure of the difference in the excitability trajectories, see next section for a formal definition), which increases and then decreases, showing a maximum at a certain time after the last input spike.

This history-dependent free evolution of the model neuron allows for spike-mediated discrimination between the two different histories by a synaptic event with proper time and amplitude: a presynaptic spike with a time and an amplitude indicated by the black filled diamond in Fig. 4.1A, upper panel, results in a postsynaptic spike after history (ISI_s,ISI_l), but only produces a subthreshold oscillation after history (ISI_l,ISI_s) (Fig. 4.1B). In this example the stimulus time has been chosen at the time of the maximal instantaneous discriminability between the two input histories, and its amplitude as the middle point between the two excitabilities g_{thr} at that time. However, any input that lies in the space between the two different excitability trajectories, corresponding to the two different input histories, can in principle (disregarding the effects of noise) discriminate between the two cases.

If the same input trains are delivered to an IF neuron with the same membrane time constant, they are still distinguishable but in this case the absolute difference between the two excitability trajectories decreases exponentially after the last spike of the train (Fig. 4.1C). Conversely, in the GIF model it first increases and then decreases, resulting in an optimal time for intrinsic discriminability.

For these linear models, we are able to derive analytical expressions for the discriminability between two input histories $\mathcal{H}_i$ and $\mathcal{H}_j$, which we will use extensively in the rest

of the chapter.

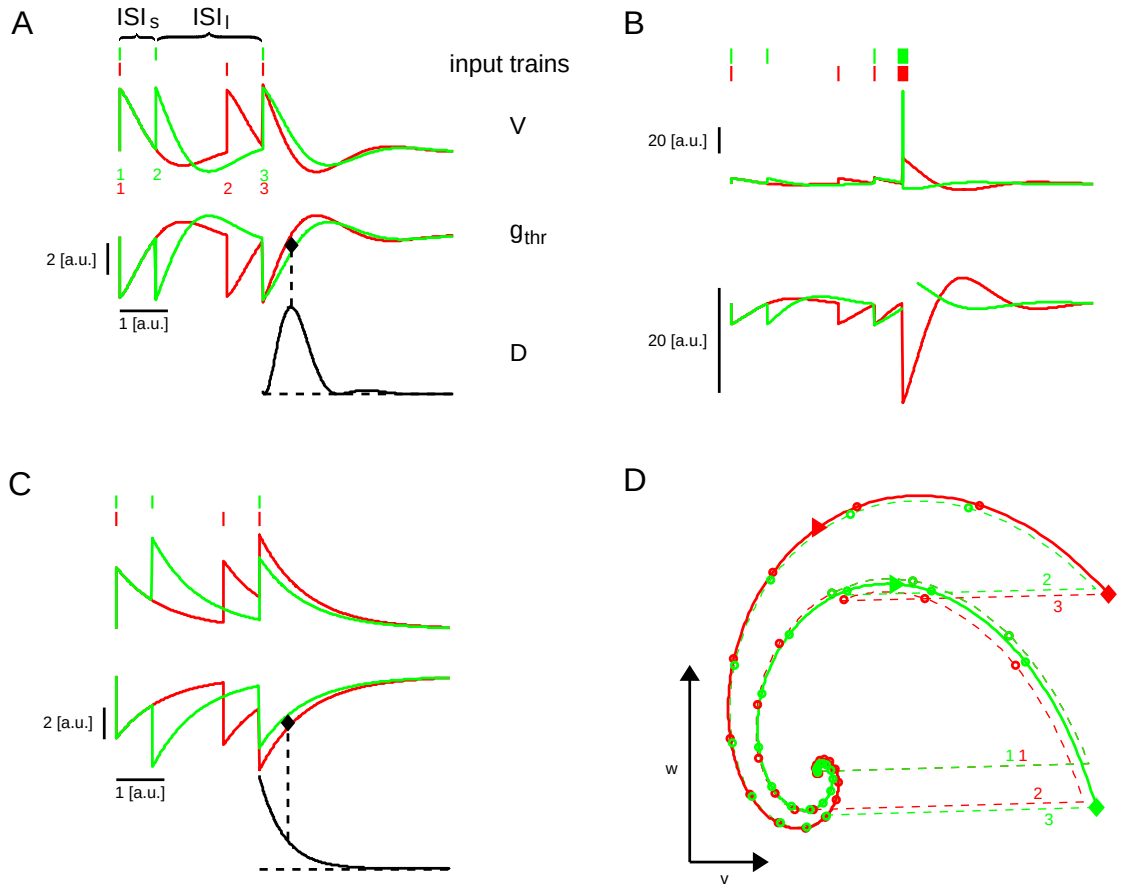

Figure 4.1: **Illustration of the history-dependent excitability concept.** Response of the GIF (A,B,D) and IF (C) model neurons to two different input trains, composed of the same ISIs. A: Voltage (top) and excitability (middle) trajectories arising from two different input trains (on top of the voltage traces). The instantaneous discriminability after the last spike of the train (black line) first increases and then decreases, resulting in an optimal time for discrimination based on intrinsic excitability (black diamond): a presynaptic spike with the strength and the timing indicated by the black diamond will be suprathreshold after the red input triplet, but subthreshold after the green input triplet. B: As in A, but with the addition of a fourth presynaptic spike with the timing and amplitude indicated by the black diamond in A. The intrinsic discriminability is not shown. C: The same as in A, for the IF model neuron. For a purely passive neuron, the intrinsic discriminability is an exponentially decreasing function of time. D: Trajectories in the phase plane (v, w) corresponding to the two input triplets in panel A. The trajectories are shown in dashed line before the last spike of the triplet, and in solid line after it. Circles are drawn every 0.25 u.t. A rightward triangle is drawn at the time of maximal discriminability (corresponding to the black diamond in A). Digits in A, D indicate the ordinal number of EPSPs in the train.

4.3.2 Instantaneous and cumulative discriminability

Living neurons *in vivo* typically receive a synaptic bombardment from thousands of presynaptic cells. It seems that the synaptic strengths of the inputs converging to a given neuron are not exponentially distributed, but might be better described by a log-normal distribution (Song et al., 2005): this corresponds to the presence of a few, strong inputs that emerge from a multitude of much weaker connections (Sherman and Guillery, 1998). The last observation, along with the fact that neurons are extremely sensitive to correlations in their inputs (Salinas and Sejnowski, 2001; Moreno et al., 2002), led us to our operational approximation.

In this study, we consider the linearization of the neuron's dynamics around its "working point", determined by its intrinsic properties and by the collective balance of the weak and asynchronous synaptic events it receives. The synaptic events will be considered as instantaneous, voltage-independent shifts in the v variable, representing the synchronous arrival of many weak EPSPs, or equivalently the synchronous arrival of a few strong EPSPs. Hence, we consider the synaptic kinetics to be much faster than the membrane time constant, or the resonant current activation rate (in the GIF model).

This approximation allows us to calculate the neuron's response to a train of presynaptic events with an iterative formula, and to calculate the discriminability based on intrinsic properties analytically (see Appendix). The discriminability between two input histories aims at measuring the difference in the corresponding evolutions of the intrinsic excitability. The most natural definition is then the square difference between the two excitability trajectories. In mathematical terms, we define the instantaneous discriminability between the input histories $\mathcal{H}_i$ and $\mathcal{H}_j$, resulting in the phase points (v_0^i, w_0^i) and (v_0^j, w_0^j) at time zero (which we set for convenience immediately after the last spike time of the input train), as

$$\mathcal{D}_{i,j}(t) = \left(g_{thr}^i(t) - g_{thr}^j(t)\right)^2 = \left(v^j(t) - v^i(t)\right)^2$$

where the last equality is due to the fact that in these linear models the firing threshold depends upon the voltage variable v only. Substituting the analytical solutions in the case of the IF and GIF models (see the Appendix for details) one obtains:

$$\mathcal{D}_{i,j}^{IF}(t) = \left(v_0^j - v_0^i\right)^2 \mathrm{e}^{-2\mu t}$$

$$\mathcal{D}_{i,j}^{GIF}(t) = \left(a\mathrm{e}^{\lambda_1 t} + b\mathrm{e}^{\lambda_2 t}\right)^2$$

where μ is the leak conductance in the IF model; λ_1 and λ_2 are the eigenvalues of the GIF model, and a and b are coefficients that depend upon the model parameters and upon the difference in initial conditions $\Delta v_0 = v_0^j - v_0^i$ and $\Delta w_0 = w_0^j - w_0^i$.

In the case of an IF neuron the instantaneous discriminability is an exponentially decreasing function of time, meaning that the intrinsic memory about the previous history will quickly vanish, and practically be lost after a few membrane time constants. In the case of a GIF model with real eigenvalues, the picture does not differ much, with the exception that now the exponential decay is governed by more than one time constant. In the case of a GIF model with intrinsic oscillations, that is a GIF model with complex conjugate eigenvalues $\lambda_{1,2} = -\mu \pm i\omega$, the instantaneous discriminability can be written more conveniently as

$$\mathcal{D}_{i,j}^{GIF}(t) = \mathrm{e}^{-2\mu t}\left(\frac{a^2+b^2}{2} + \frac{a^2-b^2}{2}\cos 2\omega t + ab\sin 2\omega t\right)$$

In this case, the instantaneous discriminability is an exponential decreasing function of time multiplied by a sinusoid. This means that for certain input histories $\mathcal{H}_i$ and $\mathcal{H}_j$, the maximal instantaneous discriminability can be achieved for times greater than zero, as in the example shown in Fig. 4.1.

The instantaneous discriminability is a measure of the square difference between two excitability trajectories originating from two input histories $\mathcal{H}_i$ and $\mathcal{H}_j$ in any moment in time. Its integral in time from zero to $+\infty$, which we call cumulative discriminability, is a measure of the information about the discriminability between the two histories $\mathcal{H}_i$ and $\mathcal{H}_j$ that could be gathered by observing the instantaneous discriminability for an infinite amount of time. This measure can be geometrically interpreted as the square area between any two excitability trajectories like those depicted in Fig. 4.1.

$$\mathcal{D}_\infty(i,j) = \int_0^\infty \left(g_{thr}^i(t) - g_{thr}^j(t)\right)^2 dt \tag{4.2}$$

After some analytical calculations (see Appendix for details) we get

$$\mathcal{D}_{\infty}^{IF}(i,j) = \frac{(v_0^j - v_0^i)^2}{2\mu}$$

$$\mathcal{D}_{\infty}^{GIF}(i,j) = -\frac{\lambda_1\lambda_2(A+B)^2 + (A\lambda_2 + B\lambda_1)^2}{2\lambda_1\lambda_2(\lambda_1+\lambda_2)}$$

If λ_1 and λ_2 are complex conjugate we can write the last expression as

$$\mathcal{D}_{\infty}^{GIF}(i,j) = \frac{a^2+b^2}{4\mu} + \frac{\mu(a^2-b^2)+2\omega ab}{4(\mu^2+\omega^2)}$$

For both models the cumulative discriminability is a quadratic function of the difference in the state variables at time zero.

It can now be appreciated that the discriminability between two input histories $\mathcal{H}_i$ and $\mathcal{H}_j$ depends on the one hand upon the free evolution from the difference in initial conditions $(\Delta v_0, \Delta w_0)$, and on the other hand upon the encoding properties of the model neuron, that is, upon how the phase point $(\Delta v_0, \Delta w_0)$ depends upon the input histories.

In our analysis we considered two different measures of the intrinsic discriminability: the cumulative discriminability and the maximal instantaneous discriminability. We did not find important differences between these measures, hence we present our results using the cumulative discriminability (which we will denote simply as $\mathcal{D}$) for its analytical simplicity.

4.3.3 Discriminability between pairs of input trains

If the input history to a neuron can be considered as a sum of stereotypical synaptic potentials, discriminability between pairs of input trains can be computed analytically in a straightforward manner for the linear models considered in this study. If input history $\mathcal{H}_i$ is composed of synaptic potentials evoked at times $t_1^i, t_2^i, ..., t_{n_i}^i$, with $t_1^i \leq t_2^i \leq ... \leq t_{n_i}^i = 0$ (without loss of generality we set the time reference at the last spike of the input train), the intrinsic discriminability between $\mathcal{H}_i$ and $\mathcal{H}_j$ can be written as

$$\mathcal{D}(i,j) = \int_0^{\infty} \left(\sum_{h=1}^{n_i} k(t - t_h^i) - \sum_{h=1}^{n_j} k(t - t_h^j) \right)^2 dt$$

where $k(t)$ is the PSP kernel, reflecting the interplay between intrinsic and synaptic properties. Hence, the only input spikes which play a role in the intrinsic discriminability are those that do not occur simultaneously in the input histories $\mathcal{H}_i$ and $\mathcal{H}_j$. An instructive example is when the two input trains are equal in the number of spikes they are made of ($n_i = n_j$), and in the spike times of each of their constituent events, except one. In this case, the previous expression reduces to

$$\mathcal{D}(i,j) = \int_0^\infty \left(k(t-t_i) - k(t-t_j)\right)^2 dt \tag{4.3}$$

where we reindexed the spike times for simplicity. In this work our focus is on intrinsic neuronal dynamics, hence we describe synaptic potentials as instantaneous shifts in the voltage variable. In this case the PSP kernels for the IF and GIF neurons are (see Appendix for details)

$$k_{IF}(t) = A\mathrm{e}^{-\mu t}\mathrm{H}(t)$$

$$k_{GIF}(t) = A\mathrm{e}^{-\mu t}\left(\cos(\omega t) + \frac{1-\mu}{\omega}\sin(\omega t)\right)\mathrm{H}(t)$$

with $\mathrm{H}(t)$ being the Heaviside functions, ensuring causality. Substituting the above expressions in (4.3) yields:

$$\mathcal{D}_{IF}(i,j) = \frac{A^2}{2\mu}\left(\mathrm{e}^{\mu t_i} - \mathrm{e}^{\mu t_j}\right)^2 \tag{4.4}$$

$$\begin{aligned}
\mathcal{D}_{GIF}(i,j) = \frac{A^2}{4\mu\omega^2\left(\mu^2+\omega^2\right)}\Big(&\left(\mathrm{e}^{2t_i\mu} + \mathrm{e}^{2t_j\mu}\right)\left((-1+\mu)^2+\omega^2\right)\left(\mu^2+\omega^2\right) - \\
&\mathrm{e}^{2t_i\mu}\mu\left((-1+\mu)^2\mu + (-2+\mu)\omega^2\right)\cos(2t_i\omega) - \\
&\mathrm{e}^{2t_j\mu}\mu\left((-1+\mu)^2\mu + (-2+\mu)\omega^2\right)\cos(2t_j\omega) - \\
&2\mathrm{e}^{(t_i+t_j)\mu}\Big(-\mu\left((-1+\mu)^2\mu + (-2+\mu)\omega^2\right)\cos((-t_i-t_j)\omega) + \\
&\left((-1+\mu)^2+\omega^2\right)\left(\mu^2+\omega^2\right)\cos((t_i-t_j)\omega) - \\
&\mu\omega\left(-1+\mu^2+\omega^2\right)\sin((-t_i-t_j)\omega)\Big) + \\
&\mu\omega\left(-1+\mu^2+\omega^2\right)\left(\mathrm{e}^{2t_i\mu}\sin(2t_i\omega) + \mathrm{e}^{2t_j\mu}\sin(2t_j\omega)\right)\Big)
\end{aligned} \tag{4.5}$$

Since we are considering linear neuron models, these results also hold if the inputs are composed of the sum of the input trains considered above, plus any term which is equal among different input histories. This situation comprises a number of illustrative cases, which we detail below.

Intrinsic discriminability between input pairs

Let input history $\mathcal{H}_i$ be composed of a pair of synaptic potentials evoked at times $t_1^i \leq t_1^i + \mathrm{ISI_i} = t_2^i = 0$, and input history $\mathcal{H}_j$ at times $t_1^j \leq t_1^j + \mathrm{ISI_j} = t_2^j = 0$. In this case the intrinsic discriminability is given by expressions (4.4) and (4.5), substituting $t_i = -\mathrm{ISI_i}$, $t_j = -\mathrm{ISI_j}$.

Intrinsic discriminability between input triplets with the same total duration

Let input history $\mathcal{H}_i$ be composed of a triplet of synaptic potentials evoked at times $t_1^i \leq t_1^i + \mathrm{ISI_1^i} = t_2^i \leq t_2^i + \mathrm{ISI_2^i} = t_3^i = 0$, and input history $\mathcal{H}_j$ at times $t_1^j = t_1^j \leq t_1^j + \mathrm{ISI_1^j} = t_2^j \leq t_2^j + \mathrm{ISI_2^j} = t_3^j = 0$. In this case the intrinsic discriminability is given by expressions (4.4) and (4.5), substituting $t_i = -\mathrm{ISI_2^i}$, $t_j = -\mathrm{ISI_2^j}$.

Intrinsic discriminability between input trains that only differ in the their second spike time

Let input history $\mathcal{H}_i$ be composed of a train of synaptic potentials evoked at times $t_1^i \leq t_2^i \leq ... \leq t_n^i = 0$, and input history $\mathcal{H}_j$ at times $t_1^j = t_1^j \leq t_2^j \leq t_3^j = t_3^j \leq ... \leq t_n^j = 0$, with $\mathrm{ISI_k^{(i,j)}} = t_{k+1}^{(i,j)} - t_k^{(i,j)}$ for $k = 1, ..., n-1$. Let T be the total duration of the input trains: $T = \sum_{k=1}^{n-1} \mathrm{ISI_k^i} = \sum_{k=1}^{n-1} \mathrm{ISI_k^j}$. In this case the intrinsic discriminability is given by expressions (4.4) and (4.5), substituting $t_i = -T + \mathrm{ISI_1^i}$, $t_j = -T + \mathrm{ISI_1^j}$:

$$\mathcal{D}_{IF}(i,j) = \frac{A^2}{2\mu} \mathrm{e}^{-2\mu T} \left(\mathrm{e}^{\mu \mathrm{ISI_1^i}} - \mathrm{e}^{\mu \mathrm{ISI_1^j}} \right)^2$$

$$\mathcal{D}_{GIF}(i,j) = \frac{A^2}{4\mu\omega^2\left(\mu^2+\omega^2\right)} \mathrm{e}^{-2\mu T} \Big(\Big(\mathrm{e}^{2\mathrm{ISI}_1^{\mathrm{i}}\mu} + \mathrm{e}^{2\mathrm{ISI}_1^{\mathrm{j}}\mu} \Big) \left((-1+\mu)^2+\omega^2\right) \left(\mu^2+\omega^2\right) - 2\mathrm{e}^{(\mathrm{ISI}_1^{\mathrm{i}}+\mathrm{ISI}_1^{\mathrm{j}})\mu} \Big(\left((-1+\mu)^2+\omega^2\right) \left(\mu^2+\omega^2\right) \cos((\mathrm{ISI}_1^{\mathrm{i}} - \mathrm{ISI}_1^{\mathrm{j}})\omega) - \mu \left((-1+\mu)^2\mu + (-2+\mu)\omega^2\right) \cos((\mathrm{ISI}_1^{\mathrm{i}} + \mathrm{ISI}_1^{\mathrm{j}} - 2T)\omega) + \mu\omega \left(-1+\mu^2+\omega^2\right) \sin((\mathrm{ISI}_1^{\mathrm{i}} + \mathrm{ISI}_1^{\mathrm{j}} - 2T)\omega) \Big) - \mu \Big(\mathrm{e}^{2\mathrm{ISI}_1^{\mathrm{i}}\mu} \left((-1+\mu)^2\mu + (-2+\mu)\omega^2\right) \cos(2(\mathrm{ISI}_1^{\mathrm{i}} - T)\omega) + \mathrm{e}^{2\mathrm{ISI}_1^{\mathrm{j}}\mu} \left((-1+\mu)^2\mu + (-2+\mu)\omega^2\right) \cos(2(\mathrm{ISI}_1^{\mathrm{j}} - T)\omega) - \omega \left(-1+\mu^2+\omega^2\right) \Big(\mathrm{e}^{2\mathrm{ISI}_1^{\mathrm{i}}\mu} \sin(2(\mathrm{ISI}_1^{\mathrm{i}} - T)\omega) + \mathrm{e}^{2\mathrm{ISI}_1^{\mathrm{j}}\mu} \sin(2(\mathrm{ISI}_1^{\mathrm{j}} - T)\omega) \Big) \Big) \Big)$$

Hence, in these linear models the intrinsic memory about the input ISIs received further back in the past decreases exponentially with time.

Figure 4.2 shows expressions (4.5) and (4.4) for our canonical GIF and IF neurons (see Methods), as functions of $\mathrm{ISI}_i{=}{-}t_i$ and $\mathrm{ISI}_j{=}{-}t_j$. It can be seen that the discriminability decreases for longer and more similar input ISIs in both models. While this decrease is non-specific for the IF neuron, a more complex structure is observed in the GIF neuron. Indeed, a local maximum is observed for the GIF model at a certain value of (ISI_i,ISI_j).

The position of the local maximum (ISI_i^{opt},ISI_j^{opt}) as a function of μ and ω cannot be obtained analytically. We performed some numerical explorations varying μ or ω, one at a time, between 20 and 500% of their initial values, starting from a few representative points in the (μ,ω) plane (Fig. 4.2C). Our results show that μ and ω interact in a non-trivial way in determining the location of the local maximum in the (ISI_i,ISI_j) plane. In general, increasing μ shifts the position of the maximum towards the closer axis, in a direction which doesn't depend much upon ω. Decreasing the intrinsic frequency ω correspondingly shifts the maximum to lower input frequencies. This shift follows straight lines in the (ISI_i,ISI_j) plane, but it bends towards the closer axis if μ is high enough. This is consistent with the intuition that a neuron with a high effective membrane rate constant will poorly discriminate between low-frequency inputs. In particular, ISI_i^{opt} scales linearly with the intrinsic period of oscillations $2\pi/\omega$ with a slope smaller than one, which decreases with increasing μ (Fig. 4.2D).

The values of the discriminability on the bisectrix $\mathrm{ISI}_i{=}\mathrm{ISI}_j$ is zero, since identical input

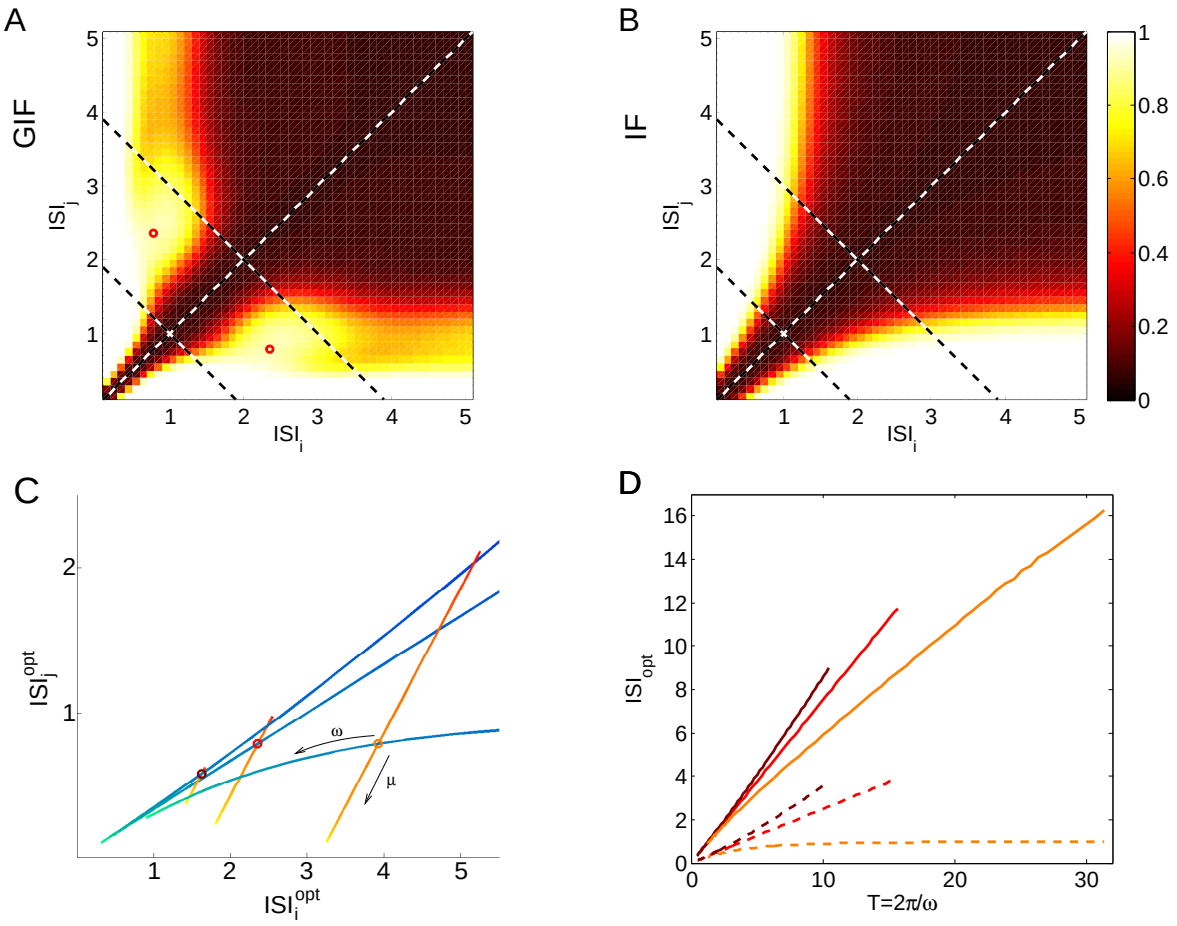

Figure 4.2: **Intrinsic excitability discriminates between input doublets.** A, B: Intrinsic discriminability between input doublets ISI_i and ISI_j for the GIF (A) and IF (B) model neurons. Intrinsic oscillations enhance discriminability for input ISIs slightly shorter than the intrinsic period π. Local maxima of $\mathcal{D}$ are indicated by red circles. Dashed lines indicate the bisectrix ISI_i=ISI_j, and the lines of constant mean ISI <ISI>=1 and <ISI>=2, along which $\mathcal{D}$ is plotted in Fig. 4.3B. $\mathcal{D}$ values have been passed through the sigmoidal function $1/(1+\exp(5(0.5-\mathcal{D})))$ to improve visualization. C: Local maximum of $\mathcal{D}$ as μ or ω are varied, one at a time, between 20 and 500% of their starting values. Shades from yellow to red indicate decreasing values of μ, shades from green to blue indicate decreasing values of ω. Local maxima corresponding to starting values for the parameters are indicated with circles. Brown Circle, $(\mu,\omega)=(0.5,3)$; Red Circle, $(\mu,\omega)=(1,2)$; Orange Circle, $(\mu,\omega)=(2,1)$. D: ISI corresponding to the local maximum of $\mathcal{D}$ as ω is varied. If (ISI_i^{opt},ISI_j^{opt}) is the position of the local maximum and $\mathrm{ISI}_i^{opt} > \mathrm{ISI}_j^{opt}$, ISI_i^{opt} is drawn with a solid line, ISI_j^{opt} with a dashed line. Color code as in C.

trains are not distinguishable. The evaluation of the intrinsic discriminability (4.5) and (4.4) along lines departing orthogonally from the bisectrix is especially interesting, since it denotes the discriminability between pairs of input trains with the same total duration, as the second-to-last spike is slightly advanced or delayed (see Fig. 4.3A).

The evaluation of (4.5) and (4.4) along (ISI$_i$=<ISI>+ΔISI/2,ISI$_j$=<ISI> $-\Delta$ISI/2) for different values of the mean ISI is plotted in Fig. 4.3B. When the average input frequency is high (with respect to the frequency of intrinsic oscillations), the discriminability increases rapidly with ΔISI in both models, but the slope is higher for the GIF neuron (mean ISI$\leq$1). When the input ISIs are so short, the post-synaptic effects of subsequent spikes add almost linearly, and the dynamic encoding mechanisms provided by the neuron's intrinsic properties play little role. In this case, the difference in discriminability is mainly determined by the free evolution of the model neurons. In this regime, higher input frequencies evoke stronger depolarizations, which in turn result in free evolutions of greater amplitude and hence greater discriminability.

For input trains with frequencies close to the GIF intrinsic frequency, the discriminability increases faster for the GIF neuron, where it reaches a plateau or local maximum (Fig. 4.3B). After this plateau, discriminability will further increase only for very short ISIs, which corresponds to almost linear summation of the postsynaptic effects. For sufficiently long mean ISI (mean ISI>2) and long ISI difference, the intrinsic discriminability reaches a maximum value (independent of the mean ISI and of the ISI difference) corresponding to the difference in initial conditions corresponding to one and two EPSPs received at rest. Indeed, when one of the constituent ISI is greater than a few membrane time constants, the neuron has time to relax to its rest state almost completely and hence loses all the information about its previous stimuli.

In order to understand these observations one needs to take into account the contributions of two different effects: 1) the dynamic encoding of input history, which determines how subsequent presynaptic spikes affect the dynamic variables of the model in a history-dependent manner, and 2) the free evolution of the system after the last spike of the train (see also Fig. 4.7).

Both these ingredients are represented in Fig. 4.3C, where the trajectories in the phase plane $(\Delta v, \Delta w)$ as the ISI difference is varied are represented together with the cumulative discriminability isolines, for several values of the ISI mean. We have shown before that the intrinsic discriminability between two input histories $\mathcal{H}_i$ and $\mathcal{H}_j$ is a function of the difference in the dynamical variables after the last spike of the input train $(\Delta v_0, \Delta w_0) = (v_0^j - v_0^i, w_0^j - w_0^i)$. Hence, the dependence of $(\Delta v_0, \Delta w_0)$ upon input frequency and ISI difference determines the dynamic encoding properties of the neuron. When the average input frequency is high, Δw changes only slightly with the ISI difference, and

the trajectories lie close to the Δv axis: in this regime the dynamic encoding mechanisms play little role. The greater the ISI difference, the greater Δv and hence the cumulative discriminability. When the average ISI is higher (mean ISI>1.5) these trajectories acquire a curved shape, which indicates that the dynamical encoding mechanism is giving a significant contribution by modulating the slow variable w in a history-dependent manner: first the phase point leaves the origin in a direction that depends upon the mean ISI, and then moves tangentially to the discriminability isolines, which is consistent with the plateau in discriminability observed in Fig. 4.3B. It is worth noting that the plateau level does not depend upon the mean input frequency, but only on the synaptic strength and the neuron's intrinsic properties, and arises as soon as one of the constituent ISI is around half the intrinsic period of the model neuron.

These results suggest that the dynamical encoding mechanisms provided by intrinsic oscillations increase the sensitivity of short-long vs. long-short ISI discrimination. To clarify this point, we made the hypothesis that $\mathcal{D}$ values above a certain threshold $\mathcal{D}_{thr}$ allow a reliable discrimination between pairs of input trains, in spite of the several non-deterministic phenomena observed in neurons (which we do not model explicitly). Hence, we defined the intrinsic sensitivity ΔISI_{thr} as the minimum ISI difference such that $\mathcal{D} \geq \mathcal{D}_{thr}$. This measure assesses the sensitivity of the intrinsic excitability in discriminating between "accelerating" and "decelerating" triplets with the same average frequency (Fig. 4.3D-F).

In the case of the IF neuron, ΔISI_{thr} can be calculated analytically by inverting expression (4.4):

$$\Delta ISI_{thr}^{IF} = \frac{1}{\mu} \ln \left[\frac{2A^2 + 2\mathcal{D}_{thr} e^{2<\text{ISI}>\mu} \mu + \sqrt{-4A^4 + \left(-2A^2 - 2\mathcal{D}_{thr} e^{2<\text{ISI}>\mu} \mu\right)^2}}{2A^2} \right]$$

The corresponding expression (4.5) for the GIF neuron is not invertible, hence we set $\mathcal{D}_{thr}$ arbitrarily at 0.5 (black horizontal line in Fig. 4.3B) and calculated ΔISI_{thr}^{GIF} numerically. For the GIF neuron, discriminability curves as a function of ΔISI are not always monotonic, and for specific parameter sets the discriminability curves crossed the threshold $\mathcal{D}_{thr}$ more than once. In these cases we did not define ΔISI_{thr} and they appear as blank spaces in Fig. 4.3D-F.

Decreasing μ results in shorter ΔISI_{thr}, and hence greater sensitivity in the discrim-

ination between different input trains (Fig. 4.3D). This is an expected result since μ is the rate of decay of the model variables to the rest state, and determines for how long the information about previous stimuli will be available in the excitability trajectory. The sensitivity is better in the GIF neuron for μ smaller than a certain value, which increases with increasing input frequency. While the sensitivity always improves with decreasing μ in the GIF neuron, it starts worsening at a certain, unrealistically low value of μ (which increases with increasing input frequency) in the IF neuron. Indeed, when the effective leak μ tends to zero, the IF neuron acts as a perfect integrator, and its membrane potential (and hence its excitability) comes to reflect solely the number of spikes received, while the precise timing of the received spikes becomes irrelevant. In this limit, ΔISI^{IF}_{thr} tends to infinity. In the same limit, the GIF neuron acts as an undamped oscillator, resulting in an infinitely high cumulative discriminability as soon as the input trains differ, and hence a vanishing small ΔISI_{thr} (Fig. 4.4). At high values of μ, the post-synaptic effects decay very fast, and significant discriminability values are achieved only when one of the two ISIs is very small. Hence, ΔISI_{thr} tends to the higher possible value of twice the mean ISI.

The effect of the intrinsic frequency ω is somewhat more complicated (Fig. 4.3E). For high input frequencies, the sensitivity improves with increasing ω, because of both the increased discriminability based on the free evolution and the greater encoding capabilities resulting from intrinsic oscillations (see also Fig. 4.7). When the intrinsic frequency ω exceeds a certain threshold (which increases with increasing input frequency), the profile of the intrinsic discriminability as a function of the ISI difference becomes oscillatory even at high input rates and can result in very low values for specific input triplets, a phenomenon conceptually remindful of destructive interference in classical wave theory (see also Fig. 4.4). For lower input frequencies, the minimal detectable difference ΔISI_{thr} as a function of ω is oscillatory: it first increases until a certain value of ω (which depends only weakly on the input frequency), then decreases, and then tends to stabilize through oscillations of progressively smaller amplitude and higher frequency. As soon as the input frequency is lower than a certain threshold, the neuron with intrinsic oscillations is less sensitive than the IF neuron for every value of ω, suggesting that intrinsic oscillations improve the intrinsic discriminability only for input trains with frequency close to, or higher than, the intrinsic frequency of oscillations.

Note that as we increase the membrane rate constant μ or the oscillation frequency ω, the damping coefficient $C_{damp} = \mathrm{e}^{-2\pi\frac{\mu}{\omega}}$ (defined as the ratio between the second and the

first peak in the free evolution of the voltage variable from an initial condition different than rest) also varies, and consequently the oscillating character of the neuron.

In order to separate the effects due to μ, ω and to the damping coefficient C_{damp}, we performed some additional calculations keeping a constant $\frac{\mu}{\omega}$ ratio of 0.5, as in the canonical GIF model. The results of this analysis are shown in Fig. 4.3F. Varying μ and ω proportionally (thus maintaining a constant damping coefficient C_{damp}) has similar effects on the sensitivity ΔISI_{thr} as varying μ while keeping ω fixed: the GIF neuron exhibits a better sensitivity (smaller ΔISI_{thr}) than the IF neuron for μ smaller than a certain threshold, which increases with increasing input frequency. When maintaining a constant damping coefficient C_{damp}, though, the increase in ΔISI_{thr} with increasing μ is smoother and the sensitivity curves are generally below the correspondent curves in Fig. 4.3D, where μ was varied while keeping ω fixed. This suggests that the steep increase in ΔISI_{thr} with increasing μ observed in Fig. 4.3D is also due to the decrease in the damping coefficient C_{damp}, in addition to the decrease in sensitivity resulting from a faster convergence to the steady state.

The results exposed in this section can be directly applied to the characterization of biological neurons, and might be used to test the physiological relevance of the phenomenon for different cell types and in different brain areas. For instance, from standard electrophysiological measures such as a neuron's (complex) impedance, we could obtain estimated values for the neuron parameters μ and ω (see for example (Schreiber et al., 2004) for a fitting procedure). On the other hand, the variance of the membrane voltage due to random fluctuations could be directly related to a value of $\mathcal{D}_{thr}$, above which discriminability values are expected to be efficiently exploitable for contextualized information processing. Such analysis could assess the robustness of the intrinsic discriminability as a function of the input frequency, or the amount of coherence in the presynaptic population needed to form a signal that could be efficiently encoded through the intrinsic dynamical mechanism described.

4.3.4 Intrinsic discriminability between random input trains

In the previous section we analyzed the input discrimination capabilities based on intrinsic single-cell dynamics between some particular, well defined inputs. In this section we wish to generalize the previous analysis and characterize the intrinsic discriminability as a

function of input statistics and intrinsic properties for random input trains. In particular we considered input trains composed of exponentially distributed ISIs. This distribution is particularly significant in neuroscience, since neurons in many brain regions exhibit a firing statistics that is well fitted by an exponential distribution with a refractory period (Shadlen and Newsome, 1998).

The average discriminability between pairs of input trains that only differ in their second to last spike can be easily calculated by integrating (4.3) over the exponential probability density:

$$E[\mathcal{D}] = \int_{-\infty}^{0}\int_{-\infty}^{0} \mathcal{D}(i,j) r_i \mathrm{e}^{r_i t_i} r_j \mathrm{e}^{r_j t_j} dt_i dt_j$$

where r_i is the mean firing rate of input history $\mathcal{H}_i$. Solving yields:

$$E[\mathcal{D}_{IF}] = \frac{A^2}{2\mu}\left(\frac{r_i}{2\mu + r_i} + \frac{r_j}{2\mu + r_j} - \frac{2r_i r_j}{(\mu + r_i)(\mu + r_j)}\right) \tag{4.6}$$

Figure 4.3 *(facing page)*: **Sensitivity of intrinsic discriminability to temporally precise inputs.** A: Input trains (left) and correspondent excitability trajectories after the last spike of the input train (right). As the input ISI difference ΔISI increases, the resultant excitability trajectories diverge and the cumulative discriminability $\mathcal{D}$ (yellow shaded area) increases. Note that the total duration of the input train is held constant. B: Intrinsic discriminability $\mathcal{D}$ as a function of ΔISI for the GIF (solid line) and IF (dashed line) neurons. The general trend is an increase in $\mathcal{D}$ with increasing ΔISI, but an oscillatory component is superimposed on this trend in the GIF neuron. Shades from brown to orange indicate increasing mean ISI (see legend). The diamond indicates the pair of ISIs used in Fig. 4.1. The threshold of putative physiological significance $\mathcal{D}_{thr}$ is depicted as a black horizontal line. C: Trajectories in the phase plane $(\Delta v, \Delta w)$ corresponding to the solid curves in B. Lines of constant discriminability are depicted as black ellipsis. D: Minimal ISI difference $\Delta\mathrm{ISI}_{thr}$ corresponding to an intrinsic discriminability above a threshold $\mathcal{D}_{thr} = 0.5$ as a function of μ, for fixed $\omega = 2$. Colors and line styles as in B. E: $\Delta\mathrm{ISI}_{thr}$ as a function of ω, for fixed $\mu = 1$. F: $\Delta\mathrm{ISI}_{thr}$ as a function of ω, scaling μ in order to maintain a fixed $\frac{\mu}{\omega}$ ratio of 0.5. Black arrows in D and E indicate the default parameter set; the correspondent curve of discriminability vs. ΔISI is depicted in panel B. The gray arrow in D indicates the value of μ used in Fig. 4.4.

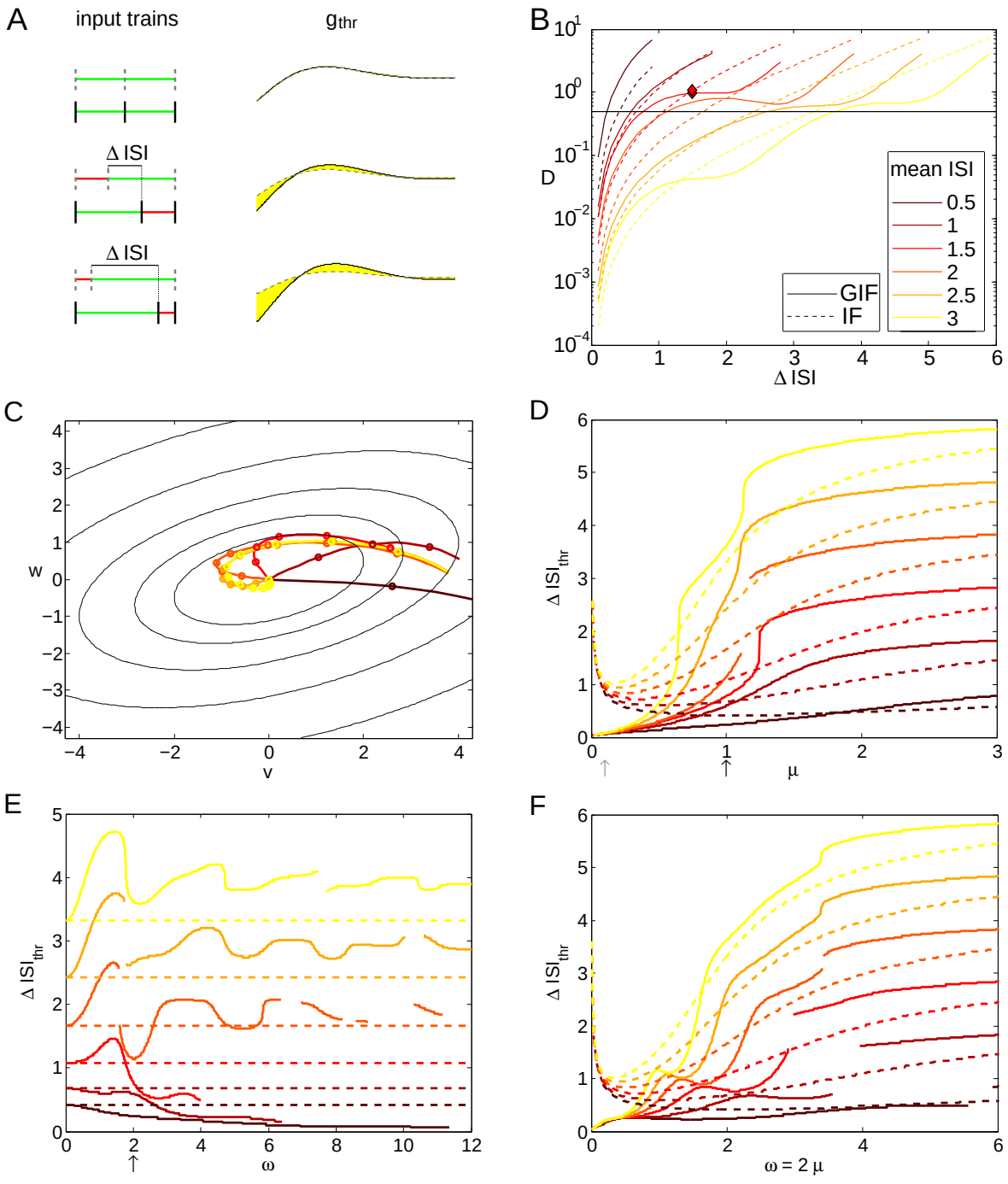
A
input trains
g_{thr}
Δ ISI
Δ ISI
B
D
Δ ISI
mean ISI
0.5
1
1.5
2
2.5
3
GIF
IF
C
w
v
D
ΔISI_{thr}
μ
E
ΔISI_{thr}
ω
F
ΔISI_{thr}
ω = 2 μ

$$E[\mathcal{D}_{GIF}] = \frac{1}{2}A^2 \left(\frac{1}{\mu} - \frac{1}{r_i + 2\mu} - \frac{1}{r_j + 2\mu} - \frac{(2 + r_i)^2}{(r_i + 2\mu)^3 + 4(r_i + 2\mu)\omega^2} + \right.$$
$$- \frac{(2 + r_j)^2}{(r_j + 2\mu)^3 + 4(r_j + 2\mu)\omega^2} + \qquad (4.7)$$
$$\left. \frac{-r_i^2\left(-1 + r_j^2\right) + (r_j + \mu)^2 + \omega^2 - r_i\left(-2\mu + r_j\left(1 + (-4 + \mu)\mu + \omega^2\right)\right)}{\mu\left((r_i + \mu)^2 + \omega^2\right)\left((r_j + \mu)^2 + \omega^2\right)} \right)$$

Expressions (4.7) and (4.6) are shown in Fig. 4.5 as a function of $<\mathrm{ISI}_i>=1/r_i$ and $<\mathrm{ISI}_j>=1/r_j$ for our canonical GIF and IF neurons (see Methods). For the GIF neuron the average discriminability between random input doublets with the same average frequency is almost as good as between random input doublets with different average frequencies, and seems to depend mainly upon the frequency of the faster input. Indeed, isolines of constant discriminability are orthogonal to the bisectrix $<\mathrm{ISI}_i>=<\mathrm{ISI}_j>$, and then run parallel to the main axes (Fig. 4.5A). This behavior corresponds to sensitivity to input ISIs rather than average rates, given that input doublets with different rates are not better discriminated than input doublets with the same rate. Conversely, the IF neuron shows a greater sensitivity to input rate: pairs of input doublets with the same average rate yield lower discriminability values than pairs of input doublets with different average rate. In fact, for a purely passive neuron, the isolines of constant discriminability are

---

Figure 4.4 *(facing page)*: **Intrinsic discriminability in the GIF and IF models for slow effective membrane rate constant μ.** Top panel: Cumulative discriminability as a function of ΔISI for input triplets of fixed duration for the GIF (solid line) and IF (dashed line) neurons. Shades from brown to orange indicate increasing mean ISI (see legend). The threshold of putative physiological significance $\mathcal{D}_{thr}$ is depicted as a black horizontal line. The symbols (red diamonds and red squares) indicate the pairs of ISIs used in the lower panels, and the resulting cumulative discriminability. Lower panels: Voltage traces of the GIF (top) and IF (middle) neurons in response to two different input trains, composed of the same ISIs, and the evolution of their instantaneous discriminability (bottom; black line for the GIF model and gray line for the IF model) after the last spike of the input train. Note the different vertical scale for the excitability in each panel. The black diamond indicates the time of maximal instantaneous discriminability in the GIF neuron, which correspond to the time of greater separation in the voltage trajectories resulting from the two different input trains. Parameter set: $(\mu, \omega) = (0.1, 2)$. Note that, as the membrane rate constant μ approaches zero, the IF neuron tends to reflect only the number of spikes received, regardless of their timing. In the same conditions, the GIF neuron will continue to oscillate indefinitely with a phase and amplitude that depend upon the precise timing of the input train.

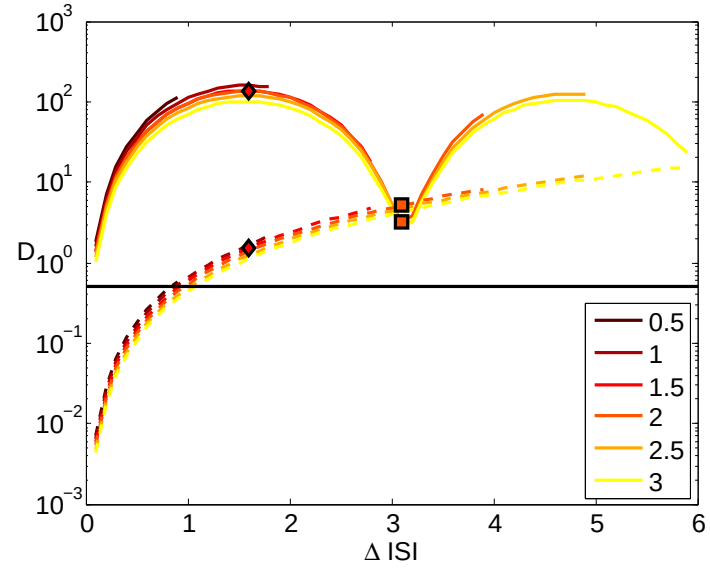
D
Δ ISI
0.5
1
1.5
2
2.5
3

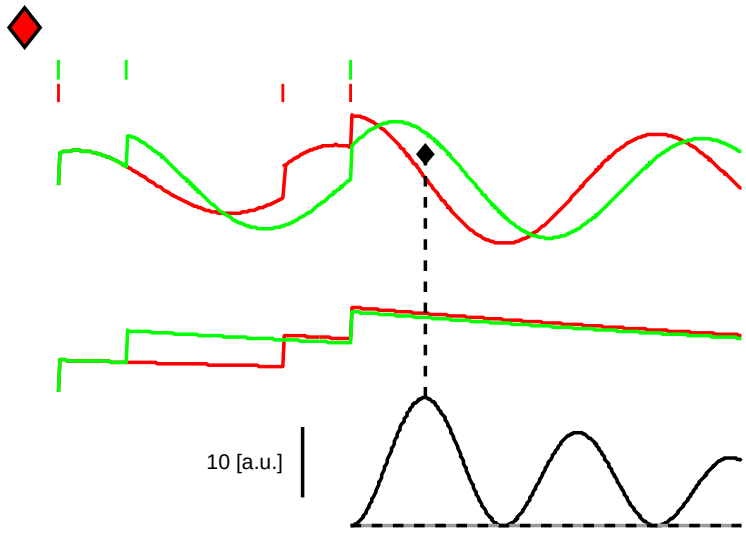
10 [a.u.]

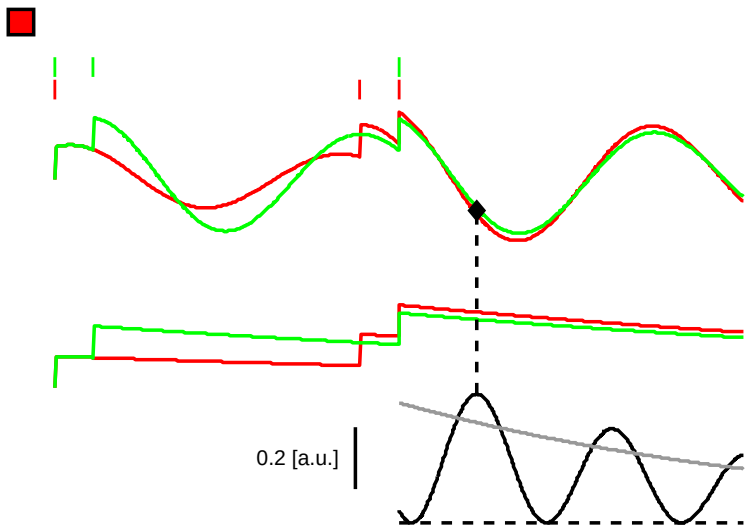
0.2 [a.u.]

approximately parallel to the bisectrix $<ISI_i>=<ISI_j>$ (Fig. 4.5B). Rate sensitivity decays for low frequency inputs, for which the average discriminability is mainly determined by the frequency of the faster input. In this regime the GIF and IF neurons behave similarly.

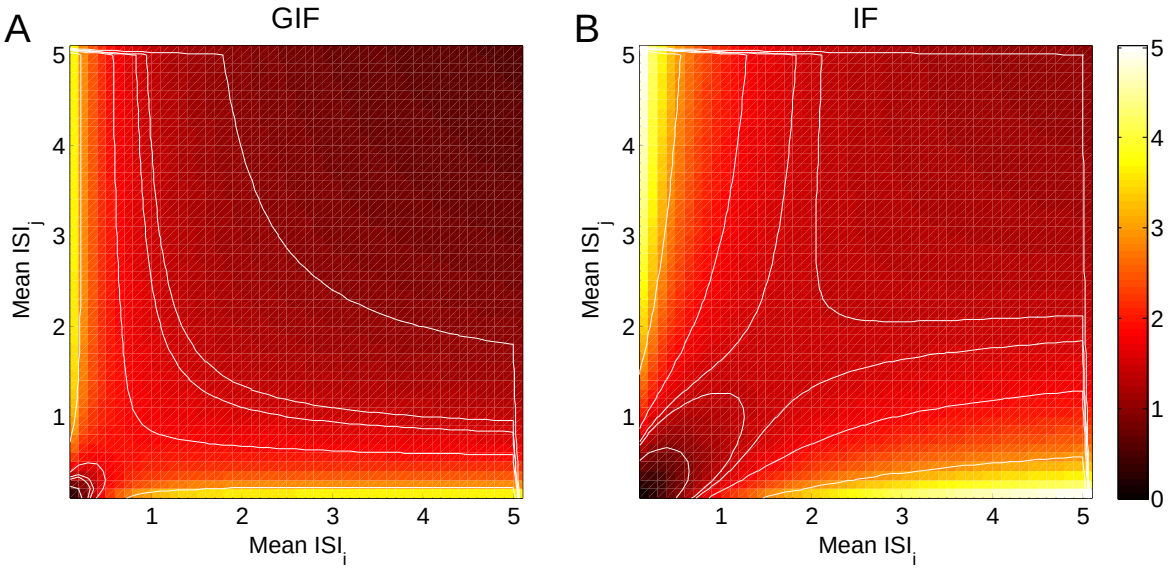

Figure 4.5: **Average discriminability between random input doublets.** Discriminability between input doublets with ISI extracted from an exponential distribution with mean values ISI_i and ISI_j, averaged over 10000 pairs. Isolines are drawn for $\mathcal{D}$ values of 1, 1.4, 1.5, 1.8, 2.8. In the range of input ISIs which interact with the intrinsic neuronal dynamics, discriminability is higher between input doublets with different frequencies than between doublets with the same frequency in the IF neuron. This is not observed in the GIF neuron, where the discriminability is mainly determined by the frequency of the faster input.

Evaluation of (4.6) and (4.7) along $r_i = r_j$ returns the average discriminability between input trains extracted from the same exponential distribution, which we plot as a function of the mean ISI in a semilog scale in Fig. 4.6A. The black line indicates the IF model, while lighter colors refers to GIF models with increasing values of the intrinsic frequency ω (see caption).

For both models, the discriminability first increases and then decreases, showing a maximum at an intermediate value of the mean ISI. For the exponential distribution, the mean equals the standard deviation: hence spike triplets with short ISIs are poorly discriminated because they are composed of very similar ISIs. Indeed, analogous calculations using gaussianly distributed ISIs (see Appendix) with a very narrow (and constant) standard deviation shows a decreasing trend for increasing mean input ISI (Fig. 4.6F), indicating that the increasing trend at high input frequencies depends upon the standard deviation

of the input.

The discriminability for long ISIs is poor too: for such distributions most of the ISIs are longer than the time span of intrinsic excitability, the neuron relaxes almost completely to its rest state and the dynamic trace reflecting its previous stimuli is lost. The maximum is achieved when the variability is great enough, yet the mean ISI is not longer than the time span of intrinsic memory.

As the intrinsic frequency ω increases, the intrinsic discriminability increases almost linearly for short input ISIs, and the peak of maximal discriminability shifts to higher input frequencies. This effect is due to two different mechanisms: on the one hand an increase in ω allows the intervention of the dynamical encoding mechanisms at higher input frequencies, and on the other hand it allows a better discriminability based on the free evolution of the model neuron (Fig. 4.7). As noted previously, the intrinsic discriminability between two input histories $\mathcal{H}_i$ and $\mathcal{H}_j$ is a function of the difference in the dynamical variables after the last spike of the input train $(\Delta v_0, \Delta w_0) = (v_0^j - v_0^i, w_0^j - w_0^i)$. Hence, the distribution of $(\Delta v_0, \Delta w_0)$ points is an indicator of the dynamic encoding properties of the neuron. Figure 4.7 shows the probability densities of $(\Delta v_0, \Delta w_0)$ for different input statistics and neuron parameters. For high frequency inputs, the dynamic encoding mechanism plays little role, and the $(\Delta v_0, \Delta w_0)$ points accumulate along a line. As the input frequency decreases, the input trains interact with the intrinsic oscillatory dynamics and the $(\Delta v_0, \Delta w_0)$ points distribute over a larger area in the $(\Delta v_0, \Delta w_0)$ phase space. As the input frequency decreases further, most input pairs result in $(\Delta v_0, \Delta w_0)$ values close to the origin. Indeed, if the input ISIs are long compared with the membrane time constant, the phase point relaxes almost completely to the rest state in between synaptic events and the intrinsic memory about previous inputs is lost. In this low frequency input regime, the intrinsic discriminability decreases slightly for increasing intrinsic frequencies, but saturates at approximately $\omega = 1$, so that an additional increase in the intrinsic frequency does not affect discriminability (Fig. 4.6A). Note that the input mean ISI that results in the greatest spread of points in the $(\Delta v_0, \Delta w_0)$ phase space, which corresponds to the optimal input frequency for dynamic encoding, decreases with increasing ω. This is consistent with the shift to higher input frequencies of the peak in the discriminability as ω is increased (Fig. 4.6A). In addition to this, increasing ω results in a greater average discriminability for $(\Delta v_0, \Delta w_0)$ points in a circular region centered at the origin, denoting a greater discriminability based on the free evolution of the model neuron.

Increasing μ results in an overall decrease of the cumulative discriminability, which is more pronounced at low input frequencies. The discriminability peak slightly shifts to higher input frequencies (Fig. 4.6B). As in the sensitivity analysis carried out in the previous section, this is an expected effect since μ is the rate of decay of the model variables to the rest state, so that greater values of μ result in faster forgetting of the previously received stimuli. This effect is more pronounced at low input rates, because the model neuron has time to converge almost completely to its rest state in between synaptic events.

The standard deviation of the mean discriminability values depicted in Fig. 4.6A,B is almost equal to the mean (not shown). Indeed, a closer inspection of the distribution of discriminability values (estimated numerically, see Methods) reveals that most ISI pairs yield very small discriminability values, while a certain subset clusters around a discriminability value that corresponds to the plateau level in Fig. 4.3B (Fig. 4.6C). This phenomenon is exclusive to the GIF neuron and it is not observed in the IF neuron, where the distribution shows a peak at zero and a smooth decline for higher values of the discriminability (Fig. 4.6D).

We interpret this phenomenon as a form of modulation of the intrinsic discriminability due to intrinsic oscillations: intrinsic oscillatory properties push the discriminability values between certain input train pairs above a certain threshold. If the threshold corresponded to a physiological limit of intrinsic discriminability, determined by the stochastic properties of neurons, this phenomenon would increase the sensitivity of the intrinsic discriminability between "accelerating" and "decelerating" input trains. This is a direct consequence of the steep rise to a plateau in the discriminability as a function of the ISI difference depicted in Fig. 4.3B.

Note that as we increase the membrane rate constant μ or the intrinsic frequency ω, the damping coefficient $C_{damp} = \mathrm{e}^{-2\pi\frac{\mu}{\omega}}$ (defined as the ratio between the second and the first peak in the free evolution of the voltage variable from an initial condition different than rest) also varies, and consequently the oscillatory character of the neuron. In order to separate the effects due to μ, ω and to the damping coefficient C_{damp}, we performed some additional simulations keeping the damping coefficient fixed, and ranging ω and μ accordingly. The results of this set of simulations are depicted in Fig. 4.6E, where the membrane rate constant μ and the intrinsic frequency ω has been changed proportionally, maintaining a constant $\frac{\mu}{\omega}$ ratio of 0.5. Increasing the intrinsic frequency ω and the membrane rate constant μ in a fixed ratio induces a slight increase in discriminability for high frequency

inputs (due to the increase in ω), but also a substantial decrease in discriminability for low input frequencies (due to the increase in μ). Also, it shifts the peak in discriminability to higher frequencies. The value of the peak decreases substantially when the cumulative discriminability is considered, but when the maximal discriminability is taken into account the decrease is minimal.

Taken together, these results can be summarized as follows: 1. Increasing the intrinsic frequency ω increases the discriminability between high frequency inputs. This happens because a fast w variable has time to activate in between synaptic events even at high input rates, enabling a dynamic encoding of input histories. In addition to this a fast intrinsic frequency increases the discriminability based on the free evolution of the neuron model. 2. Decreasing the membrane rate constant μ increases the discriminability especially for middle and low frequency inputs, because of the widening of the integration window of the neuron, and because the slower exponential decay of the instantaneous discriminability results in a stronger and longer-lasting memory of the immediate past.

4.4 Discussion

Neurons are dynamical entities which act on several time scales; this endows them naturally with a capacity for short-term memory or context-dependent processing. The history of inputs to a neuron is dynamically encoded in its state-dependent, time-varying properties: each synaptic event induces some modifications in the neuron dynamical state which depend

---

Figure 4.6 *(facing page)*: **Intrinsic discriminability as a function of input statistics for different model neurons.** A: Mean discriminability between input triplets with exponentially distributed ISIs, as a function of the input mean ISI, for the GIF and the IF neuron. Shades from brown to orange indicate GIF neurons with increasing values of the intrinsic frequency ω (see legend), while the black line indicates the IF neuron. The membrane rate constant μ was fixed at its canonical value of 1. B: The same as in A, but μ has been varied while ω was fixed at its canonical value of 2. Shades from brown to orange indicate increasing values of μ (see legend). GIF neurons, solid lines; IF neurons, dashed lines. C, D: Probability densities of the discriminability between input triplets with exponentially distributed ISIs, as a function of the input mean ISI, for the GIF (C) and the IF (D) neuron. E: The same as in A and B, but μ and ω have been scaled proportionally in order to maintain a fixed $\frac{\mu}{\omega}$ ratio of 0.5. Lighter colors indicate greater values of μ and ω. F: The same as in A, for gaussianly distributed input ISIs. Summarizing, increasing ω increases the discriminability at high input rates, while decreasing μ increases the discriminability especially for middle and low frequency inputs.

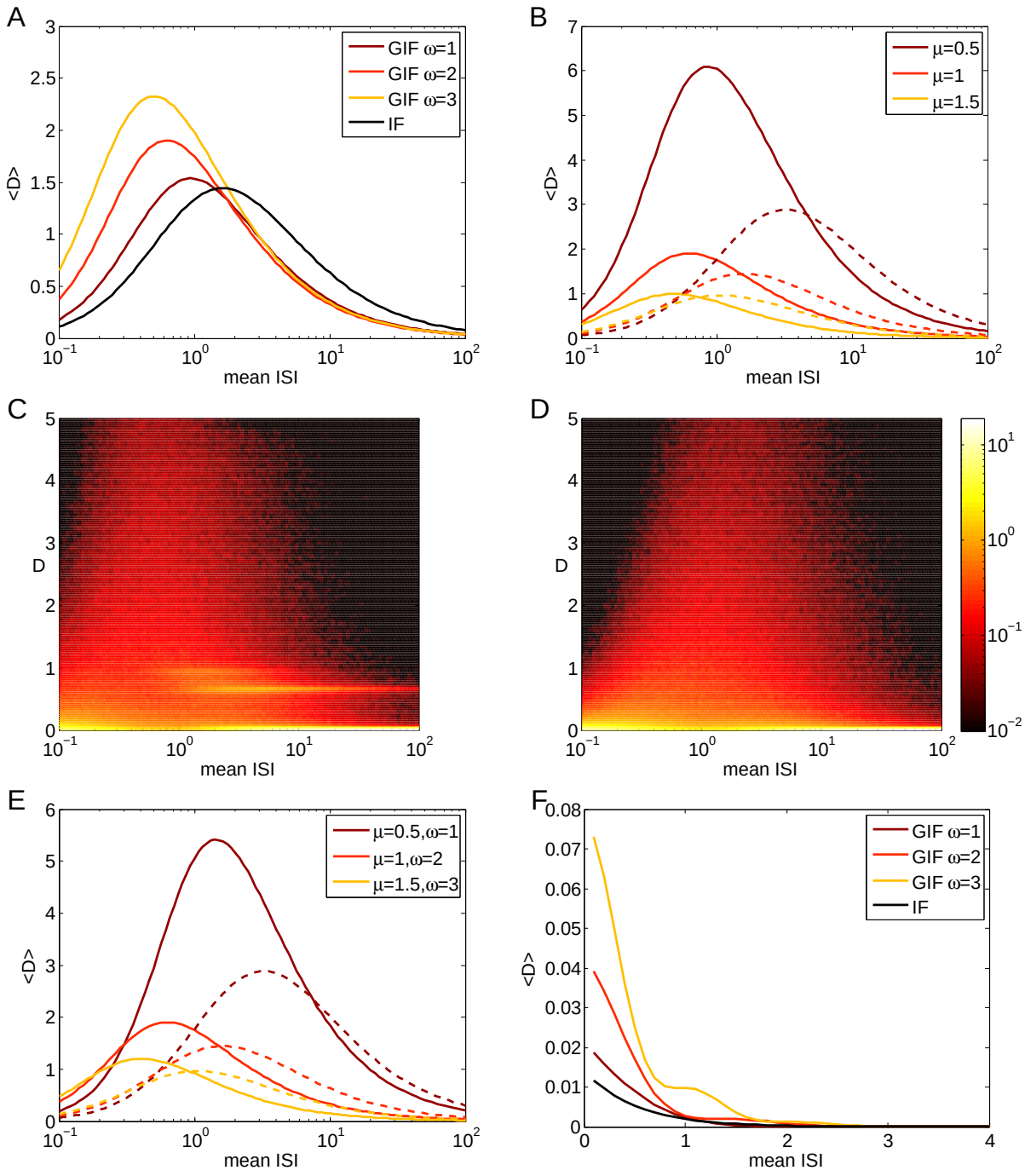
A
B
C
D
E
F
GIF ω=1
GIF ω=2
GIF ω=3
IF
μ=0.5
μ=1
μ=1.5
μ=0.5,ω=1
μ=1,ω=2
μ=1.5,ω=3
<D>
D
mean ISI

upon the previously received stimuli and their timing. In order to map intrinsic neuronal state to a physiologically, spike-related measure, we introduced the concept of history-dependent neuronal excitability, which we define as the minimal strength of a synaptic event that can cause the neuron to fire. As the neuron's dynamics unfolds in a history-dependent manner, the time evolution of the intrinsic excitability carries information about the history of stimulation in the immediate past, allowing for context-dependent signal processing. This framework allows us to compare the context-dependent processing capabilities of different neuron types.

4.4.1 History-dependent discriminability for different subthreshold dynamics

For the sake of illustration we considered linear models with a fixed voltage threshold for spike generation, namely the IF and (oscillating) GIF neuron models. Their simplicity is useful in dissecting the relative contribution of very general dynamical mechanisms (such as passive and inductive membrane dynamics) to the emergence and properties of history-dependent processing. The IF neuron, described by a single dynamical variable with a single time constant, is a standard model of a passive membrane. The GIF neuron is a natural extension of the single variable IF model which includes an additional dynamical variable that varies linearly with voltage, and comes to represent the (linearized) net effect of voltage gated ionic currents. Of particular interest when dealing with temporally selective

---

Figure 4.7 *(facing page)*: **Intrinsic discriminability is determined by the interplay of the dynamic encoding and the free evolution.** Probability distributions of the difference in the dynamical variables immediately after the last spike of the input train $(\Delta v_0, \Delta w_0)$ for different values of the average input ISI, which increases along the rows (0.1, 0.2, 0.5, 1, 2, 3, 5). The isolines of the cumulative discriminability as a function of $(\Delta v_0, \Delta w_0)$ are represented as white lines. Isolines are drawn for discriminability values of 1, 2, 4, 8, 32 and 64, starting from the center. Probability densities are normalized to the peak value in each plot. For high frequency inputs, the dynamic encoding mechanism plays little role, and the $(\Delta v_0, \Delta w_0)$ points accumulate along a line. As the input frequency decreases, the input trains interact with the intrinsic oscillatory dynamics and the $(\Delta v_0, \Delta w_0)$ points distribute over a larger area in the $(\Delta v_0, \Delta w_0)$ phase space. Note that the input mean ISI that results in the greatest spread of points in the $(\Delta v_0, \Delta w_0)$ phase space, which corresponds to the optimal input frequency for dynamic encoding, decreases with increasing ω. In addition to this, increasing ω results in a greater average discriminability for $(\Delta v_0, \Delta w_0)$ points in a circular region centered at the origin, denoting a greater discriminability based on the free evolution of the model neuron.

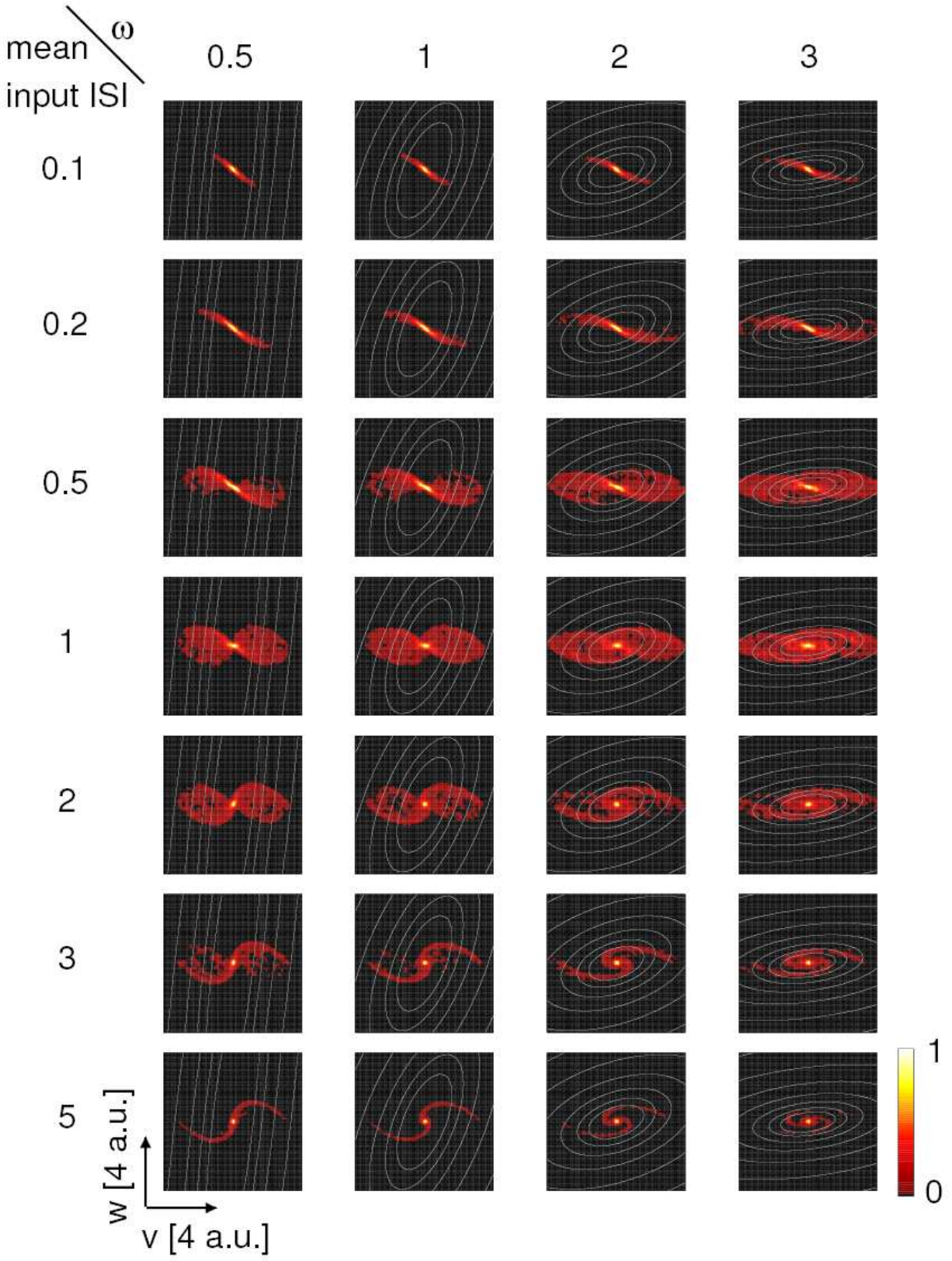
mean input ISI
ω
0.5
1
2
3
0.1
0.2
0.5
1
2
3
5
w [4 a.u.]
v [4 a.u.]
1
0

dynamical mechanisms is the oscillating GIF neuron, where the effect of the slow variable is to counteract voltage changes and the model dynamics is characterized by a pair of complex conjugate eigenvalues, thus exhibiting damped oscillatory responses to perturbing inputs. These simple linear models allowed the use of iterative formulae for calculating their response to input trains, and analytic expressions for the calculation of the intrinsic discriminability between pairs of input trains. The consequences and possible drawbacks of using these models are discussed in detail in the section "Limitations of the current approach".

Both the IF and the GIF neuron exhibit history-dependent processing capabilities, which could allow the discrimination between different input trains even when they share the same average frequency or even the same constituent ISIs. In fact, history-dependent responses are a general feature of any dynamical system, and can be studied conveniently with any dynamic description of neuronal behavior (for example, through a set of differential equations). In this case, the neuron model does not implement a static input-output transformation, but one that is modulated by its state variables, which in turn reflect the previous history of stimuli and responses. The GIF model, though, is particularly sensitive to the precise timing of input stimuli, while the IF neuron discriminates better between inputs with different average frequencies (Fig. 4.5). This suggests that passive neurons are better suited to rate-based computation, while neurons with subthreshold oscillations are advantageous for information processing in a temporal coding scheme. Since context-dependent processing is observed even in these simple, linear models, we expect it to be a general feature of neuronal computation. Furthermore, we expect these history-dependent processing capabilities to become more complex and modulable as more realistic model neurons are considered, and as more time scales come into play.

One of the most important differences between the IF and the oscillating GIF model is that the intrinsic discriminability between two different input histories decreases exponentially with time for the IF neuron, while intrinsic oscillations result in an intrinsic discriminability that is an exponentially decreasing function of time multiplied by a sinusoid. This means that for certain input histories and neuron parameters, the instantaneous discriminability can reach its maximum a few u.t. after the last spike of the input train (Fig. 4.1A). Thus, when a certain neuron "decides" to transmit or block a certain piece of information depending upon the current context in the immediate past, intrinsic oscillations allow the reverberation of this information a few u.t. after the last spike of the input train

which defines the context. Conversely, in passive neurons this information exponentially wanes.

Another important difference between oscillating and non-oscillating neurons regards the sensitivity to small differences in the input histories. For instance, when the discriminability between an accelerating and a decelerating input triplet with the same constituent ISIs is considered, the discriminability as a function of input ISI difference grows faster in the oscillating GIF neuron than in the purely passive IF neuron (Fig. 4.3B). Hence, if discriminability differences could be exploited as soon as they exceed a certain threshold, the oscillating GIF would exhibit an increased sensitivity in the discrimination between accelerating and decelerating triplets. This increase depends upon the input statistics though: the oscillating neuron discriminates better than the correspondent passive neuron between input triplets with frequency higher than a certain value, which decreases as the membrane rate constant μ decreases (Fig. 4.3D). These results suggest that while a passive neuron can provide context-dependent processing capabilities in a broad frequency range (which nevertheless depends upon the membrane rate constant μ), subthreshold oscillations enhance discriminability at high input frequencies and short ISI differences. Considering that discriminability differences below a certain threshold might not be physiologically exploitable for context-dependent processing, subthreshold oscillations increase the sensitivity between different input trains as a function of the difference between their constituent ISIs.

Finally, the theoretical framework provided by the neuronal excitability concept allowed the assessment of the temporal extension of the intrinsic memory (section 4.3.3). As the neuron receives successive EPSPs in a train, each EPSP drives the neuron's dynamical variables so that they come to reflect mainly the last input ISI, and the relative contribution of previous ISIs to the intrinsic excitability gradually wanes. In these linear models the intrinsic discriminability of the first and second ISIs in a train decreases exponentially with the train length, and the rate of decay is not influenced by intrinsic oscillations. The exponential forgetting is a consequence of the small number of time scales interacting in these simple linear models (one for the IF, two for the GIF neuron). It would not be surprising if a subthreshold dynamics with multiple time scales might lead to a more gradual forgetting, for instance a power-law forgetting, as it is observed in multiple time scale synaptic models (Fusi et al., 2005). Indeed, a neuron model with a multiple time-scale current efficiently encodes input history over several time-scales (Gilboa et al., 2005). Power-law forgetting curves could also arise from the interaction among many heterogeneous linear elements

with exponentially decaying individual traces (Anderson, 2001; Sikström, 2002).

Computer simulations allow the assessment of history-dependent excitability for arbitrary neuron models, and with arbitrary accuracy. In the absence of an analytical description for the excitability, it can be computed numerically by generating, in any moment in time, multiple branches of a given simulation, corresponding to different values of the conductance of an applied synaptic event. This technique allows the numerical measurement of the intrinsic excitability, defined as the minimal conductance of a synaptic event capable of generating a spike, in a certain instant. Iterating this procedure over successive time steps allows the reconstruction of the excitability trajectory with arbitrary temporal resolution. The measurement of the intrinsic excitability in living cells is constrained by the stability of the cell's properties, which will inevitably posit some limit upon the achievable resolution. Nevertheless, we believe that the experimental confirmation of the ideas exposed in this work is possible. In particular, an optimized dynamic clamp protocol (Prinz et al., 2004a) can be established, which could be used to probe the intrinsic discriminability as a function of input statistics, or simulated network state (Fellous et al., 2003), with the minimum number of trials. These experiments will further our understanding of the relationships between single-cell properties, network state, and the temporal discriminability properties of single neurons. If the neuron considered exhibits chaotic dynamics in the subthreshold regime, the integral which defines the cumulative discriminability (4.2) might not converge. In this case, the memory about the previously received inputs, intended as the input-specific perturbation of the neuron's trajectory, persists for an infinite amount of time. This result is consistent with our interpretation of intrinsic discriminability as a measure of the amplitude and temporal extension of the transient mnemonic trace.

4.4.2 Limitations of the current approach

Even if the computational mechanisms outlined in this work are general and apply to both living and model neurons, and might be relevant even to non-neural systems with history-dependent dynamics (Wolf et al., 2008), the detailed analysis were carried out with linear models with one (in the case of the IF neuron) or two (for the GIF neuron) time scales. These models arise from a linearized approximation around the stable state, and are useful to describe the subthreshold response to weak inputs. Still, they might not be adequate to study neuronal networks that can operate in different regimes, or that exhibit local or global transitions between up and down states (Stern et al., 1997; Lampl et al., 1999;

Cossart et al., 2003). For instance, when a real neuron (or a non-linear neuron model) is clamped to different holding voltages with a proper injected DC current, the jacobian matrix resulting from linearization around this new stable state is in general different from that obtained at equilibrium and in the absence of external currents. This implies that its resonant and passive properties will strongly depend upon the voltage the neuron is held at, or, in more physiological conditions, on the state of the subset of the circuit impinging on it (Destexhe et al., 2003). We predict that the computational consequences of history-dependent intrinsic excitability could be especially relevant in the down state, where the effective membrane time constant is slow and the membrane potential is far from threshold. In particular, we can speculate that the proposed mechanisms might contribute to the selection of the subset of neurons which will take part in the up state, depending upon the present context.

Another simplification adopted is the spike generation mechanism, implemented as a fixed voltage threshold in the IF and GIF models. It is possible that in certain conditions this simplification might provide a biased estimate of the excitability (which depends on both the synaptic dynamics and the spike generation mechanism). For instance, the interplay between the spike generation mechanism and the synaptic filtering properties can affect single-neuron processing, especially at high input rates (Fourcaud-Trocmé et al., 2003). Moreover, neurons that display intrinsic oscillations are likely to be dynamically close to an Andronov-Hopf bifurcation, hence their firing threshold might be better described by a curved manifold rather than by a fixed voltage threshold. This issue will be addressed in future work, where the influence of the spike generation mechanisms and its interplay with synaptic kinetics will be assessed by using computational models of increasing realism.

In this work we have assessed the influence of subthreshold damped oscillations arising from intrinsic neuronal dynamics upon information discrimination. In several brain areas and functional conditions sustained oscillations of the membrane potential have been observed. These oscillations are thought to arise mainly through network mechanisms (Buzsaki, 2006), even if intrinsic oscillatory dynamics at the single cell level can also play a role (Llinas, 1988). Since membrane oscillations arising from network mechanisms are the result of external oscillatory input currents, they do not affect intrinsic discriminability in the linear subthreshold approximation considered here (see Section 2.3). Sustained subthreshold oscillations can also arise from intrinsic mechanisms in the presence of a subthreshold limit cycle or strange attractor. In this case intrinsic discriminability is

expected to depend upon the state vector at the time of each applied synaptic potential, and its characterization can be accomplished through numerical analysis.

In this chapter we considered an idealized scenario in which the neuron sits at its stable point, receives a train of instantaneous EPSPs with constant amplitude, and it is then free to evolve according to its intrinsic dynamics alone. The adoption of linear models guarantees that the presented results also hold if the input histories include fluctuating currents ("frozen noise"), as long as they are equal among different input histories. Furthermore, intrinsic discriminability does not depend upon the neuron state at the moment of input arrival in linear models. Nevertheless, it is not clear whether intrinsic discriminability could still serve as a reliable indicator of the current context in a complex, non-linear neuron as the input histories include unknown time-varying components. From a dynamical perspective, the consistent encoding of incoming information could still be achieved if the neuron state is driven to a restricted portion of its state space before receiving its temporally-structured inputs. This task could be accomplished by network oscillations (Buzsaki, 2006; Schaefer et al., 2006): periodic inhibition could format the continuous stream of incoming synaptic events in blocks of fixed temporal duration, by driving the neuron to a restricted portion of its state space at each peak of the total inhibitory drive (Li et al., 2006). This periodic "reset" would allow the consistent contextualization of the EPSPs on a cycle-by-cycle basis. Periodic excitation could play a similar role. For networks operating in an asynchronous, irregular firing regime, results from random dynamical system theory (Arnold, 2003) reveal that in certain conditions a neuron injected with a pseudo-random stimulus will soon forget its initial state and converge to a stochastic, time-varying attractor (Tateno and Pakdaman, 2004; Pakdaman, 2002). Hence, temporally structured inputs time-locked to the stochastic attractor might be consistently encoded through the proposed mechanism even in non-linear neurons. In this case, the transient memory trace induced by the external stimulus would gradually wane as the neuron trajectory converges to the stochastic attractor corresponding to a given noise realization. Nevertheless, more work is needed in the field in order to clarify the interplay between sensitivity and reliability in neuronal network dynamics (Legenstein and Maass, 2007; van Vreeswijk and Sompolinsky, 1996; Izhikevich and Edelman, 2008).

One last remark regards the definition of neuronal excitability as the minimal excitatory synaptic strength capable of firing the neuron. In the translation from the state vector to a scalar, spike-related measure of the neuron's propensity to firing, we defined neuronal

excitability as the minimal excitatory synaptic strength capable of firing the neuron. While such a translation is useful for the comparison between different neuron types, the exact definition we propose might sound arbitrary. For instance, neurons receiving an intense barrage of EPSPs and IPSPs might fire mostly because of a reduction in the total inhibitory conductance, rather than because of an increment in the total excitatory drive (Rudolph et al., 2007). A generalization of the intrinsic excitability that takes into account post-inhibitory rebound spiking and more general threshold manifolds will be necessary to gain insight into this issue. While the exact definition of intrinsic excitability is somewhat arbitrary, the general concept presented is powerful enough to foster the study of single-neuron discrimination properties, which has been largely disregarded in the literature.

4.4.3 Consequences at the network level

The presence of an intrinsic memory in each processing unit is likely to have profound consequences at the network level, and to foster the emergence of complex functions in biological circuits. It is now widely accepted that network function is not entirely specified by the network connectivity, but depends upon its neuromodulatory state, and its history of activity and afferent inputs (see, for example, (Saideman et al., 2007; Proekt et al., 2004; Fellous et al., 2003), reviewed in (Nadim et al., 2008)). Sometimes the same network can produce the same output in different network states, which are only revealed if specific electrophysiological or pharmacological manipulations are applied to the network (Saideman et al., 2007; Kintos et al., 2008). On the other hand, the state of the network shapes the input-output transformation performed by its constituent neurons, by setting the statistics of the synaptic currents that a representative neuron in the network receives (Fellous et al., 2003; Destexhe et al., 2003; Fontanini and Katz, 2008; Steriade, 2004). We believe that the presence of context-dependent processing capabilities at the single-cell level, or even down to the dendritic domain level, coupled with the domain-specific interneuron innervation (Klausberger and Somogyi, 2008), is a key feature in the emergence of multifunctionality in neuronal networks.

Traditionally, neuronal network computations have been interpreted within a static framework. For instance, in associative neural networks, the synaptic weights determine the set of attractors toward which any initial network state will evolve, after a transient which is thought to bear no relevant information (Hopfield, 1982). This framework has been experimentally reinforced through working memory studies which revealed how clue-

specific subset of neurons remained continuously active during the delay period in delayed match-to-sample tasks (see (Funahashi and Takeda, 2002; Wang, 2001) for review). More refined experimental paradigms which separated the clue and the target both in time and space revealed a more dynamical network processing: individual neurons can shift their tuning from a purely stimulus-driven sensitivity to the encoding of prospective actions, during the course of the delay period or over the experimental session (Quintana and Fuster, 1992, 1999; Rainer et al., 1999; Takeda and Funahashi, 2002; Baeg et al., 2003). These experiments have shown that working memory cannot be clearly disentangled from perception, expectation, prediction, and other cognitive computations, since they rely upon largely overlapping neuronal networks. Instead, it seems that transient dynamics in the brain underlie the joint representation of memory clues and what the brain does with them (see also (Scheich et al., 2005)).

In the last few years new theoretical paradigms have been proposed, which are better suited to the interpretation of transient and dynamical computation in neuronal networks (reviewed in (Buonomano and Maass, 2009; Rabinovich et al., 2008, 2006; Durstewitz et al., 2008; Destexhe and Contreras, 2006; Tsuda, 2001)). In particular, some authors have proposed that the variety of time scales involved in neuronal network dynamics, and their distributed nature among many constituent neurons and synapses, form a general purpose computing substrate from which the useful information can be extracted at any given time by properly trained read-out neurons (Maass et al., 2002; Buonomano, 2000; Karmarkar and Buonomano, 2007). In these models (commonly referred to as "state-dependent networks" or "liquid state machines") the distributed synaptic dynamics encodes input history in an analogous way as we discussed in this chapter for a single neuron: each input to the network will have an effect that depends upon the previous network history. In contrast to the linear, few dimensional single-cell models considered in this work, liquid state machines retain some information about past stimuli for periods of time that are much longer than the slower time scale in the system. This behavior is due to their lack of attractors and "edge of chaos" dynamics (Bertschinger and Natschläger, 2004), and to the reverberation of activity through positive feedback. These characteristics make them exquisitely sensitive to small perturbations, whose contributions linger for a long time in the network dynamics.

We believe that the contributions of this work to the theory of state-dependent networks are twofold. On the one hand, the complex dynamical entities in these models are the synaptic connections, while the intrinsic neuronal dynamics is commonly reduced to a

purely passive description. We believe that intrinsic neuronal processes also play a part in determining the complex dynamics of neural microcircuits: as we showed in this chapter, the intrinsic properties determine the evolution of neuronal excitability as a function of the previous history, and will eventually determine whether future stimuli will result in a post synaptic spike or not. On the other hand, when the network state is considered and related to network performance, only the voltage variable of each neuron and the strength of each synapse are taken into account, while internal variables are disregarded (Karmarkar and Buonomano, 2007). This chapter shows that the information contained in single-neuron dynamics is not only that which is transmitted to other neurons in the network through spike-mediated synaptic transmission, but also includes the intrinsic subthreshold dynamics which affects the way a neuron responds to incoming stimuli. Hence, an assessment of their information processing capabilities should take into account all the dynamical variables of the model (synaptic and intrinsic), this being the only level of description that unambiguously defines the microcircuit high-dimensional input-output mapping to an arbitrary spatiotemporal stimulus.

In addition to this, there is a substantial heterogeneity in the intrinsic properties of individual cells in several brain regions, which goes beyond the categorization in neuronal subtypes commonly accepted in the literature (Soltesz, 2005). Nevertheless, most theoretical approaches to neuronal network dynamics have considered the individual cells as homogeneous, or divided in two or few homogeneous populations (for example, excitatory and inhibitory populations (Brunel, 2000)). More recent studies have revealed that neuronal heterogeneity might not be just an epiphenomenon, but might serve specific computational purposes, like the improvement of information representation in a population code (Shamir and Sompolinsky, 2006; Chelaru and Dragoi, 2008), or the generation of complex dynamics in recurrent networks (White et al., 1998). Furthermore, intrinsic neuronal properties and synaptic connectivity are expected to be correlated, given that intrinsic oscillations bias weight dynamics under spike-timing dependent synaptic plasticity (Baroni and Varona, 2010). Hence we strongly encourage the inclusion of a realistic level of heterogeneity in the intrinsic properties of individual cells, as it is likely to highlight new important roles for the wide diversity of intrinsic and synaptic properties in the nervous system.

4.5 Appendix

4.5.1 Integration of the IF neuron model

The differential equation describing the IF model can be solved analytically given the initial conditions of the dynamical variables. In the absence of synaptic input ($I_{syn} = 0$), the solution to (4.1) reads

$$v(t) = v_0 \mathrm{e}^{-\mu t}$$

where v_0 is the initial condition of the voltage variable at time $t = 0$. Hence, in the absence of post synaptic spikes (see Methods), the response of the model neuron to a train of synaptic events at times $(t_0^s, t_1^s, \ldots, t_{n-1}^s)$ can be calculated by iterating the following map:

$$v_i = (v_{i-1} + A)\mathrm{e}^{-\mu \mathrm{ISI_i}}$$

for $i = 1, \ldots, n-1$, where $\mathrm{ISI}_i = t_i^s - t_{i-1}^s$, A is the synaptic strength (assumed for simplicity to be equal among synaptic events), and v_i is the voltage variable just before the arrival of the synaptic event at time t_i^s. The voltage variable after the last spike of the train is calculated as

$$v_n = (v_{n-1} + A)$$

and will be used to calculate the discriminability (see the next section). In all our simulations we set the initial condition for the v variables at the rest state ($v_0 = 0$). The differential equations describing the GIF model have been solved as described in the previous chapter.

4.5.2 Analytical derivation of the discriminability

We define the neuronal excitability in any moment in time as the minimal synaptic strength capable of firing the neuron. The instantaneous intrinsic discriminability between two input histories is then defined, in any moment in time, as the square difference between the excitabilities corresponding to the two input histories. That is,

$$\mathcal{D}_{i,j}(t) = \left(g^i_{thr}(t) - g^j_{thr}(t)\right)^2 = \left(v^j(t) - v^i(t)\right)^2 \tag{4.8}$$

where the last equality is due to the fact that in these linear models the firing threshold depends upon the voltage variable v only. The main measures of intrinsic discriminability we considered are the maximal instantaneous discriminability (maximal value of (4.8)) and the cumulative discriminability, defined as the integral in time from zero to $+\infty$ of the instantaneous discriminability:

$$\mathcal{D}^{\infty}_{i,j} = \int_0^{\infty} \left(g^i_{thr}(t) - g^j_{thr}(t)\right)^2 dt = \int_0^{\infty} \left(v^j(t) - v^i(t)\right)^2 dt$$

The instantaneous and the cumulative discriminability can be computed analytically for the IF and GIF neuron, given the initial conditions for the dynamical variables.

Analytical derivation of the discriminability: IF neuron

For the IF model neuron the instantaneous discriminability can be written as a function of the initial conditions for the voltage variable v^i_0 and v^j_0, corresponding to the neuron's state after input history $\mathcal{H}_i$ and $\mathcal{H}_j$, respectively:

$$\mathcal{D}_{i,j}(t) = \left(v^j(t) - v^i(t)\right)^2 = (v^j_0 - v^i_0)^2 \mathrm{e}^{-2\mu t}$$

This expression integrated from zero to $+\infty$ gives the cumulative discriminability:

$$\mathcal{D}^{\infty}_{i,j} = \int_0^{\infty} \left(v^j(t) - v^i(t)\right)^2 dt = (v^j_0 - v^i_0)^2 \int_0^{\infty} \mathrm{e}^{-2\mu t} dt = \frac{(v^j_0 - v^i_0)^2}{2\mu}$$

Analytical derivation of the discriminability: GIF neuron

For the GIF model neuron the instantaneous discriminability can be written as a function of the initial conditions for the dynamical variables (v^i_0, w^i_0) and (v^j_0, w^j_0), corresponding to the neuron's state after input history $\mathcal{H}_i$ and $\mathcal{H}_j$, respectively:

$$\mathcal{D}_{i,j}(t) = \left(g^i_{thr}(t) - g^j_{thr}(t)\right)^2 = \mathrm{e}^{-2\mu t} \left[(a_j - a_i)\cos(\omega t) + (b_j - b_i)\sin(\omega t)\right]^2$$

where we set $a_{i,j} = v_0^{i,j}$ and $b_{i,j} = \frac{v_0^{i,j}(1-\mu) - w_0^{i,j}(1-2\mu+\mu^2+\omega^2)}{\omega}$. Calculating the square product of the bracketed expression and applying some trigonometric equalities one obtains:

$$\mathcal{D}_{i,j}(t) = \mathrm{e}^{-2\mu t}\left[(a_j - a_i)^2\frac{1+\cos(2\omega t)}{2} + (b_j - b_i)^2\frac{1-\cos(2\omega t)}{2} + (a_j - a_i)(b_j - b_i)\sin(2\omega t)\right]$$

and finally

$$\mathcal{D}_{i,j}(t) = \mathrm{e}^{-2\mu t}\left(\frac{a^2+b^2}{2} + \frac{a^2-b^2}{2}\cos 2\omega t + ab\sin 2\omega t\right)$$

with $a = a_j - a_i$ and $b = b_j - b_i$.

The above expression integrated from zero to $+\infty$ gives the cumulative discriminability:

$$\mathcal{D}_{i,j}^{\infty} = \frac{a^2+b^2}{4\mu} + \frac{\mu(a^2-b^2) + 2\omega ab}{4(\mu^2+\omega^2)}$$

where the indefinite integrals

$$\int \mathrm{e}^{ax}\cos bx = \frac{b}{a^2+b^2}\mathrm{e}^{ax}\sin bx + \frac{a}{a^2+b^2}\mathrm{e}^{ax}\cos bx$$
$$\int \mathrm{e}^{ax}\sin bx = \frac{a}{a^2+b^2}\mathrm{e}^{ax}\sin bx - \frac{b}{a^2+b^2}\mathrm{e}^{ax}\cos bx$$

have been used. Thus, it is a quadratic function in $\Delta v = v_j - v_i$ and $\Delta w = w_j - w_i$, whose orientation and eccentricity are determined by the neuron's parameters μ and ω.

Average discriminability in the presence of Gaussian inputs

The average discriminability in the presence of Gaussian inputs can be calculated as

$$E[\mathcal{D}] = \int_{-\infty}^{0}\int_{-\infty}^{0}\mathcal{D}(i,j)\frac{4}{\mathrm{erfc}\left(\frac{m_i}{\sqrt{2}\sigma}\right)\mathrm{erfc}\left(\frac{m_j}{\sqrt{2}\sigma}\right)2\pi\sigma^2}\mathrm{e}^{-\frac{(t_i-m_i)^2}{2\sigma^2}}\mathrm{e}^{-\frac{(t_j-m_j)^2}{2\sigma^2}}dt_i dt_j$$

where the factors $\mathrm{erfc}\left(\frac{m_i}{\sqrt{2}\sigma}\right)$ and $\mathrm{erfc}\left(\frac{m_j}{\sqrt{2}\sigma}\right)$ take into account the fact that ISIs cannot be non-positive. The standard deviations are assumed equal for both distributions for simplicity. If $\mathcal{D}(i,j) = \mathcal{D}_{IF}(i,j)$ solving yields:

$$E[\mathcal{D}_{IF}] = \left(A^2 \left(\mathrm{e}^{2\mu\left(\mathrm{m_i}+\mu\sigma^2\right)} \mathrm{erfc}\left(\frac{\mathrm{m_j}}{\sqrt{2}\sigma} \right) \mathrm{erfc}\left(\frac{\left(2\mu + \frac{\mathrm{m_i}}{\sigma^2}\right)\sigma}{\sqrt{2}} \right) - \right.$$
$$2\mathrm{e}^{\mu\left(\mathrm{m_i}+\mathrm{m_j}+\mu\sigma^2\right)} \mathrm{erfc}\left(\frac{\left(\mu + \frac{\mathrm{m_i}}{\sigma^2}\right)\sigma}{\sqrt{2}} \right) \mathrm{erfc}\left(\frac{\left(\mu + \frac{\mathrm{m_j}}{\sigma^2}\right)\sigma}{\sqrt{2}} \right) +$$
$$\left. \mathrm{e}^{2\mu\left(\mathrm{m_j}+\mu\sigma^2\right)} \mathrm{erfc}\left(\frac{\mathrm{m_i}}{\sqrt{2}\sigma} \right) \mathrm{erfc}\left(\frac{\left(2\mu + \frac{\mathrm{m_j}}{\sigma^2}\right)\sigma}{\sqrt{2}} \right) \right) \Big/ \left(2\mu \mathrm{erfc}\left(\frac{\mathrm{m_i}}{\sqrt{2}\sigma} \right) \mathrm{erfc}\left(\frac{\mathrm{m_j}}{\sqrt{2}\sigma} \right) \right)$$

In the case of the GIF neuron we further assumed $m_i = m_j = m$ for simplicity, obtaining

$$E[\mathcal{D}_{GIF}] = \frac{A^2 \mathrm{e}^{2m\mu+\sigma^2\left(\mu^2-5\omega^2\right)}}{8\mu\omega^2\left(\mu^2+\omega^2\right)\mathrm{erfc}\left(\frac{m}{\sqrt{2}\sigma}\right)^2} \left(2\mathrm{e}^{4\sigma^2\omega^2} \left(\mathrm{e}^{-2i\left(m+\mu\sigma^2\right)\omega} \mu(-1+\mu-i\omega)^2 \right.\right.$$
$$(\mu+i\omega)\mathrm{erfc}^2\left(\frac{m+\sigma^2(\mu-i\omega)}{\sqrt{2}\sigma} \right) -$$
$$2\left((-1+\mu)^2+\omega^2\right)\left(\mu^2+\omega^2\right)\mathrm{erfc}\left(\frac{m+\sigma^2(\mu-i\omega)}{\sqrt{2}\sigma} \right)\mathrm{erfc}\left(\frac{m+\sigma^2(\mu+i\omega)}{\sqrt{2}\sigma} \right) +$$
$$\left. \mathrm{e}^{2i\left(m+\mu\sigma^2\right)\omega}\mu(\mu-i\omega)(-1+\mu+i\omega)^2\mathrm{erfc}^2\left(\frac{m+\sigma^2(\mu+i\omega)}{\sqrt{2}\sigma} \right) \right) +$$
$$2\mathrm{erfc}\left(\frac{m}{\sqrt{2}\sigma}\right) \left(2\mathrm{e}^{\sigma^2\left(\mu^2+5\omega^2\right)} \left((-1+\mu)^2+\omega^2\right)\left(\mu^2+\omega^2\right)\mathrm{erfc}\left(\frac{m+2\mu\sigma^2}{\sqrt{2}\sigma} \right) - \right.$$
$$\mathrm{e}^{\sigma^2\left(\mu^2+3\omega^2\right)}\mu \left(\mathrm{e}^{-2i\left(m+2\mu\sigma^2\right)\omega}(-1+\mu-i\omega)^2(\mu+i\omega)\mathrm{erfc}\left(\frac{m+2\sigma^2(\mu-i\omega)}{\sqrt{2}\sigma} \right) + \right.$$
$$\left. \left. \left. \mathrm{e}^{2i\left(m+2\mu\sigma^2\right)\omega}(\mu-i\omega)(-1+\mu+i\omega)^2\mathrm{erfc}\left(\frac{m+2\sigma^2(\mu+i\omega)}{\sqrt{2}\sigma} \right) \right) \right) \right)$$

Although the imaginary unit i appears in the above expression, it always evaluates to real values if the model parameters are real.

Chapter 5

Spike timing-dependent plasticity is affected by the interplay of intrinsic and network oscillations

Abstract

In the previous chapters, we studied the effects of intrinsic neuronal properties upon the recognition and generation of temporally precise spike trains. In this chapter, we explore the effects of intrinsic neuronal properties upon the weight dynamics arising from an activity-dependent plasticity rule. In particular, we focus upon a form of Hebbian learning which is sensitive to the precise timing of pre- and postsynaptic firing patterns, known as spike timing-dependent plasticity (STDP). This form of plasticity has been reported in several neuronal systems, and it is thought to underlie structure formation during development, and learning and memory in later life. In this chapter we show that the intrinsic properties of the postsynaptic neuron might have a deep influence on STDP dynamics by shaping the causal correlation between the pre- and the postsynaptic spike trains. The cell-specific effect of STDP is particularly evident in the presence of an oscillatory component in a cell input. In this case, the cell-specific phase response to an oscillatory modulation biases the oscillating afferents towards potentiation or depression, depending upon the intrinsic dynamics of the postsynaptic neuron and the period of the modulation.

Keywords: STDP, single-neuron dynamics, intrinsic oscillations, network oscillations, learning, self-organization.

5.1 Introduction

Experimental results have revealed a form of Hebbian learning which is extremely sensitive to the precise timing of pre- and postsynaptic firing patterns. In particular, in paired-pulse experiments (where brief suprathreshold current pulses are injected in the pre- and postsynaptic cell at a fixed temporal delay) LTP was observed when the evoked presynaptic spike led the postsynaptic spike (thus contributing to postsynaptic firing), while LTD was observed when the evoked presynaptic spike lagged behind the postsynaptic one ((Markram et al., 1997; Bi and Poo, 1998); reviewed in (Dan and Poo, 2004; Bi and Poo, 2001)).

In the last few years, several theoretical works have stemmed from this experimental observations, predicting an important role for STDP in self-organization of neural micro-circuits (Lubenov and Siapas, 2008; Kang et al., 2008; Kempter et al., 2001; Song and Abbott, 2001; Câteau et al., 2008), learning of input correlations (Song et al., 2000; Gütig et al., 2003; Meffin et al., 2006), and output firing rate normalization (Song et al., 2000; Tegnér and Kepecs, 2002; Rubin et al., 2001).

While the influence of different STDP rules upon the weight dynamics and the stationary weight distribution has been studied extensively (reviewed in (Morrison et al., 2008; Kepecs et al., 2002)), only recently there has been some attention drawn to the influence of single-cell intrinsic properties in STDP dynamics (Câteau et al., 2008). The intrinsic dynamics of the postsynaptic cell determine the integration of subthreshold stimuli and the spike generation mechanism (see, for example, (Richardson et al., 2003; Schreiber et al., 2004; Baroni and Varona, 2007; Gutkin et al., 2005)), thus directly affect the cross-correlation between the input and the output spike trains. This consideration suggests that the intrinsic postsynaptic dynamics can potentially have a great impact upon the weight dynamics arising from a certain STDP rule.

In addition to shaping the input-output transformation performed, single-cell intrinsic properties determine the response to oscillatory stimuli. Oscillations of multiple, interacting frequencies are very common in the nervous system (Buzsaki, 2006; Buzsaki and Draguhn, 2004), and the phase of the response of a neuron embedded in an oscillating network is strongly biased by its intrinsic properties (Tateno, 2007; Netoff et al., 2005; Narayanan and Johnston, 2008; Bland et al., 2005). In some neural structures, proteic and morphological characteristics of single cells seem to be precisely tuned in order to produce the observed network dynamics (Whittington and Traub, 2003; Gloveli et al., 2005). Since

synaptic plasticity is highly sensitive to the precise timing of pre- and postsynaptic firing, the presence of an oscillatory component in a cell input is expected to reveal cell-specific biases in the STDP dynamics which would pass unnoticed in the absence of oscillations.

In this chapter we consider a feedforward neuronal architecture where one postsynaptic cell receives a synaptic bombardment from several hundred presynaptic afferents, and compare the stationary weight distributions arising from the same STDP rule and presynaptic firing statistics, but different postsynaptic intrinsic properties. In particular, we compare a purely passive Integrate and Fire (IF) model with an inductive Generalized Integrate and Fire (GIF) model with subthreshold oscillations.

Our results suggest that the intrinsic properties of the postsynaptic cell quantitatively affect the stationary weight distribution under different STDP rules when the input firing patterns are uncorrelated. More interestingly, a sinusoidal modulation of the firing rate of a subset of the presynaptic population reveals qualitative and important differences in the weight dynamics between the IF and the GIF model, which are the focus of this chapter.

5.2 Methods

5.2.1 Neuron models

We considered the Integrate and Fire (IF) and the Generalized Integrate and Fire (GIF), introduced in chapters 4 and 3, respectively. The numerical values of the parameters used here are: $v_{thr} = 20$, $v_{reset} = -4$, $t_{refr} = 0.3$, $\alpha = 1$ and $\beta = 4$ (resulting in complex conjugate eigenvalues $-1 \pm 2i$, denoting subthreshold dampened oscillations with period π), while the intrinsic rate constant of the IF neuron (denoted as μ in section 4) has been set at 1. Given the wide frequency range of intrinsic oscillations observed in mammalian brains, which spans at least two order of magnitude (from 0.5 Hz until 50 Hz (Hutcheon and Yarom, 2000)), we preferred to keep our models dimensionless.

5.2.2 Synaptic description

In general, synaptic dynamics interact with intrinsic neuronal dynamics (Muresan and Savin, 2007), both at the level of a single synaptic potential (in shaping the PSP profile), as during an intense synaptic bombardment from many afferents (in determining the output statistics). Calibration of the synaptic parameters in order to achieve similar PSP profile

in different neurons is possible, but still involves a certain degree of subjectivity regarding which features of the synaptic response should be made equal. In order to guarantee equal postsynaptic effects in different neuron models, we modelled PSPs as instantaneous, voltage independent shifts in the voltage variable:

$$I_{syn} = \sum_{n=1}^{N} \sum_{t_n^s} g_n^{syn} \delta(t - t_n^s) \tag{5.1}$$

where $N = 250$ is the number of afferents, and g_n^{syn} is the synaptic strength of afferent number n. If the synaptic dynamics is fast with respect to the intrinsic neuronal dynamics, this approximation is reasonable (see, for example, (Lubenov and Siapas, 2008)). Furthermore, this choice guarantees a clear separation between the synaptic and the intrinsic dynamics, and assures that the observed differences between the GIF and IF neuron are due to their intrinsic dynamics only. We discretized the simulations in time steps of size $dt = 0.01$ u.t., and in each time step we generated a presynaptic input pattern in which each afferent which is not in its refractory period has a probability p_n of firing. Once an afferent fires, it will not be able to generate another spike for $t_{refr} = 0.3$ u.t..

We divided the afferent population into three subsets: $N_{exc} = 170$ Poisson excitatory afferents with a constant firing probability $p_{exc} = 0.0033$, corresponding to a mean ISI of 3 u.t.; $N_{osc} = 30$ Poisson excitatory afferents with a sinusoidally modulated firing probability $p_{osc} = p_{exc}\left(1 + A_{sin} \sin\left(\frac{2\pi}{T} t\right)\right)$ with period $T = \pi$ (except in Figure 5.4 and 5.6 where it has been varied in a range, and in Figure 5.5 where $T = 1.2743$ or $T = 7.8476$) and modulation amplitude $A_{sin} = 0.5$; $N_{inh} = 50$ Poisson inhibitory afferents with a constant firing probability $p_{inh} = p_{exc} = 0.0033$. The synaptic strengths of the excitatory connections $g_n^{syn} = g_{syn}^{exc} w_n$ are obtained by multiplying the corresponding synaptic weights w_n (which are bounded in the interval [0,1] and subject to STDP) by a scaling factor $g_{syn}^{exc} = 4$. The synaptic strengths of the inhibitory connections are fixed at $g_{syn}^{inh} = 6$.

At the beginning of each simulation the synaptic weights w_n of the excitatory population are homogeneously initialized at their maximal value of 1. These values result in fast and regular postsynaptic firing at a frequency close to the maximal frequency allowed by the refractory period. In this regime the STDP weight dynamics strongly depress most synapses in a non-specific way due to the relative predominance of depression over potentiation (Figure 5.1 and 5.2A, B), until the postsynaptic neuron sets in a lower frequency irregular firing regime. The regular and the irregular firing regimes display large differences not only

in their firing statistics, but also in their response to a sinusoidal modulation (Richardson et al., 2003). Thus we disregarded the first $30 \cdot 10^3$ u.t. of simulation output and focused our analysis on the subsequent evolution of the synaptic weights through STDP in the low frequency, irregular firing regime, during which the mean and the standard deviation of the output ISIs (Inter Spike Intervals) can be considered stationary, as well as the phase of the response to the sinusoidal modulation. This irregular firing regime is more relevant for neuronal physiology, since neurons in many brain areas exhibit highly irregular firing patterns (Shadlen and Newsome, 1998).

All the simulations have been run for $5 \cdot 10^6$ u.t.. Convergence has been assured by visual inspection of the output data and it has always been reached within $2 \cdot 10^6$ u.t. of simulation time.

The sinusoidal modulation in the input rate induces a modulation of the firing probability, which we fit to a sinusoidal function $r_{out}\left(1 + A_g \sin\left(\frac{2\pi}{T}t + \phi\right)\right)$ to obtain the modulation gain A_g and phase ϕ plotted in Figure 5.4, 5.5 and 5.6.

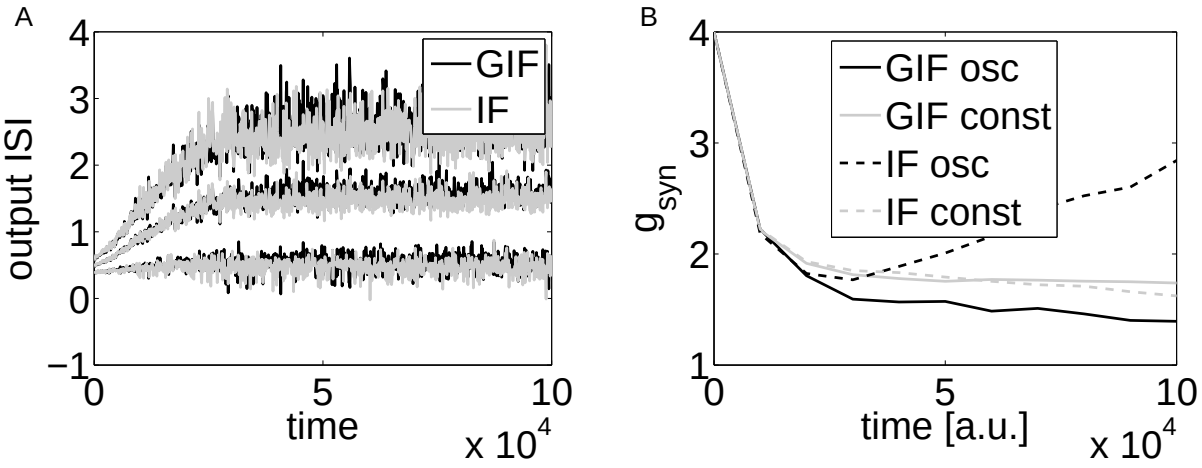

Figure 5.1: The initial parameters result in high frequency regular firing, and unspecific depression of synaptic strengths. A: Evolution of the mean ISI over time for the first 100000 u.t. of simulation. Mean ISI and mean ISI ± standard deviation, calculated over non overlapping windows of 100 u.t., are plotted for the GIF (black line) and IF (gray line) neuron. B: Evolution of the average synaptic strengths over time for the first 100000 u.t. of simulation. Different colours indicate different afferent populations, different line styles indicate different postsynaptic intrinsic properties (see legend).

5.2.3 STDP model

The excitatory synaptic connections are plastic and evolve according to the STDP rule described in (Gütig et al., 2003). In brief, every pair of a presynaptic and a postsynaptic action potentials with time difference $\Delta t = t_{post} - t_{pre}$ induces a weight change given by

$$\Delta w = G(\Delta t|w) = \begin{cases} -\lambda f_-(w)K(\Delta t) & \text{if } \Delta t \leq 0 \\ \lambda f_+(w)K(\Delta t) & \text{if } \Delta t > 0 \end{cases} \tag{5.2}$$

where $K(\Delta t) = e^{-|\Delta t|/\tau}$ is the STDP window function, λ is a learning rate, and $f_\pm(w)$ describe the weight dependence of the STDP rule:

$$f_+ = (1-w)^\mu \qquad f_- = \alpha w^\mu \tag{5.3}$$

where μ is a parameter included in [0,1] which determines the weight dependence of the STDP rule. If $\mu = 0$, $G(\Delta t|w)$ results is the familiar weight independent (additive) STDP rule like in (Song et al., 2000); if $\mu = 1$ one recovers the multiplicative STDP rule like in (Rubin et al., 2001). Note that if $\mu > 0$ the effect of potentiation vanishes as w approaches 1, and so does the effect of depression as w approaches 0, preventing the synaptic efficacies from leaving the allowed range [0,1]. We chose $\mu = 0.02$, a weak weight dependence which corresponds to symmetry breaking in the absence of correlations in the inputs (not shown). The details of the STDP rule are not critical though: since our results depend on the phase response of the model neurons, we expect any temporally asymmetric STDP rule to yield similar results. The parameter α describes the asymmetry between depression and potentiation; we set it at a value slightly greater than 1 ($\alpha = 1.05$) to assure than uncorrelated pre- and postsynaptic firing yield synaptic depression. The numerical values for the other parameters are $\lambda = 0.002$ and $\tau = 0.8$. In most simulations a higher value of λ could be used, resulting in faster convergence to the steady state. Nevertheless, when the phase response is close to zero or positive, small random fluctuations could have a great effect upon the weight dynamics (see the next section). In this situation a small learning rate λ assures a time scale separation between the intrinsic neuronal dynamics, which determine the response to a sinusoidal modulation embedded in a random synaptic bombardment, and the weight dynamics.

5.3 Results

Over time scales shorter than $1/\lambda$, the input-output correlation can be considered stationary and the mean weight drift can be obtained from (5.2) by integrating over the time difference Δt, weighted by its correspondent probability:

$$< \Delta w >= \int_{-\infty}^{\infty} G(\Delta t|w) P_t(\Delta t|w) d\Delta t \tag{5.4}$$

The dependence upon the intrinsic neuronal properties of the postsynaptic cell is included in the input-output correlation term $P_t(\Delta t|w) =< \rho^{pre}(t)\rho^{post}(t+\Delta t, w) >_t$ where $\rho^{pre}(t) = \sum_k \delta(t - t_k^{pre})$ and $\rho^{post}(t, w) = \sum_k \delta(t - t_k^{post})$ are the pre- and postsynaptic spike trains, and $< \cdot >_t$ indicates averaging over time.

The postsynaptic intrinsic properties affect the integration of incoming stimuli, and determine the input-output transformation performed. For instance, an EPSP evoked on a regular spiking neuron at a certain point of its firing cycle can advance or delay its phase depending upon the intrinsic properties of the postsynaptic neuron (Gutkin et al., 2005; Galan et al., 2005; Oprisan and Canavier, 2002; Ermentrout, 1996). Furthermore, the stimulus features which most effectively result in a postsynaptic spike depend upon the type of excitability and the dynamical mechanism of spike generation (Mato and Samengo, 2008).

Intrinsic neuronal properties (in particular, intrinsic oscillations) affect the neuron's behavior in response to a sinusoidal modulation (Richardson et al., 2003). In the irregular firing regime, a purely passive neuron like an IF always follows a sinusoidal modulation with some delay, while a GIF neuron with intrinsic oscillations can synchronize to an input modulation or even lead ahead of it, depending upon its intrinsic frequency and the frequency of the modulation ((Richardson et al., 2003), see also Figure 5.4A).

When the synaptic afferents to a neuron are composed of two different populations, one with a constant firing frequency and another with a sinusoidally modulated firing frequency, the phase with which the postsynaptic neuron follows the sinusoidal modulation determines if the oscillating population will differentiate from the non-oscillating population, and in which direction, through the STDP dynamics. Indeed, an IF neuron which follows a sinusoidal modulation with a phase delay will on average fire after most of the neurons in the oscillating population (Figure 5.3B), leading to a selective strengthening of

the synapses belonging to this group (Figure 5.2D). Conversely, the GIF neuron follows the same sinusoidal modulation without any significant phase difference (Figure 5.3A), hence its spikes will be symmetrically distributed with respect to the oscillating population (see also Figure 5.3C, D), leading to no net potentiation nor depression with respect to the

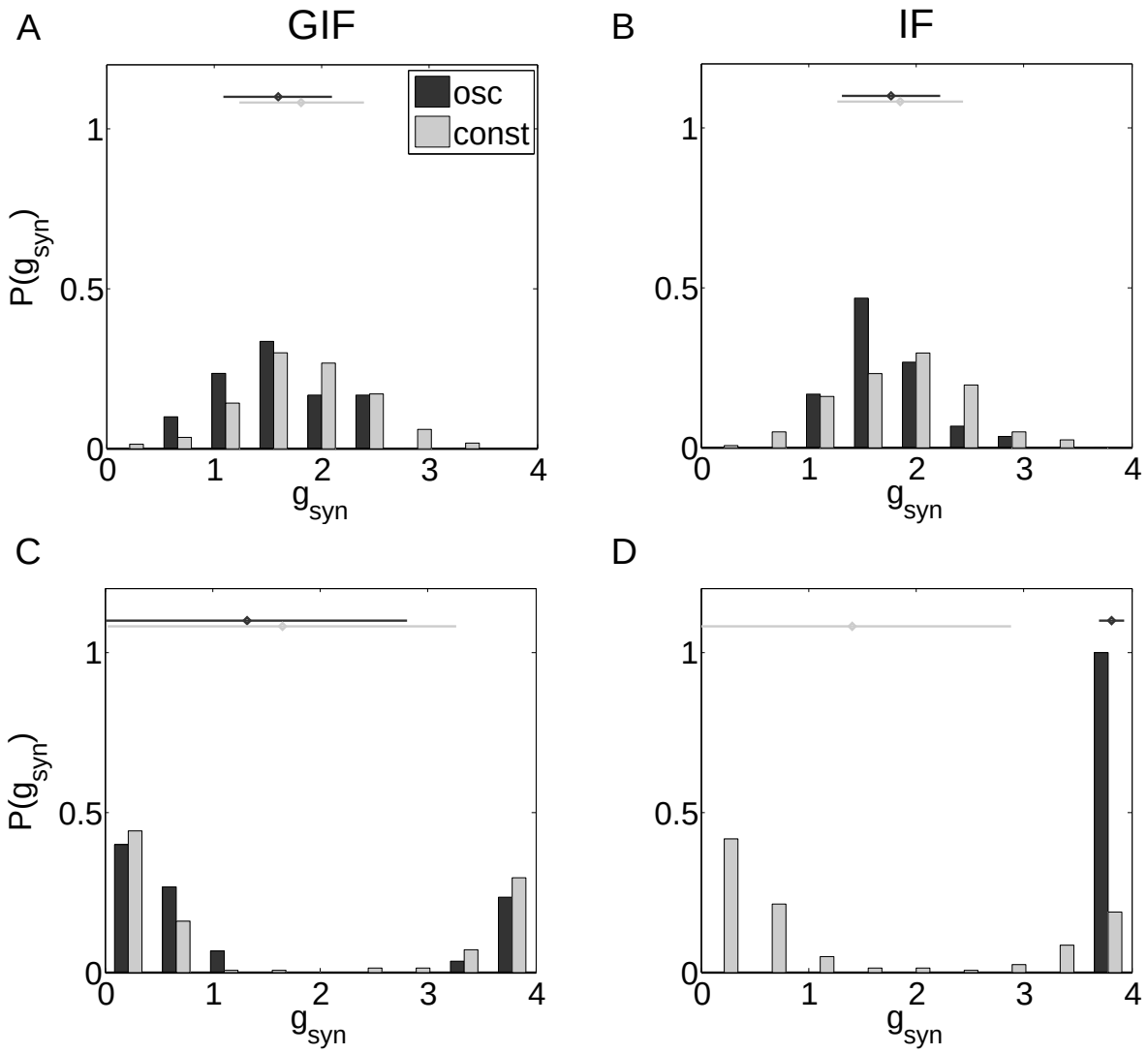

Figure 5.2: Intrinsic neuronal properties determine the dynamics and the equilibrium distribution of the weights under STDP. Distributions of the synaptic weights for the GIF (left) and IF (right) neuron model at the beginning of the low frequency, irregular firing regime (top) and at equilibrium (bottom). For each afferent population, the diamond indicates the mean of the weight distribution and the horizontal line its standard deviation. In the initial high frequency, regular firing regime the synapses are depressed in a non-specific way and reach a unimodal distribution where the oscillatory and non-oscillatory populations overlap (A, B). After learning, the weight distributions are bimodal for both neuron types but while the two populations are still largely overlapping for the GIF neuron (C), the oscillatory population is significantly more potentiated for the IF neuron (D).

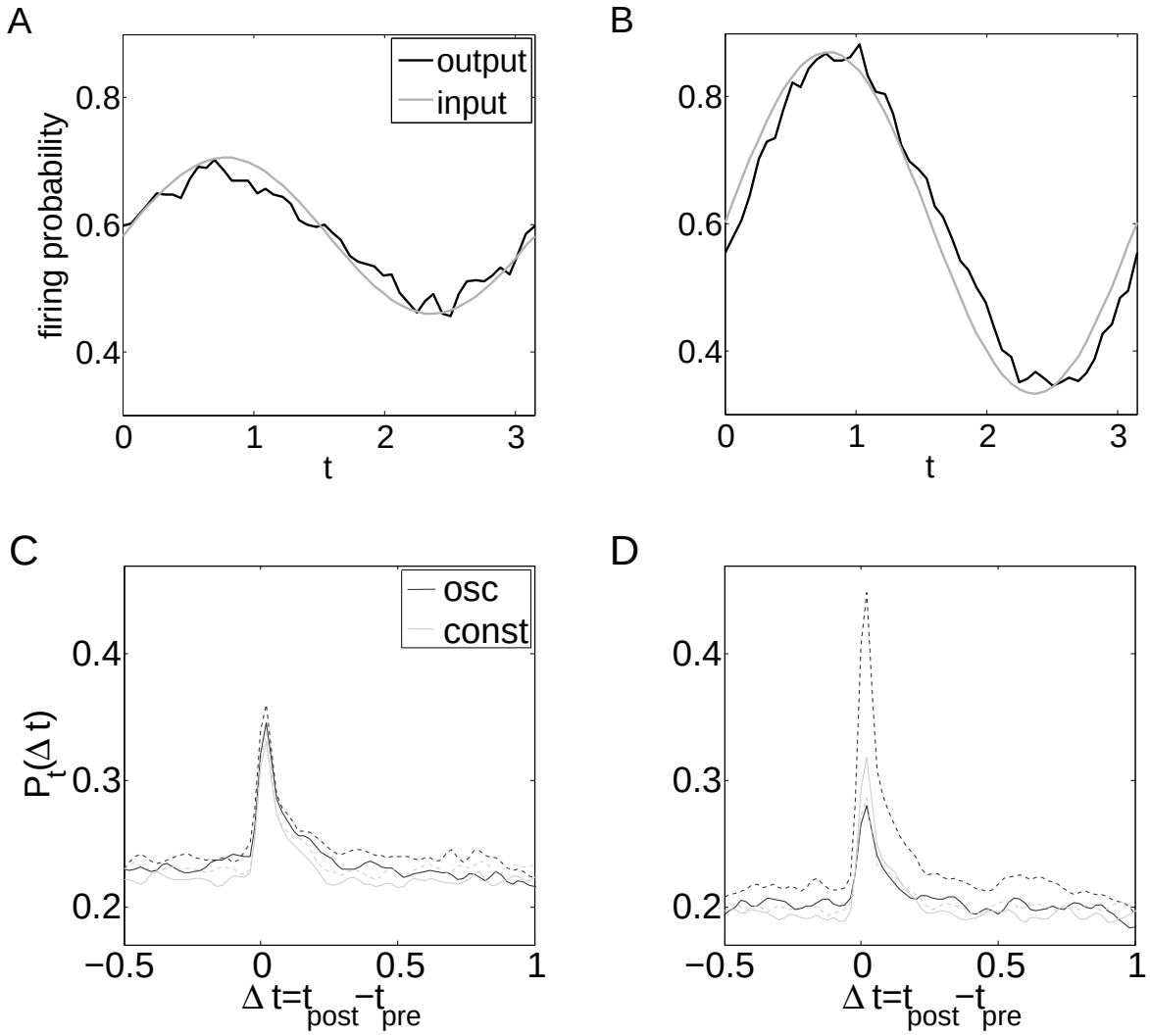

Figure 5.3: Intrinsic neuronal properties determine the phase of the oscillating response, and hence the input-output cross-correlation. A, B: The firing probability along the cycle at the end of the simulation (black line) is plotted together with the sinusoidal modulation of the input firing rate (gray). While the output is in phase with the input for the GIF neuron (left), there is a delay for the IF neuron (right). Moreover, the gain in the IF neuron is increased due to potentiation of the oscillating population. C, D: $P_t(\Delta t)$ is plotted for the oscillatory (black) and non-oscillatory (gray) population for the GIF (solid line) and IF (dashed line) neuron at the beginning of the irregular firing regime (left) and at the end of the simulation (right). At the beginning of the irregular firing regime the oscillating afferents are slightly more efficient in firing the postsynaptic cell due to their common sinusoidal modulation. This can be deduced from the broader input-output correlation and the higher peak. Note that the broadening of the input-output correlation in the oscillating population has an important component for negative Δt pairs in the GIF neuron, while it mainly affects positive Δt pairs in the IF neuron, reflecting the different phase responses of the two neuron types. After learning the input-output correlation has clearly increased for the oscillating subgroup in the IF neuron.

non-oscillating population (Figure 5.2C).

To quantify the degree of separation between the oscillating and the non-oscillating

populations, we computed the ratio between the mean conductance in the two subgroups $R =< g_{osc} > / < g_{const} >$. Figure 5.4 shows the relationship between R and the phase of the sinusoidal response: as expected from our theoretical considerations, the sign of the phase lag determines if the oscillating subgroup will be potentiated or depressed. A negative phase (the postsynaptic neuron lags behind the sinusoidal modulation) results in relative potentiation of the oscillating subgroup of afferents ($R > 1$), while a positive phase leads to relative depression of the oscillatory population ($R < 1$). This general relationship does not hold for very short input periods T, for which a very negative phase results in no differentiation or only slight potentiation of the oscillating subgroup: at very high input frequencies a postsynaptic spike lagging behind a given cycle can also be considered as leading ahead the next cycle, so that as soon as the STDP window becomes comparable in width with the input oscillation period the effects of potentiation and depression tend to cancel out. Measures of the separation between the two different populations which also take into account the standard deviation of the two distributions yielded similar results. In spite of this general tendency, there are some additional differences between the GIF and the IF models which cannot be explained solely on the basis of the phase of the sinusoidal response. For example, for a certain range of negative phase lags there is a stronger potentiation of the oscillating subgroup in the GIF neuron (Figure 5.4B).

The cell-specific potentiation or depression of the oscillating population affects in turn the postsynaptic firing statistics, and in particular the gain of the oscillatory component of the postsynaptic response (Figure 5.5 and 5.6). In particular, a sinusoidal modulation which results in negative phase lag (the postsynaptic cell lags behind the sinusoidal modulation) leads to a selective strengthening of the oscillatory population, which in turn produces an increase in the sinusoidal gain. The opposite trend is observed for modulation periods and postsynaptic intrinsic properties which result in positive phase lag (the postsynaptic cell leads ahead of the sinusoidal modulation). This dynamics is shown in Figure 5.5, where the amplitude gain A_g and the separation index R are plotted for the GIF and IF neurons along a typical simulation for two representative values of the modulation period T. For short modulation periods ($T = 1.2743$ in the plotted example, the non-integer values are due to the logarithmically spaced values for T) both GIF and IF neurons lag behind the sinusoidal modulation, their oscillating afferents are potentiated and their sinusoidal gain is consequently increased (Figure 5.5A, C). For modulation periods slightly greater than the intrinsic period π, the GIF and the IF neurons behave in a qualitative different way:

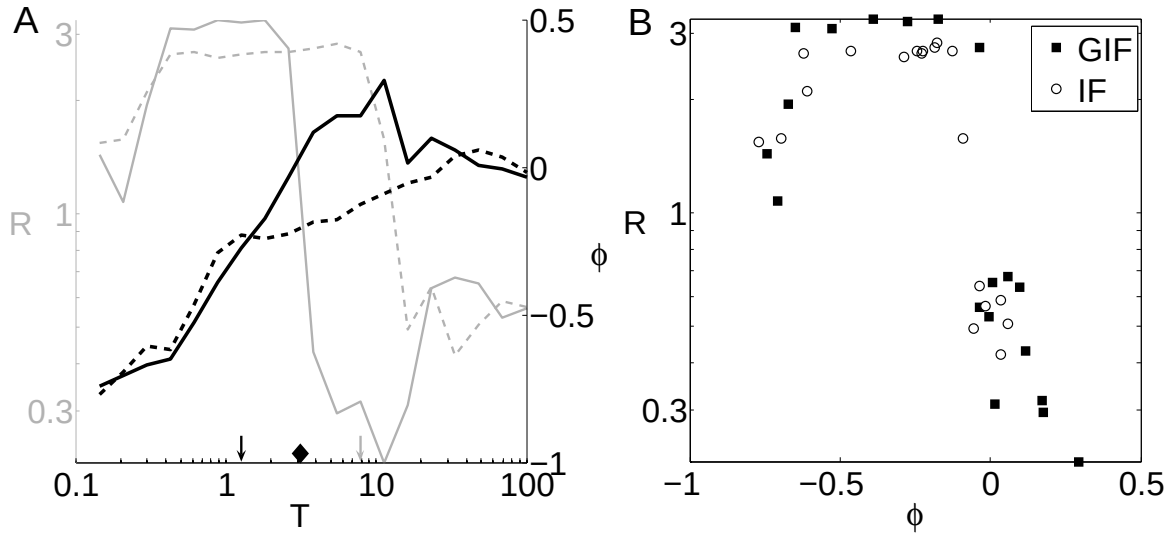

Figure 5.4: The phase of the sinusoidal response determines the mean drift of the oscillating population. A: Ratio between the mean oscillatory conductance and the mean non-oscillatory conductance $R =< g_{osc} > / < g_{const} >$ and phase of the sinusoidal response ϕ for the GIF (solid line) and IF (dashed line) models as a function of the period of the sinusoidal modulation. While the IF neuron always lags behind, the GIF neuron can synchronize with or even lead ahead of the sinusoidal input modulation. The sign of the phase determines the potentiation ($R > 1$) or depression ($R < 1$) of the oscillating population with respect to the other afferents. The black diamond indicates the intrinsic period for the GIF neuron considered, and the input period used in the simulations plotted in Figure 5.2. The black and the gray arrows indicate the input periods used in the simulations plotted in Figure 5.5. B: R ratio for the GIF (filled squares) and IF (empty circles) models after learning is plotted versus the correspondent phase.

the IF neuron still lags behind the sinusoidal modulation, while the GIF neuron leads ahead of it, resulting in an opposite trend in their separation index R and consequently in their gain A_g (compare panels A and C). This cell-specific regulation of the sinusoidal gain through STDP is also apparent in Figure 5.6, where the gain for the GIF (solid) and IF models (dashed) is plotted at the beginning (light gray) and at the end (dark gray) of the simulations, for input periods T spanning three orders of magnitude. For all tested input periods, the difference in gain at the beginning of the simulations is rather small, but it increases dramatically through the action of STDP for those input periods which result in qualitatively different behavior in the GIF and IF neuron (with T in the interval $(3, 10)$ approximately, the phase is positive for the GIF neuron and negative for the IF neuron). Conversely, the difference in gain between the two neuron models remains small for very short or very long modulation periods, for which the two models display similar phase shifts. Note the negative peak in A_g for the GIF neuron, which corresponds to maximal phase advance and consequently maximal relative depression of the oscillating subgroup

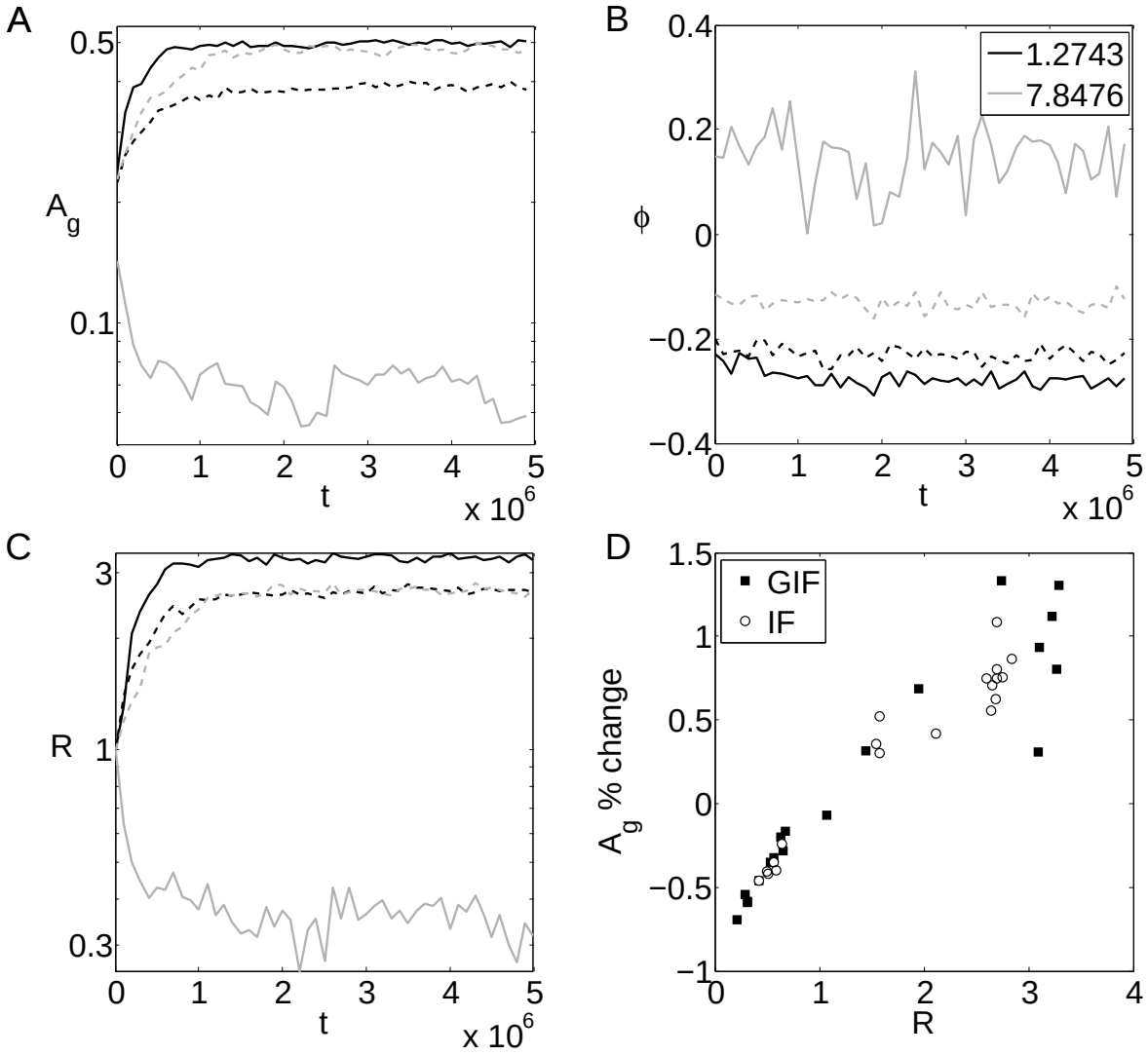

Figure 5.5: Evolution of some relevant quantities along a typical simulation for the GIF (solid line) and IF (dashed line) model, for two different values of the input modulation period. A: Sinusoidal gain A_g. B: Sinusoidal phase ϕ. C: R ratio. D: The relative potentiation of the oscillating population is the main determinant of the change in the sinusoidal gain due to STDP.

(compare Figure 5.6 with Figure 5.4A).

To further clarify the relation between the R index and the sinusoidal gain, we lumped all the data obtained with different T for the same neuron model, and plotted the percentual change in sinusoidal gain A_g during learning versus R for the GIF (filled squares) and IF models (empty circles) (Figure 5.5D). This figure shows that the relationship between the sinusoidal gain change and the oscillating / non-oscillating ratio R is almost linear, with a R value of 1 (indifferentiation between the two subgroup of afferents) resulting in no gain change. This suggests that the evolution of the sinusoidal gain along a simulation is mainly

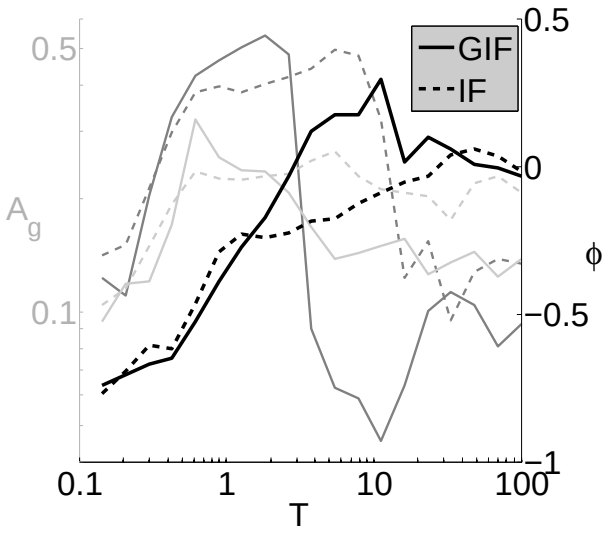

Figure 5.6: Gain and phase of the sinusoidal modulation as a function of the period T of the modulation. The gain is plotted at the beginning of the irregular firing regime (light gray) and at the end of the simulation (dark gray).

driven by the relative potentiation or depression of the oscillating subgroup.

The effect of STDP on the phase lag of the different model neurons is somewhat more subtle. When the postsynaptic neuron lags behind the sinusoidal modulation, the oscillating afferents are potentiated with respect to the other afferents, and keep the postsynaptic cell at a constant, negative phase. Conversely, when the postsynaptic neuron leads ahead of the sinusoidal modulation, the oscillating afferents are depressed and their entrainment of the postsynaptic cell is less efficient, resulting in low sinusoidal gain and variable, positive phase (Figure 5.5C).

5.4 Discussion

In this chapter we considered a simplified framework, in which a single postsynaptic cell receives a synaptic bombardment from several hundred presynaptic afferents in a purely feedforward configuration. While the adoption of a simplified model is useful in dissecting the minimal dynamical mechanisms required for the observed behavior, the introduction of additional biological details might significantly alter, or extend, our results. In this section we discuss the main assumptions of our model which are not expected to hold in biological neural networks, discuss how they might affect our results, and suggest future work which will further unravel the complex interplay between neuronal properties and

synaptic plasticity.

In our approach we did not take into account propagation delays along neurites. However, the effects of linear, frequency-independent propagation delays can easily be predicted in the current framework. If we consider an axonal conductance delay τ_a from the soma of the presynaptic neuron until the synaptic contact, and a dendritic conductance delay τ_d from the synaptic contact until the soma of the postsynaptic cell (equal among afferents for simplicity), we expect the phase response to be delayed by $(\tau_a + \tau_d)/T$, where T is the period of the sinusoidal modulation. This will result in a shrinking of the frequency range with positive phase response, suggesting a bias towards potentiation of the oscillating population. However, this latter effect depends upon the relative magnitude of the axonal and dendritic conductance delays. Given that synaptic modifications depends upon the relative timing of the pre- and postsynaptic activity as observed at the synaptic site (more precisely, upon the time difference between the calcium influx through synaptically gated postsynaptic channels and the postsynaptic depolarization due to a backpropagating action potential (Markram et al., 1997)), we could substitute Δt in equation (5.2) with $\Delta t_{syn} = t_{post}^{syn} - t_{pre}^{syn} = \Delta t + (\tau_d - \tau_a)$. Since in most cases the propagation delay along the axon is greater than along the dendrite, we would expect a rightward shift of the temporal dependence of STDP, with zero phase lag observed at the somae resulting in synaptic depression, thus partially compensating for the downward shift in the phase response.

The adoption of a more realistic synaptic description, i.e. exponentially decaying synaptic conductances or alpha functions, is also expected to increase the phase lag, because the synaptic current will peak a certain time after its onset. We performed some exploratory simulations with exponential synapses, and indeed observed a general downward shift in the phase response and consequently a bias towards potentiation of the oscillating population (not shown). As the synaptic dynamics interacts with the intrinsic dynamics, the differences between the IF and GIF neuron which could not be attributed to the phase response are bigger than in the present case, and deserve further study which will be addressed in the future. The adoption of linear neuron models might also seem unrealistically simple. However, these simple models with parameters obtained from linearization around the steady state of realistic, conductance-based model neurons have proven to replicate faithfully the response to a weak sinusoidal modulation of their realistic counterparts, even when embedded in strong background noise (Richardson et al., 2003). Still, it is possible that a more realistic spike generation mechanism might affect the neuronal response to a

sinusoidal modulation, especially at high input rates (Fourcaud-Trocmé et al., 2003). This possibility will be addressed in future work.

In our model, the oscillating population follows a sinusoidally modulated Poisson statistics, without any additional temporal structure. Hence, if the postsynaptic cell is in phase with the input modulation, one particular presynaptic neuron will sometimes lead, sometimes lag the postsynaptic response so that the mean synaptic drift it will experience is zero. Conversely, if the oscillating population activity were temporally structured, a differentiation of the oscillating population from the rest of the afferents could still be observed. For instance, if a subset of the oscillating population were imposed to fire earlier on average than the other afferents of the oscillating population, this subset would be expected to undergo potentiation.

Another assumption of our feedforward model which is not expected to hold in generic neuronal networks is the independence between inhibition and excitation. Inhibition if often correlated with excitation, either because of excitatory-inhibitory loops in the same brain area, or because of common inputs from other brain areas which target both interneurons and principal cells (Buzsáki, 1984; Pouille and Scanziani, 2001; Wang et al., 2007). This interdependence might bias synapse strengthening in a cell-specific way. For example, inhibition which shortly precedes excitation increases the responsiveness and reliability of neurons with subthreshold oscillations, but not of purely passive neurons (Mato and Samengo, 2008).

In our model inhibitory connections are fixed, and plasticity of excitatory synaptic weights is the only mechanism responsible for adjusting the spiking statistics of the postsynaptic cell from the initial high frequency, regular spiking regime to the low frequency, irregular firing regime which is commonly observed in the brain. This results in a dependence of the output firing statistics after learning upon the initial values of the synaptic weights. Even if most experimental and theoretical studies have focused on synaptic plasticity of excitatory (typically glutamatergic) synapses, inhibitory connections are also known to undergo activity-dependent plasticity (Gaiarsa et al., 2002), which, at least in some systems, exhibits a high sensitivity to the relative timing of pre- and postsynaptic spiking (Haas et al., 2006). Contrary to the anti-homeostatic effect of excitatory STDP, which tends to strenghten the stronger synapses, the effect of inhibitory STDP is homeostatic, increasing the inhibitory effect if it was not sufficient to prevent the postsynaptic cell from firing. It will be worth exploring whether the interaction of these complementary mechanisms might

result in robust self-organization of network dynamics and, in a feedforward network like the one presented here, in convergence to a given output statistics from a broad range of initial synaptic weights.

5.5 Conclusions

Intrinsic neuronal properties may affect the integration of incoming stimuli in a nontrivial way. For instance, an EPSP evoked on a regular spiking neuron can advance or delay the occurrence of the next spike, depending upon the intrinsic properties of the postsynaptic neuron and the exact time in which it is delivered.

Intrinsic neuronal properties (in particular, intrinsic oscillations) affect the neuron behavior in response to a sinusoidal modulation embedded in a random synaptic bombardment (Richardson et al., 2003). In the irregular firing regime, a purely passive neuron like an IF always follows a sinusoidal modulation with some delay, while a GIF neuron with intrinsic oscillations can synchronize to an input modulation or even lead ahead of it, depending upon its intrinsic frequency and the frequency of the sinusoidal modulation.

The phase of the sinusoidal response determines the net drift that will affect the weights of the oscillating population: if the phase is positive (the postsynaptic neuron leads ahead of the presynaptic sinusoidal modulation) the oscillating population will experience a net depressing effect (most postsynaptic spikes will lead the presynaptic spikes originating from this population), while if the phase is negative (the postsynaptic neuron follows the sinusoidal modulation with some delay) the oscillating population will be potentiated.

The net weight drift experienced by the oscillating population affects in turn the postsynaptic firing statistics, and in particular the sinusoidal gain response. If the postsynaptic neuron follows the sinusoidal modulation with some delay, as in the case of the passive IF neuron, the oscillating population will undergo potentiation and will increase the gain of the sinusoidal modulation. Conversely, if the postsynaptic neuron is synchronized with the sinusoidal modulation, the net weight drift on the oscillating population will be the same as the one experienced by the other afferents, hence the sinusoidal gain will stay constant. Thus, it seems that STDP might have a regulatory effect upon the sinusoidal gain in the presence of oscillatory inputs, by increasing the oscillatory input to target cells which follow the modulation with some delay, while not affecting or even decreasing the oscillatory

inputs to target cells which display intrinsic oscillations in resonance with the frequency of the oscillatory modulation.

Since both network oscillations and intrinsic resonant neurons are widespread in many brain areas, we believe that this mechanism might be highly relevant for structure formation during both development and mature life. For example, we could hypothesize that the distribution of intrinsic neuronal properties in a certain brain area might impose some restrictions upon the possible wiring schemes, thus contributing to the specification of network connectivity and possibly decreasing the amount of information about wiring which needs to be genetically encoded. This effect is expected to be especially relevant in higher and evolutionarily more recent neural structures, where the heterogeneity of intrinsic properties is higher (Freund and Buzsáki, 1996; Markram et al., 2004; Somogyi and Klausberger, 2005). Intrinsic single-cell properties might tune incoming connections in order to enhance responsiveness to neuronal assemblies which tend to fire at a certain phase of network oscillations, thus fostering specialization and multiplexing in network processing (Friedrich et al., 2004). According to our numerical results, we expect passive neurons to be driven mostly by synchronized presynaptic assemblies which fire at the peak of the oscillatory input component, while neurons with subthreshold oscillations might more often develop strong connections from neurons which tend to fire earlier than their other afferents.

Finally, single-cell processing is a distributed phenomenon. Single domains along the neuronal morphology can be characterized by specific intrinsic properties (Johnston and Narayanan, 2008), interneuron innervation (Klausberger and Somogyi, 2008) and local plasticity rules (Froemke et al., 2005; Letzkus et al., 2006; Saudargiene et al., 2005). The investigation about the complex interplay between network oscillations, the heterogeneity of intrinsic neuronal dynamics, and the local nature of synaptic plasticity is likely to be of key importance for understanding information processing in the nervous system.

Chapter 6

Conclusions

6.1 Main results of the present thesis

The main results of this work can be summarized by chapter as follows:

Chapter 2

- Calcium and voltage dynamics are bidirectionally coupled; this interaction results in some features which are highly restrained, while others are free to evolve almost independently.
- The bidirectional coupling between voltage and calcium is better described when multiple temporal scales are taken into account. The interaction between dynamics on different temporal scales can be the basis for contextual information processing in single neurons.

Chapter 3

- The interplay between subthreshold damped oscillations and after-spike effects results in complex input-output mappings in single neurons.
- Simple linear models with after-spike reset can reproduce much of the observed features of input-output relationships of detailed conductance-based models.

Chapter 4

- A formal definition of history-dependent excitability allows the quantitative assessment of the mnemonic features of intrinsic neuronal dynamics.
- Subthreshold oscillations enhance single-cell information discrimination at high input rates.
- Neurons with subthreshold oscillations are advantageous for information processing based on a temporal coding scheme, while passive neurons are better suited to computation based on a rate coding scheme.

Chapter 5

- The intrinsic properties of the postsynaptic cell can have a deep impact upon weight dynamics arising from activity-dependent plasticity rules.
- An oscillatory component in the input to a cell will impose a certain phase which depends upon its intrinsic properties, which in turn will bias the weight dynamics arising from a temporally sensitive synaptic plasticity rule.

Taken together, these results clearly point to a key role for the interaction between dynamics on multiple time scales in the generation and recognition of precisely timed neuronal patterns, as well as in structure formation mediated by activity dependent synaptic plasticity rules.

The discriminability properties at the single cell level which we describe in sections 3 and 4 constitute a local form of information contextualization which could have profound consequences at the network level. Though not formally demonstrated yet, a network composed of complex and heterogeneous individual units, each of them capable of decisions which depend in a non-trivial way upon the previous input-output history, will show a range of collective behaviors which is not reproducible by networks of homogeneous units with mainly passive intrinsic properties. Indeed, numerous experimental studies have reported a high degree of neuronal heterogeneity in various brain areas, and have inspired several theoretical works investigating the effects of heterogeneity in network computation, with respect to both the generated dynamics and the coding capabilities. However, the range of heterogeneities considered in these studies is quite restricted and does not encompass the wide range of different active properties observed in real neurons, hence the effects of neuronal heterogeneity in network information processing is only partially understood.

Some of the main results of this thesis constitute theoretical predictions that can be verified experimentally. For example, in chapter 4 we provide clear guidelines for the design of an experimental protocol aimed at characterizing the intrinsic discriminability properties of neuronal cells. This protocol could be implemented in a dynamic clamp software, probing the mnemonic features based on intrinsic single-cell dynamics in an automatized manner and with the minimum number of trials. The impact of single cell neuronal properties in network dynamics can now be tested experimentally with optogenetic techniques (Boyden et al., 2005; Miller, 2006), which allow the modification of single-cell intrinsic properties of a selected cell class in a highly controlled fashion.

Even if we only considered a feed-forward architecture, our results about the effects of intrinsic neuronal properties upon weight dynamics can be confirmed through the simultaneous analysis of intrinsic neuronal properties and the distribution of incoming connection weights. Such data is difficult to obtain, especially in an amount which could lead to statistically significant results, but might become available in the near future thanks to the technological advances in large scale multielectrode array and imaging recordings, combined with sophisticated stimulation and analysis tools.

6.2 Concluding remarks

A single neuron is by itself a highly complex biological entity. When billions of them are connected in a network by synaptic and neuromodulatory links which are themselves dynamically complex, the concepts of causation, top-down and bottom-up information transfer can only offer a partial description of the resulting behavior. In fact, the resulting dynamics might be better understood in the framework of complex emerging phenomena. This framework challenges the Aristotelian view of mechanistic sequences of "causes" and "effects", which is inevitably hard-wired in the common intuition of western society, while it stresses the circular relationship between complex individuals and the complex dynamics of the networks they belong to. Every individual is constrained by the activity of the population, but even a single individual affects the emerging population outcome, especially if the system is endowed with chaotic dynamical features.

From my personal perspective, I believe that a comparison with social sciences is useful for understanding the relationship between reductionism and complexity in computational neuroscience. Even if the wide diversity of personal characters, personalities, skills and attitudes is a key ingredient in the evolutionary success of human societies, extremely simple "social-physics" models (also known as human thermodynamics approaches, to highlight the strong reductionism commonly applied to individuals in these models) can explain and successfully predict a wealth of social phenomena, from political preferences, attitude towards crime to the transfer and evolution of cultural traits (Ball, 2004).

As highly complex individuals embedded in topologically complex networks, neuronal cells might seem all alike when viewed from a population perspective. Notably, when their morphological, physiological and molecular complements are assessed in detail, they all look quite different. In spite of the strong efforts towards defining a widely agreeable taxonomy

of neuronal types, the variability observed within neuronal classes is so broad that such taxonomies are becoming hard to justify. Within a neuronal class, which is usually defined by the morphological characteristics of the cell, the neurotransmitter it releases and the proteic complement it expresses, individual neurons differ in the precise distribution of ion channels along their morphology (affecting the input-output transformation they perform), and maybe more importantly, in the position they hold in the network: that is, in the identity of their pre and post synaptic targets (Chou et al., 2010). Recent data revealed that both the number of connection per neuron and their strength are scale-free (Song et al., 2005). This means that a few strong connections emerge from a sea of weaker ones, and that a small minority of cells constitute "hubs" of network computation, connecting to a much greater number of neurons than the average. This heterogeneity is probably one of the key ingredient in the emergence of complex functions in neuronal networks.

So far, reductionist approaches in computational neuroscience have obtained important successes in explaining several biophysical and cognitive phenomena within simple mathematical frameworks. At the single cell level, two-variable model neurons can explain the rapid up-stroke of membrane voltage during the generation of an action potential, and the subsequent refractory behavior (Fitzhugh, 1961; Morris and Lecar, 1981). Three-variable neurons can reproduce, as parameters are varied, many different dynamical classes of bursting behavior (Izhikevich, 2006). At the network level, relatively simple mathematical models give satisfactory explanations of several cognitive phenomena, from working memory (Wang, 2001) to dead-reckoning navigation (Maurer and McNaughton, 2007), from visual illusions (Bressloff et al., 2002; Schwartz et al., 2009) to time perception (Karmarkar and Buonomano, 2007), recently reaching hard to define concepts such as consciousness (Dehaene and Changeux, 2005), often providing a close match with psychophysical data.

In contrast, the inclusion of all the available biophysical knowledge in a neuronal model is seldom, or hardly ever, justified. It is surely tempting to include a great level of realism in neuronal simulations, in part as an effort towards "realistic" modelling, which allows the direct association between mathematical variables in the model and experimentally measurable quantities in the biology, and in part because of the strong interest from the general media about artificial life in general, and artificial intelligence in particular. Nevertheless, the more biophysical details are incorporated in a model, the more difficult is the interpretation of the obtained dynamics. Not only the huge parameter space of these models is

difficult or impossible to constrain. Even if we could constrain experimentally each of the intervening parameters, it would be hard or impossible to identify the biophysical features which are responsible for the given phenomenon under study. Indeed, it is possible that these extremely detailed simulations would produce an output which is not statistically different from one obtained from much simpler versions of the model.

Hence, it is useful to gradually increase the level of detail in models, with the awareness that different biophysical mechanisms could have similar dynamical outcomes, and that proper function in the nervous system is likely to rely upon a machinery of redundant biophysical mechanisms, whose relative contribution could be modulated by complex signalling networks which could act in a homeostatic fashion to guarantee the correct physiological performance of the system, and its robustness in the face of external (environmental) or internal (developmental, pathological) changes. Complementarily, it is also useful to simplify existing models based on a great level of biophysical detail, in order to determine which properties are key in order to reproduce each of the observed features of the biological system.

Bibliography

Abarbanel, H. D. and Talathi, S. S. (2006). Neural circuitry for recognizing interspike interval sequences. *Physical review letters*, 96(14).

Abbott, L. F. and van Vreeswijk, C. (1993). Asynchronous states in networks of pulse-coupled oscillators. *Physical Review E*, 48(2):1483–1490.

Abbott, L. F., Varela, J. A., Sen, K., and Nelson, S. B. (1997). Synaptic depression and cortical gain control. *Science*, 275(5297):220–224.

Amit, D. J. and Brunel, N. (1997). Model of global spontaneous activity and local structured activity during delay periods in the cerebral cortex. *Cerebral cortex (New York, N.Y. : 1991)*, 7(3):237–252.

Anderson, R. B. (2001). The power law as an emergent property. *Memory & cognition*, 29(7):1061–1068.

Arganda, S., Guantes, R., and de Polavieja, G. G. (2007). Sodium pumps adapt spike bursting to stimulus statistics. *Nature neuroscience*, 10(11):1467–1473.

Arnold, L. (2003). *Random Dynamical Systems (Springer Monographs in Mathematics)*. Springer.

Baeg, E. H., Kim, Y. B., Huh, K., Mook-Jung, I., Kim, H. T., and Jung, M. W. (2003). Dynamics of population code for working memory in the prefrontal cortex. *Neuron*, 40(1):177–188.

Baker, S. N. and Lemon, R. N. (2000). Precise spatiotemporal repeating patterns in monkey primary and supplementary motor areas occur at chance levels. *J Neurophysiol*, 84(4):1770–1780.

Ball, P. (2004). *Critical Mass: How One Thing Leads to Another*. Farrar, Straus and Giroux, 1st edition.

Baluska, F. and Mancuso, S. (2009a). Deep evolutionary origins of neurobiology: Turning the essence of 'neural' upside-down. *Communicative & integrative biology*, 2(1):60–65.

Baluska, F. and Mancuso, S. (2009b). Plant neurobiology: from sensory biology, via plant communication, to social plant behavior. *Cognitive processing*, 10 Suppl 1.

Barlow, H. (1996). Intraneuronal information processing, directional selectivity and memory for spatio-temporal sequences. *Network (Bristol, England)*, 7(2):251–259.

Baroni, F. (2005). Effects of slow modulation in the temporal structure of neural spiking activity. Master's thesis, Escuela Politecnica Superior, Universidad Autonoma de Madrid.

Baroni, F., Torres, J. J., and Varona, P. (2005). Interacting slow and fast dynamics in precise spiking-bursting neurons. *LNCS*, 3561:106–115.

Baroni, F., Torres, J. J., and Varona, P. (2010). History-dependent excitability as a single-cell substrate of transient memory for information discrimination. Submitted to Journal of Computational Neuroscience.

Baroni, F. and Varona, P. (2007). Subthreshold oscillations and neuronal input-output relationships. *Neurocomputing*, 70(10-12):1611–1614.

Baroni, F. and Varona, P. (2010). Spike timing-dependent plasticity is affected by the interplay of intrinsic and network oscillations. *Journal of Physiology, Paris*, 104(1-2):91–98.

Beggs, J. M. (2008). The criticality hypothesis: how local cortical networks might optimize information processing. *Philosophical Transactions of the Royal Society A: Mathematical, Physical and Engineering Sciences*, 366(1864):329–343.

Beggs, J. M. and Plenz, D. (2003). Neuronal avalanches in neocortical circuits. *J. Neurosci.*, 23(35):11167–11177.

Beggs, J. M. and Plenz, D. (2004). Neuronal avalanches are diverse and precise activity patterns that are stable for many hours in cortical slice cultures. *J. Neurosci.*, 24(22):5216–5229.

Berridge, M. J. (1998). Neuronal calcium signaling. *Neuron*, 21:13–26.

Bertschinger, N. and Natschläger, T. (2004). Real-time computation at the edge of chaos in recurrent neural networks. *Neural Comput.*, 16(7):1413–1436.

Bi, G.-q. and Poo, M.-m. (1998). Synaptic modifications in cultured hippocampal neurons: Dependence on spike timing, synaptic strength, and postsynaptic cell type. *J. Neurosci.*, 18(24):10464–10472.

Bi, G. Q. and Poo, M. M. (2001). Synaptic modification by correlated activity: Hebb's postulate revisited. *Annual Review of Neuroscience*, 24(1):139–166.

Bland, B. H., Konopacki, J., and Dyck, R. (2005). Heterogeneity among hippocampal pyramidal neurons revealed by their relation to theta-band oscillation and synchrony. *Experimental neurology*, 195(2):458–474.

Borgmann, A., Hooper, S. L., and Buschges, A. (2009). Sensory feedback induced by front-leg stepping entrains the activity of central pattern generators in caudal segments of the stick insect walking system. *J. Neurosci.*, 29(9):2972–2983.

Boyden, E. S., Zhang, F., Bamberg, E., Nagel, G., and Deisseroth, K. (2005). Millisecond-timescale, genetically targeted optical control of neural activity. *Nature neuroscience*, 8(9):1263–1268.

Bressloff, P. C., Cowan, J. D., Golubitsky, M., Thomas, P. J., and Wiener, M. C. (2002). What geometric visual hallucinations tell us about the visual cortex. *Neural computation*, 14(3):473–491.

Briggman, K. L. and Kristan, W. B. (2008). Multifunctional pattern-generating circuits. *Annual Review of Neuroscience*, 31(1):271–294.

Brunel, N. (2000). Dynamics of sparsely connected networks of excitatory and inhibitory spiking neurons. *Journal of computational neuroscience*, 8(3):183–208.

Bucher, D., Prinz, A. A., and Marder, E. (2005). Animal-to-animal variability in motor pattern production in adults and during growth. *J. Neurosci.*, 25(7):1611–1619.

Buonomano, D. V. (2000). Decoding temporal information: A model based on short-term synaptic plasticity. *J Neurosci*, 20(3):1129–1141.

Buonomano, D. V. and Maass, W. (2009). State-dependent computations: spatiotemporal processing in cortical networks. *Nature Reviews Neuroscience*, 10(2):113–125.

Buzsáki, G. (1984). Feed-forward inhibition in the hippocampal formation. *Progress in neurobiology*, 22(2):131–153.

Buzsaki, G. (2006). *Rhythms of the Brain*. Oxford University Press, USA, 1 edition.

Buzsaki, G. and Draguhn, A. (2004). Neuronal oscillations in cortical networks. *Science*, 304(5679):1926–1929.

Calabrese, R. L. (1979). The roles of endogenous membrane properties and synaptic interaction in generating the heartbeat rhythm of the leech, hirudo medicinalis. *The Journal of experimental biology*, 82:163–176.

Calabrese, R. L., Nadim, F., and Olsen, O. H. (1995). Heartbeat control in the medicinal leech: a model system for understanding the origin, coordination, and modulation of rhythmic motor patterns. *Journal of neurobiology*, 27(3):390–402.

Campos, D., Aguirre, C., Serrano, E., de Borja Rodríguez, F., de Polavieja, G. G., and Varona, P. (2007). Temporal structure in the bursting activity of the leech heartbeat cpg neurons. *Neurocomputing*, 70(10-12):1792–1796.

Câteau, H., Kitano, K., and Fukai, T. (2008). Interplay between a phase response curve and spike-timing-dependent plasticity leading to wireless clustering. *Physical review. E, Statistical, nonlinear, and soft matter physics*, 77(5 Pt 1).

Chelaru, M. I. and Dragoi, V. (2008). Efficient coding in heterogeneous neuronal populations. *Proceedings of the National Academy of Sciences of the United States of America*, 105(42):16344–16349.

Chou, Y.-H. H., Spletter, M. L., Yaksi, E., Leong, J. C., Wilson, R. I., and Luo, L. (2010). Diversity and wiring variability of olfactory local interneurons in the drosophila antennal lobe. *Nature neuroscience*, 13(4):439–449.

Cole, K. S. (1932). Electric phase angle of cell membranes. *J. Gen. Physiol.*, 15(6):641–649.

Cole, K. S. (1941). Rectification and inductance in the squid giant axon. *J. Gen. Physiol.*, 25(1):29–51.

Coombes, S., Lord, G. J., and Owen, M. R. (2003). Waves and bumps in neuronal networks with axo-dendritic synaptic interactions. *Physica D: Nonlinear Phenomena*, 178(3-4):219–241.

Cooper, S. and Adrian, E. D. (1923). The frequency of discharge from the spinal cord in the frog. *J Physiol*, 58(2-3):209–229.

Cossart, R., Aronov, D., and Yuste, R. (2003). Attractor dynamics of network up states in the neocortex. *Nature*, 423(6937):283–288.

Dallman, J. E., Davis, A. K., and Moody, W. J. (1998). Spontaneous activity regulates calcium-dependent k+ current expression in developing ascidian muscle. *The Journal of Physiology*, 511(3):683–693.

Dan, Y. and Poo, M. M. (2004). Spike timing-dependent plasticity of neural circuits. *Neuron*, 44(1):23–30.

de Polavieja, G. G., Harsch, A., Kleppe, I., Robinson, H. P., and Juusola, M. (2005). Stimulus history reliably shapes action potential waveforms of cortical neurons. *The Journal of neuroscience : the official journal of the Society for Neuroscience*, 25(23):5657–5665.

De Valois, R. L. L., Jacobs, G. H. H., and Jones, A. E. E. (1962). Effects of increments and decrements of light on neural discharge rate. *Science*, 136(3520):986–988.

deCharms, R. C. and Merzenich, M. M. (1996). Primary cortical representation of sounds by the coordination of action-potential timing. *Nature*, 381(6583):610–613.

Dehaene, S. and Changeux, J.-P. P. (2005). Ongoing spontaneous activity controls access to consciousness: a neuronal model for inattentional blindness. *PLoS biology*, 3(5):e141+.

Destexhe, A. and Contreras, D. (2006). Neuronal computations with stochastic network states. *Science*, 314(5796):85–90.

Destexhe, A., Rudolph, M., and Pare, D. (2003). The high-conductance state of neocortical neurons in vivo. *Nat Rev Neurosci*, 4(9):739–751.

Durstewitz, Daniel, Deco, and Gustavo (2008). Computational significance of transient dynamics in cortical networks. *European Journal of Neuroscience*, 27(1):217–227.

Egorov, A. V., Hamam, B. N., Fransén, E., Hasselmo, M. E., and Alonso, A. A. (2002). Graded persistent activity in entorhinal cortex neurons. *Nature*, 420(6912):173–178.

Ermentrout, B. (1996). Type i membranes, phase resetting curves, and synchrony. *Neural computation*, 8(5):979–1001.

Euston, D. R., Tatsuno, M., and Mcnaughton, B. L. (2007). Fast-forward playback of recent memory sequences in prefrontal cortex during sleep. *Science*, 318(5853):1147–1150.

Fairhall, A. and Bialek, W. (2003). *Adaptive Spike Coding.*, pages 90–94. The MIT press.

Falcke, M., Huerta, R., Rabinovich, M. I., Abarbanel, H. D., Elson, R. C., and Selverston, A. I. (2000). Modeling observed chaotic oscillations in bursting neurons: the role of calcium dynamics and ip3. *Biological cybernetics*, 82(6):517–527.

Fellous, J.-M. M., Rudolph, M., Destexhe, A., and Sejnowski, T. J. (2003). Synaptic background noise controls the input/output characteristics of single cells in an in vitro model of in vivo activity. *Neuroscience*, 122(3):811–829.

Fitzhugh, R. (1961). Impulses and physiological states in theoretical models of nerve membrane. *Biophysical journal*, 1(6):445–466.

Fontanini, A. and Katz, D. B. B. (2008). Behavioral states, network states and sensory response variability. *Journal of neurophysiology*.

Fourcaud-Trocmé, N., Hansel, D., van Vreeswijk, C., and Brunel, N. (2003). How spike generation mechanisms determine the neuronal response to fluctuating inputs. *J Neurosci*, 23(37):11628–11640.

Freund, T. F. and Buzsáki, G. (1996). Interneurons of the hippocampus. *Hippocampus*, 6(4):347–470.

Friedrich, R. W., Habermann, C. J., and Laurent, G. (2004). Multiplexing using synchrony in the zebrafish olfactory bulb. *Nature neuroscience*, 7(8):862–871.

Froemke, R. C., Poo, M.-M., and Dan, Y. (2005). Spike-timing-dependent synaptic plasticity depends on dendritic location. *Nature*, 434(7030):221–225.

Fuhrmann, G., Segev, I., Markram, H., and Tsodyks, M. (2002). Coding of temporal information by activity-dependent synapses. *J Neurophysiol*, 87(1):140–148.

Funahashi, S. and Takeda, K. (2002). Information processes in the primate prefrontal cortex in relation to working memory processes. *Reviews in the neurosciences*, 13(4):313–345.

Fusi, S., Drew, P. J., and Abbott, L. F. (2005). Cascade models of synaptically stored memories. *Neuron*, 45(4):599–611.

Gaiarsa, J. L., Caillard, O., and Ben-Ari, Y. (2002). Long-term plasticity at gabaergic and glycinergic synapses: mechanisms and functional significance. *Trends in neurosciences*, 25(11):564–570.

Galan, R. F., Ermentrout, B. G., and Urban, N. N. (2005). Efficient estimation of phase-resetting curves in real neurons and its significance for neural-network modeling. *Physical Review Letters*, 94(15).

Garcia, P. S. S., Wright, T. M. M., Cunningham, I. R. R., and Calabrese, R. L. L. (2008). Coordination of motor neurons by the leech heartbeat central pattern generator: Modeling the role of the inhibitory input and electrical coupling. *Journal of neurophysiology*.

Gerstner, W. and Kistler, W. M. (2002). *Spiking Neuron Models*. Cambridge University Press, 1 edition.

Gerstner, W. and Naud, R. (2009). How good are neuron models? *Science*, 326(5951):379–380.

Gilboa, G., Chen, R., and Brenner, N. (2005). History-dependent multiple-time-scale dynamics in a single-neuron model. *J Neurosci*, 25:6479–6489.

Gloveli, T., Dugladze, T., Rotstein, H. G., Traub, R. D., Monyer, H., Heinemann, U., Whittington, M. A., and Kopell, N. J. (2005). Orthogonal arrangement of rhythm-generating microcircuits in the hippocampus. *Proc Natl Acad Sci U S A*, 102(37):13295–13300.

Grashow, R., Brookings, T., and Marder, E. (2009). Reliable neuromodulation from circuits with variable underlying structure. *Proceedings of the National Academy of Sciences*, 106(28):11742–11746.

Grillner, S. and Zangger, P. (1979). On the central generation of locomotion in the low spinal cat. *Experimental Brain Research*, 34(2):241–261.

Gutfreund, Y., yarom, Y., and Segev, I. (1995). Subthreshold oscillations and resonant frequency in guinea-pig cortical neurons: physiology and modelling. *The Journal of physiology*, 483 (Pt 3):621–640.

Gütig, R., Aharonov, R., Rotter, S., and Sompolinsky, H. (2003). Learning input correlations through nonlinear temporally asymmetric hebbian plasticity. *J Neurosci*, 23(9):3697–3714.

Gutkin, B. S., Ermentrout, B. G., and Reyes, A. D. (2005). Phase-response curves give the responses of neurons to transient inputs. *J Neurophysiol*, 94(2):1623–1635.

Haas, J. S., Nowotny, T., and Abarbanel, H. D. (2006). Spike-timing-dependent plasticity of inhibitory synapses in the entorhinal cortex. *Journal of neurophysiology*, 96(6):3305–3313.

Hill, A. V. (1936). Excitation and Accommodation in Nerve. *Royal Society of London Proceedings Series B*, 119:305–355.

Hille, B. (2001). *Ion Channels of Excitable Membranes (3rd Edition)*. Sinauer Associates, 3rd casebound edition.

Hodgkin, A. L. and Huxley, A. F. (1952). A quantitative description of membrane current and its application to conduction and excitation in nerve. *J Physiol*, (London) 117:500–544.

Hooper, S. L. (1998). Transduction of temporal patterns by single neurons. *Nat Neurosci*, 1(8):720–726.

Hooper, S. L., Buchman, E., Weaver, A. L., Thuma, J. B., and Hobbs, K. H. (2009). Slow conductances could underlie intrinsic phase-maintaining properties of isolated lobster (panulirus interruptus) pyloric neurons. *The Journal of neuroscience : the official journal of the Society for Neuroscience*, 29(6):1834–1845.

Hopfield, J. J. (1982). Neural networks and physical systems with emergent collective computational abilities. *Proceedings of the National Academy of Scientists*, 79:2554–2558.

Hopfield, J. J. (2004). Encoding for computation: Recognizing brief dynamical patterns by exploiting effects of weak rhythms on action-potential timing. *Proceedings of the National Academy of Sciences of the United States of America*, 101(16):6255–6260.

Hutcheon, B. and Yarom, Y. (2000). Resonance, oscillation and the intrinsic frequency preferences of neurons. *Trends Neurosci*, 23:216–222.

Ikegaya, Y., Aaron, G., Cossart, R., Aronov, D., Lampl, I., Ferster, D., and Yuste, R. (2004). Synfire chains and cortical songs: temporal modules of cortical activity. *Science (New York, N.Y.)*, 304(5670):559–564.

Ivanov, A. I. and Calabrese, R. L. (2000). Intracellular ca2+ dynamics during spontaneous and evoked activity of leech heart interneurons: low-threshold ca currents and graded synaptic transmission. *J Neurosci*, 20:4930–4943.

Ivanov, A. I. and Calabrese, R. L. (2003). Modulation of spike-mediated synaptic transmission by presynaptic background ca2+ in leech heart interneurons. *J Neurosci*, 23:1206–1218.

Izhikevich, E. M. (2001). Resonate-and-fire neurons. *Neural Netw*, 14(6-7):883–894.

Izhikevich, E. M. (2006). *Dynamical Systems in Neuroscience: The Geometry of Excitability and Bursting*. The MIT press.

Izhikevich, E. M., Desai, N. S., and Walcott, E. C. (2003a). Bursts as a unit of neural information: selective communication via resonance. *Trends Neurosci*, 26:161–167.

Izhikevich, E. M., Desai, N. S., Walcott, E. C., and Hoppensteadt, F. C. (2003b). Bursts as a unit of neural information: selective communication via resonance. *Trends in neurosciences*, 26(3):161–167.

Izhikevich, E. M. and Edelman, G. M. (2008). Large-scale model of mammalian thalamocortical systems. *Proceedings of the National Academy of Sciences*, 105(9):3593–3598.

Johnson, H. A. and Buonomano, D. V. (2007). Development and plasticity of spontaneous activity and up states in cortical organotypic slices. *J. Neurosci.*, 27(22):5915–5925.

Johnston, D. and Narayanan, R. (2008). Active dendrites: colorful wings of the mysterious butterflies. *Trends in Neurosciences*, 31(6):309–316.

Kang, S., Kitano, K., and Fukai, T. (2008). Structure of spontaneous up and down transitions self-organizing in a cortical network model. *PLoS Comput Biol*, 4(3):e1000022+.

Karmarkar, U. R. and Buonomano, D. V. (2007). Timing in the absence of clocks: Encoding time in neural network states. *Neuron*, 53(3):427–438.

Kavalali and Ege, T. (2007). Multiple vesicle recycling pathways in central synapses and their impact on neurotransmission. *The Journal of Physiology*, 585(3):669–679.

Kempter, R., Leibold, C., Wagner, H., and van Hemmen, J. L. (2001). Formation of temporal-feature maps by axonal propagation of synaptic learning. *Proc Natl Acad Sci U S A*, 98(7):4166–4171.

Kepecs, A., van Rossum, M. C., Song, S., and Tegner, J. (2002). Spike-timing-dependent plasticity: common themes and divergent vistas. *Biological cybernetics*, 87(5-6):446–458.

Keren, N., Peled, N., and Korngreen, A. (2005). Constraining compartmental models using multiple voltage recordings and genetic algorithms. *Journal of neurophysiology*, 94(6):3730–3742.

Kintos, N., Nusbaum, M. P., and Nadim, F. (2008). A modeling comparison of projection neuron- and neuromodulator-elicited oscillations in a central pattern generating network. *Journal of computational neuroscience*, 24(3):374–397.

Kistler, W. M., Gerstner, W., and Hemmen (1997). Reduction of the hodgkin-huxley equations to a single-variable threshold model. *Neural Computation*, 9(5):1015–1045.

Klausberger, T. and Somogyi, P. (2008). Neuronal diversity and temporal dynamics: The unity of hippocampal circuit operations. *Science*, 321(5885):53–57.

Kleppe, I. C. and Robinson, H. P. (2006). Correlation entropy of synaptic input-output dynamics. *Phys Rev E Stat Nonlin Soft Matter Phys*, 74(4 Pt 1).

Kobayashi, R., Tsubo, Y., and Shinomoto, S. (2009). Made-to-order spiking neuron model equipped with a multi-timescale adaptive threshold. *Frontiers in computational neuroscience*, 3.

Komendantov, A. O. and Kononenko, N. I. (1996). Deterministic chaos in mathematical model of pacemaker activity in bursting neurons of snail, helix pomatia. *Journal of theoretical biology*, 183(2):219–230.

Kropff, E. and Treves, A. (2008). The emergence of grid cells: Intelligent design or just adaptation? *Hippocampus*, 18(12):1256–1269.

Lampl, I., Reichova, I., and Ferster, D. (1999). Synchronous membrane potential fluctuations in neurons of the cat visual cortex. *Neuron*, 22(2):361–374.

Lapicque, L. (1907). Recherches quantitatifs sur l'excitation electrique des nerfs traitée comme une polarisation. *J. Physiol. (Paris)*, 9:620–635.

Latorre, R., Rodríguez, F. B., and Varona, P. (2006). Neural signatures: multiple coding in spiking-bursting cells. *Biological cybernetics*, 95(2):169–183.

Legenstein, R. and Maass, W. (2007). Edge of chaos and prediction of computational performance for neural circuit models. *Neural Networks*, 20(3):323–334.

Leibold, C., Gundlfinger, A., Schmidt, R., Thurley, K., Schmitz, D., and Kempter, R. (2008). Temporal compression mediated by short-term synaptic plasticity. *Proceedings of the National Academy of Sciences*, pages 0708711105+.

Letzkus, J. J., Kampa, B. M., and Stuart, G. J. (2006). Learning rules for spike timing-dependent plasticity depend on dendritic synapse location. *The Journal of neuroscience : the official journal of the Society for Neuroscience*, 26(41):10420–10429.

Levi, R., Marinazzo, D., Chamorro, P., Rodriguez, F. B., and Varona, P. (2010). Causal relationships between calcium and membrane potential in cpg neurons. Society for Neuroscience Annual Meeting Abstract.

Li, C., Chen, L., and Aihara, K. (2006). Transient resetting: A novel mechanism for synchrony and its biological examples. *PLoS Comput Biol*, 2(8).

Linsdell, P. and Moody, W. J. (1995). Electrical activity and calcium influx regulate ion channel development in embryonic xenopus skeletal muscle. *J. Neurosci.*, 15(6):4507–4514.

Liu, A., Golowasch, J., Marder, E., and Abbott, F. (1998). A model neuron with activity-dependent conductances regulated by multiple calcium sensor. *J Neurosci*, 18:2309–2320.

Llinas, R. R. (1988). The intrinsic electrophysiological properties of mammalian neurons: insights into central nervous system function. *Science*, 242(4886):1654–1664.

Loewenstein, Y. and Sompolinsky, H. (2003). Temporal integration by calcium dynamics in a model neuron. *Nature neuroscience*, 6(9):961–967.

Lubenov, E. V. and Siapas, A. G. (2008). Decoupling through synchrony in neuronal circuits with propagation delays. *Neuron*, 58(1):118–131.

Luczak, A., Barthó, P., Marguet, S. L., Buzsáki, G., and Harris, K. D. (2007). Sequential structure of neocortical spontaneous activity in vivo. *Proceedings of the National Academy of Sciences of the United States of America*, 104(1):347–352.

Luthi, A. and Mccormick, D. A. (1998). Periodicity of thalamic synchronized oscillations: the role of ca2+-mediated upregulation of ih. *Neuron*, 20(3):553–63.

Maass, W., Natschläger, T., and Markram, H. (2002). Real-time computing without stable states: A new framework for neural computation based on perturbations. *Neural Computation*, 14(11):2531–2560.

Mao, B. Q., Hamzei-Sichani, F., Aronov, D., Froemke, R. C., and Yuste, R. (2001). Dynamics of spontaneous activity in neocortical slices. *Neuron*, 32(5):883–898.

Marder, E., Abbott, L. . F., Turrigiano, G. g., Liu, Z., and Golowasch, J. (1996). Memory from the dynamics of intrinsic membraneÂ currents. *PNAS*, 93(24):13481–13486.

Marder, E. and Calabrese, R. L. (1996). Principles of rhythmic motor pattern production. *Physiol Rev*, 76:687–717.

Marin, B., Baroni, F., Varona, P., and Pinto, R. (2009). Temporal structure of bursting patterns as representation of input history. *BMC Neuroscience*, 10(Suppl 1):P101+.

Markram, H., Lübke, J., Frotscher, M., and Sakmann, B. (1997). Regulation of synaptic efficacy by coincidence of postsynaptic aps and epsps. *Science (New York, N.Y.)*, 275(5297):213–215.

Markram, H., Toledo-Rodriguez, M., Wang, Y., Gupta, A., Silberberg, G., and Wu, C. (2004). Interneurons of the neocortical inhibitory system. *Nature Reviews Neuroscience*, 5(10):793–807.

Mato, G. and Samengo, I. (2008). Type i and type ii neuron models are selectively driven by differential stimulus features. *Neural computation*, 20(10):2418–2440.

Maurer, A. P. and McNaughton, B. L. (2007). Network and intrinsic cellular mechanisms underlying theta phase precession of hippocampal neurons. *Trends in neurosciences*, 30(7):325–333.

Meech, R. W. (1978). Calcium-dependent potassium activation in nervous tissues. *Annual review of biophysics and bioengineering*, 7:1–18.

Meffin, H., Besson, J., Burkitt, A. N., and Grayden, D. B. (2006). Learning the structure of correlated synaptic subgroups using stable and competitive spike-timing-dependent plasticity. *Physical review. E, Statistical, nonlinear, and soft matter physics*, 73(4 Pt 1).

Meister, M., Lagnado, L., and Baylor, D. A. (1995). Concerted signaling by retinal ganglion cells. *Science (New York, N.Y.)*, 270(5239):1207–1210.

Miller, G. (2006). Optogenetics. shining new light on neural circuits. *Science (New York, N.Y.)*, 314(5806):1674–1676.

Moreno, R., de la Rocha, J., Renart, A., and Parga, N. (2002). Response of spiking neurons to correlated inputs. *Phys Rev Lett*, 89(28 Pt 1).

Morris, C. and Lecar, H. (1981). Voltage oscillations in the barnacle giant muscle fiber. *Biophysical journal*, 35(1):193–213.

Morrison, A., Diesmann, M., and Gerstner, W. (2008). Phenomenological models of synaptic plasticity based on spike timing. *Biol. Cybern.*, 98(6):459–478.

Muller, K. J., Nicholls, J. G., and Stent, G. S. (1981). *Neurobiology of the Leech*. Cold Spring Harbor Laboratory.

Muresan, R. C. and Savin, C. (2007). Resonance or integration? self-sustained dynamics and excitability of neural microcircuits. *J Neurophysiol*, 97(3):1911–1930.

Nadasdy, Z., Hirase, H., Czurko, A., Csicsvari, J., and Buzsaki, G. (1999). Replay and time compression of recurring spike sequences in the hippocampus. *J. Neurosci.*, 19(21):9497–9507.

Nadim, F., Brezina, V., Destexhe, A., and Linster, C. (2008). State dependence of network output: Modeling and experiments. *J. Neurosci.*, 28(46):11806–11813.

Nadim, F., Manor, Y., Kopell, N., and Marder, E. (1999). Synaptic depression creates a switch that controls the frequency of an oscillatory circuit. *Proc Natl Acad Sci U S A*, 96(14):8206–8211.

Narayanan, R. and Johnston, D. (2008). The h channel mediates location dependence and plasticity of intrinsic phase response in rat hippocampal neurons. *The Journal of neuroscience : the official journal of the Society for Neuroscience*, 28(22):5846–5850.

Nayak, T. K. and Sikdar, S. K. (2007). Time-dependent molecular memory in single voltage-gated sodium channel. *The Journal of membrane biology*, 219(1-3):19–36.

Netoff, T., Acker, C., Bettencourt, J., and White, J. (2005). Beyond two-cell networks: Experimental measurement of neuronal responses to multiple synaptic inputs. *Journal of Computational Neuroscience*, 18(3):287–295.

Nowotny, T., Levi, R., and Selverston, A. I. (2008). Probing the dynamics of identified neurons with a data-driven modeling approach. *PloS one*, 3(7).

Nowotny, T., Szücs, A., Levi, R., and Selverston, A. I. (2007). Models wagging the dog: are circuits constructed with disparate parameters? *Neural computation*, 19(8):1985–2003.

Olshausen, B. A. and Field, D. J. (2004). Sparse coding of sensory inputs. *Current opinion in neurobiology*, 14(4):481–487.

Oprisan, S. A. and Canavier, C. C. (2002). The influence of limit cycle topology on the phase resetting curve. *Neural computation*, 14(5):1027–1057.

Oram, M. W., Wiener, M. C., Lestienne, R., and Richmond, B. J. (1999). Stochastic nature of precisely timed spike patterns in visual system neuronal responses. *Journal of neurophysiology*, 81(6):3021–3033.

Pakdaman, K. (2002). The reliability of the stochastic active rotator. *Neural Comput*, 14(4):781–792.

Plenz, D. and Thiagarajan, T. (2007). The organizing principles of neuronal avalanches: cell assemblies in the cortex? *Trends in Neurosciences*, 30(3):101–110.

Pouille, F. and Scanziani, M. (2001). Enforcement of temporal fidelity in pyramidal cells by somatic feed-forward inhibition. *Science*, 293(5532):1159–1163.

Prinz, A. A., Abbott, L. F., and Marder, E. (2004a). The dynamic clamp comes of age. *Trends Neurosci*, 27(4):218–224.

Prinz, A. A., Bucher, D., and Marder, E. (2004b). Similar network activity from disparate circuit parameters. *Nat Neurosci*, 7:1345–1352.

Proekt, A., Brezina, V., and Weiss, K. R. (2004). Dynamical basis of intentions and expectations in a simple neuronal network. *Proceedings of the National Academy of Sciences of the United States of America*, 101(25):9447–9452.

Quintana, J. and Fuster, J. M. (1992). Mnemonic and predictive functions of cortical neurons in a memory task. *Neuroreport*, 3(8):721–724.

Quintana, J. and Fuster, J. M. (1999). From perception to action: temporal integrative functions of prefrontal and parietal neurons. *Cereb Cortex*, 9(3):213–221.

Rabinovich, M. I., Huerta, R., Varona, P., and Afraimovich, V. S. (2008). Transient cognitive dynamics, metastability, and decision making. *PLoS Comput Biol*, 4(5):e1000072+.

Rabinovich, M. I., Varona, P., Selverston, A. I., and Abarbanel, H. D. I. (2006). Dynamical principles in neuroscience. *Reviews of Modern Physics*, 78(4):1213+.

Rainer, G., Rao, S. C., and Miller, E. K. (1999). Prospective coding for objects in primate prefrontal cortex. *The Journal of neuroscience : the official journal of the Society for Neuroscience*, 19(13):5493–5505.

Ramaswamy, S., Baroni, F., Varona, P., and Depolavieja, G. (2007). Time-scales in the interplay between calcium and voltage dynamics. *Neurocomputing*, 70(10-12):1949–1953.

Reyes, M., Huerta, R., Rabinovich, M., and Selverston, A. (2008). Artificial synaptic modification reveals a dynamical invariant in the pyloric cpg. *European Journal of Applied Physiology*, 102(6):667–675.

Richardson, M. J., Brunel, N., and Hakim, V. (2003). From subthreshold to firing-rate resonance. *J Neurophysiol*, 89(5):2538–2554.

Ripley, S. H. and Wiersma, C. A. (1953). The effect of spaced stimulation of excitatory and inhibitory axons of the crayfish. *Physiol. comp. et oeco.*, 3:1–17.

Roxin, A., Brunel, N., and Hansel, D. (2005). Role of delays in shaping spatiotemporal dynamics of neuronal activity in large networks. *Physical review letters*, 94(23).

Rubin, J., Lee, D. D., and Sompolinsky, H. (2001). Equilibrium properties of temporally asymmetric hebbian plasticity. *Physical Review Letters*, 86(2):364+.

Rudolph, M., Pospischil, M., Timofeev, I., and Destexhe, A. (2007). Inhibition determines membrane potential dynamics and controls action potential generation in awake and sleeping cat cortex. *The Journal of neuroscience : the official journal of the Society for Neuroscience*, 27(20):5280–5290.

Saideman, S. R., Blitz, D. M., and Nusbaum, M. P. (2007). Convergent motor patterns from divergent circuits. *The Journal of neuroscience : the official journal of the Society for Neuroscience*, 27(25):6664–6674.

Salinas, E. and Sejnowski, T. J. (2001). Correlated neuronal activity and the flow of neural information. *Nat Rev Neurosci*, 2(8):539–550.

Saudargiene, A., Porr, B., and Wörgötter, F. (2005). Local learning rules: predicted influence of dendritic location on synaptic modification in spike-timing-dependent plasticity. *Biol Cybern*, 92(2):128–138.

Schaefer, A. T., Angelo, K., Spors, H., and Margrie, T. W. (2006). Neuronal oscillations enhance stimulus discrimination by ensuring action potential precision. *PLoS biology*, 4(6).

Scheich, H., Ohl, F. W., Schulze, H., Hess, A., and Brechmann, A. (2005). *What is reflected in sensory neocortical activity: External stimuli or what the cortex does with them?*, pages 343–366. Computational Neuroscience Series. Oxford University Press, USA.

Scholz, J. P. and Schöner, G. (1999). The uncontrolled manifold concept: identifying control variables for a functional task. *Experimental brain research. Experimentelle Hirnforschung. Expérimentation cérébrale*, 126(3):289–306.

Schreiber, S., Erchova, I., Heinemann, U., and Herz, A. V. (2004). Subthreshold resonance explains the frequency-dependent integration of periodic as well as random stimuli in the entorhinal cortex. *J Neurophysiol*, 92(1):408–415.

Schwartz, O., Sejnowski, T. J., and Dayan, P. (2009). Perceptual organization in the tilt illusion. *Journal of vision*, 9(4).

Scoville, W. B. and Milner, B. (1957). Loss of recent memory after bilateral hippocampal lesions. *Journal of neurology, neurosurgery, and psychiatry*, 20(1):11–21.

Segundo, J. P., Moore, G. P., Stensaas, L. J., and Bullock, T. H. (1963). Sensitivity of neurones in aplysia to temporal pattern of arriving impulses. *J Exp Biol*, 40(4):643–667.

Seung, H. S., Lee, D. D., Reis, B. Y., and Tank, D. W. (2000). The autapse: a simple illustration of short-term analog memory storage by tuned synaptic feedback. *Journal of computational neuroscience*, 9(2):171–185.

Shadlen, M. N. and Newsome, W. T. (1998). The variable discharge of cortical neurons: Implications for connectivity, computation, and information coding. *J. Neurosci.*, 18(10):3870–3896.

Shamir, M., Ghitza, O., Epstein, S., and Kopell, N. (2009). Representation of time-varying stimuli by a network exhibiting oscillations on a faster time scale. *PLoS Comput Biol*, 5(5):e1000370+.

Shamir, M. and Sompolinsky, H. (2006). Implications of neuronal diversity on population coding. *Neural Comput.*, 18(8):1951–1986.

Sherman, S. M. and Guillery, R. W. (1998). On the actions that one nerve cell can have on another: distinguishing "drivers" from "modulators". *Proc Natl Acad Sci U S A*, 95(12):7121–7126.

Shoham, S., O'Connor, D. H., and Segev, R. (2006). How silent is the brain: is there a "dark matter" problem in neuroscience? *Journal of comparative physiology. A, Neuroethology, sensory, neural, and behavioral physiology*, 192(8):777–784.

Sikström, S. (2002). Forgetting curves: implications for connectionist models. *Cognitive psychology*, 45(1):95–152.

Soltesz, I. (2005). *Diversity in the Neuronal Machine: Order and Variability in Interneuronal Microcircuits*. Oxford University Press, USA.

Somogyi, P. and Klausberger, T. (2005). Defined types of cortical interneurone structure space and spike timing in the hippocampus. *The Journal of physiology*, 562(Pt 1):9–26.

Song, S. and Abbott, L. F. (2001). Cortical development and remapping through spike timing-dependent plasticity. *Neuron*, 32(2):339–350.

Song, S., Miller, K. D., and Abbott, L. F. (2000). Competitive hebbian learning through spike-timing-dependent synaptic plasticity. *Nature Neuroscience*, 3(9):919–926.

Song, S., Sjöström, P. J., Reigl, M., Nelson, S., and Chklovskii, D. B. (2005). Highly nonrandom features of synaptic connectivity in local cortical circuits. *PLoS Biol*, 3(3).

Steriade, M. (2004). Neocortical cell classes are flexible entities. *Nat Rev Neurosci*, 5(2):121–134.

Stern, E. A., Kincaid, A. E., and Wilson, C. J. (1997). Spontaneous subthreshold membrane potential fluctuations and action potential variability of rat corticostriatal and striatal neurons in vivo. *Journal of neurophysiology*, 77(4):1697–1715.

Szücs, A., Pinto, R. D., Rabinovich, M. I., Abarbanel, H. D. I., and Selverston, A. I. (2003). Synaptic modulation of the interspike interval signatures of bursting pyloric neurons. *J Neurophysiol*, 89:1363–1377.

Takeda, K. and Funahashi, S. (2002). Prefrontal task-related activity representing visual cue location or saccade direction in spatial working memory tasks. *Journal of neurophysiology*, 87(1):567–588.

Tateno, T. (2007). Phase resetting curves and oscillatory stability in interneurons of rat somatosensory cortex. *Biophysical Journal*, 92(2):683–695.

Tateno, T. and Pakdaman, K. (2004). Random dynamics of the morris-lecar neural model. *Chaos (Woodbury, N.Y.)*, 14(3):511–530.

Tegnér, J. and Kepecs, A. (2002). An adaptive spike-timing-dependent plasticity rule. *Neurocomputing*, 44-46:189–194.

Teramae, J.-N. and Fukai, T. (2005). A cellular mechanism for graded persistent activity in a model neuron and its implications in working memory. *Journal of Computational Neuroscience*, 18(1):105–121.

Thoby-Brisson, M. and Simmers, J. (1998). Neuromodulatory inputs maintain expression of a lobster motor pattern-generating network in a modulation-dependent state: Evidence from long-term decentralization in vitro. *J. Neurosci.*, 18(6):2212–2225.

Thompson, W. J. and Stent, G. S. (1976). Neuronal control of heartbeat in the medicinal leech. *Journal of Comparative Physiology A: Neuroethology, Sensory, Neural, and Behavioral Physiology*, 111(3):281–307.

Thomson, A. M. and Deuchars, J. (1994). Temporal and spatial properties of local circuits in neocortex. *Trends in neurosciences*, 17(3):119–126.

Tobin, A.-E. E. and Calabrese, R. L. (2006). Endogenous and half-center bursting in morphologically inspired models of leech heart interneurons. *Journal of neurophysiology*, 96(4):2089–2106.

Todorov, E. (2004). Optimality principles in sensorimotor control. *Nature neuroscience*, 7(9):907–915.

Tsodyks, M. and Markram, H. (1997). The neural code between neocortical pyramidal neurons depends on neurotransmitter release probability. *Proceedings of the National Academy of Sciences of the United States of America*, 94(2):719–723.

Tsuda, I. (2001). Toward an interpretation of dynamic neural activity in terms of chaotic dynamical systems. *Behav Brain Sci*, 24(5).

Turrigiano, G. G., Marder, E., and Abbott, L. F. (1996). Cellular short-term memory from a slow potassium conductance. *J Neurophysiol*, 75(2):963–966.

Ullah, G. and Schiff, S. J. (2009). Tracking and control of neuronal hodgkin-huxley dynamics. *Physical review. E, Statistical, nonlinear, and soft matter physics*, 79(4 Pt 1).

van Vreeswijk, C. and Sompolinsky, H. (1996). Chaos in neuronal networks with balanced excitatory and inhibitory activity. *Science*, 274(5293):1724–1726.

Vanier, M. C. and Bower, J. M. (1999). A comparative survey of automated parameter-search methods for compartmental neural models. *Journal of computational neuroscience*, 7(2):149–171.

Varona, P., Torres, J. J., Huerta, R., Abarbanel, H. D., and Rabinovich, M. I. (2001). Regularization mechanisms of spiking-bursting neurons. *Neural networks : the official journal of the International Neural Network Society*, 14(6-7):865–875.

Wang, H.-P., Spencer, D., Fellous, J.-M., and Sejnowski, T. J. (2010). Synchrony of thalamocortical inputs maximizes cortical reliability. *Science*, 328(5974):106–109.

Wang, X., Wei, Y., Vaingankar, V., Wang, Q., Koepsell, K., Sommer, F. T., and Hirsch, J. A. (2007). Feedforward excitation and inhibition evoke dual modes of firing in the cat's visual thalamus during naturalistic viewing. *Neuron*, 55(3):465–478.

Wang, X.-J. (2001). Synaptic reverberation underlying mnemonic persistent activity. *Trends in Neurosciences*, 24(8):455–463.

Warrick, H. R. M. and Marder, E. (1991). Modulation of neural networks for behavior. *Annu Rev Neurosci*, 14:39–57.

Wehr, M. and Laurent, G. (1996). Odour encoding by temporal sequences of firing in oscillating neural assemblies. *Nature*, 384(6605):162–166.

Wessel, R., Kristan, W. B., and Kleinfeld, D. (1999). Dendritic ca(2+)-activated k(+) conductances regulate electrical signal propagation in an invertebrate neuron. *J Neurosci*, 19:8319–8326.

White, J. A., Chow, C. C., Ritt, J., Soto-Treviño, C., and Kopell, N. (1998). Synchronization and oscillatory dynamics in heterogeneous, mutually inhibited neurons. *J Comput Neurosci*, 5(1):5–16.

Whittington, M. A. and Traub, R. D. (2003). Interneuron diversity series: inhibitory interneurons and network oscillations in vitro. *Trends in neurosciences*, 26(12):676–682.

Wiersma, C. A. and Adams, R. T. (1950). The influence of nerve impulse sequence on the contractions of different crustacean muscles. *Physiol. comp. et oeco.*, 2:20–33.

Winograd, M., Destexhe, A., and Sanchez-Vives, M. V. (2008). Hyperpolarization-activated graded persistent activity in the prefrontal cortex. *Proceedings of the National Academy of Sciences of the United States of America*, 105(20):7298–7303.

Wolf, D. M., Fontaine-Bodin, L., Bischofs, I., Price, G., Keasling, J., and Arkin, A. P. (2008). Memory in microbes: quantifying history-dependent behavior in a bacterium. *PLoS ONE*, 3(2).

Yuste, R., MacLean, J. N., Smith, J., and Lansner, A. (2005). The cortex as a central pattern generator. *Nature reviews. Neuroscience*, 6(6):477–483.

Zhang, W. and Linden, D. J. (2003). The other side of the engram: experience-driven changes in neuronal intrinsic excitability. *Nat Rev Neurosci*, 4(11):885–900.

Zhang, Y., Bose, A., and Nadim, F. (2008). Predicting the activity phase of a follower neuron with a-current in an inhibitory network. *Biological cybernetics*, 99(3):171–184.

Zhurov, Y. and Brezina, V. (2006). Variability of motor neuron spike timing maintains and shapes contractions of the accessory radula closer muscle of aplysia. *The Journal of neuroscience : the official journal of the Society for Neuroscience*, 26(26):7056–7070.

Zucker, R. S. and Regehr, W. G. (2002). Short-term synaptic plasticity. *Annual Review of Physiology*, 64(1):355–405.